uOttawa

L'Université canadienne
Canada's university

FACULTÉ DES ÉTUDES SUPÉRIEURES ET POSTOCTORALES

uOttawa

L'Université canadienne
Canada's university

FACULTY OF GRADUATE AND POSDOCTORAL STUDIES

Gabriel Machado
AUTEUR DE LA THÈSE / AUTHOR OF THESIS

Ph.D. (Earth Sciences)
GRADE / DEGREE

Department of Earth Sciences
FACULTÉ, ÉCOLE, DÉPARTEMENT / FACULTY, SCHOOL, DEPARTMENT

Crystal size distribution of feldspar crystals from granitic rocks or Eurajoki (Finland) and the South Mountain Batholith (Nova Scotia, Canada)

TITRE DE LA THÈSE / TITLE OF THESIS

Anthony Fowler
DIRECTEUR (DIRECTRICE) DE LA THÈSE / THESIS SUPERVISOR

CO-DIRECTEUR (CO-DIRECTRICE) DE LA THÈSE / THESIS CO-SUPERVISOR

EXAMINATEURS (EXAMINATRICES) DE LA THÈSE / THESIS EXAMINERS

Frederik Agterberg

André Lalonde

Jaroslav Dostal

Richard Taylor

Michael Higgins

Gary W. Slater
Le Doyen de la Faculté des études supérieures et postdoctorales / Dean of the Faculty of Graduate and Postdoctoral Studies

Crystal size distribution of feldspar crystals from granitic rocks of Eurajoki (Finland) and the South Mountain Batholith (Nova Scotia, Canada)

By

Gabriel Machado

A thesis submitted to the School of Graduate Studies and Research

in partial fulfillment of the requirements

for the degree of Ph.D. in Earth Sciences

Ottawa-Carleton Geoscience Centre

and

University of Ottawa

Your file Votre référence
ISBN: 978-0-494-50743-8
Our file Notre référence
ISBN: 978-0-494-50743-8

Abstract

Crystal size distributions (CSDs) studies of igneous rocks allow the quantification of sizes of mineral and contribute to a better understanding of crystallization conditions. Since most CSD studies have been made on mafic and felsic volcanic rocks and mafic plutonic rocks, one of the goals of this research was to do a large number of CSDs on feldspar crystals from two well-known granitic localities: the Eurajoki stock (Finland) and the South Mountain Batholith (Nova Scotia, Canada).

Crystal size data were measured at different scales and on different media (outcrop, rock slabs and thin sections). CSDs were constructed from the data collected at the various scales using the program *CSD corrections* and plotted as amalgamated CSDs for each sample.

CSDs of potassic felspars from Eurajoki samples were curved upwards and the characteristic lengths indicate three populations of crystals sizes. It is proposed that potassic feldspar crystals have been texturally coarsened likely because the Eurajoki melts were emplaced in a hot environment. This minimized undercooling and the temperature was buffered by latent heat of fusion near the liquidus. Thus large crystals grew at the expense of smaller ones. With cooling, nucleation and growth of small crystals resumed, yielding the different crystals sizes populations observed.

CSDs of plagioclase and potassic felspars from the South Mountain Batholith were also curved upwards and the characteristic lengths indicate two populations of crystals sizes, except for the muscovite leucogranites from the stage 2 plutons, where CSDs are straight. Textural coarsening formed the larger crystals, megacrysts, in the South Mountain Batholith. Here the constant ascent of new magma into the plutons slowed undercooling and buffered the temperature producing the right conditions for textural coarsening.

Résumé

L'étude de la Distribution de la Taille des Cristaux (DTC) dans les roches ignées permet de quantifier la taille des cristaux et de mieux comprendre leurs conditions de cristallisation. Compte tenu que la plupart des études de DTC publiées concernaient les roches mafiques volcaniques et plutoniques ainsi que les roches felsiques volcaniques, le but de cette recherche consistait à calculer un grand nombre de DTC pour les cristaux de feldspath de deux masses granitiques déjà bien étudiées : Eurajoki en Finlande et le South Mountain Batholith en Nouvelle-Écosse au Canada afin de mieux comprendre leur formation.

Les données nécessaires à la production de DTC ont été mesurées à différentes échelles et sur différents supports (affleurement, plaque d'échantillon de roche et lame mince). Les graphiques de DTC ont été faits en combinant les données obtenues à différentes échelles pour chaque échantillon et en utilisant le programme *CSD corrections*.

Les DTC des cristaux de feldspath potassique provenant des échantillons de Eurajoki sont courbées vers le haut et les longueurs caractéristiques indiquent trois différentes populations de tailles de cristaux. Il est proposé que les cristaux de feldspath potassique ont subit un accroissement textural (textural coarsening) parce que le magma de Eurajoki a été mis en place dans un environnement ayant une température élevée. Cette situation a minimisé la surfusion (undercooling) et la température a été tamponnée près du liquidus par la chaleur latente de fusion. Les gros cristaux ont alors continué de croître aux dépends des plus petits,

qui se sont résorbés. À la reprise du refroidissement, la nucléation et la croissance de petits cristaux ont recommencé, donnant ainsi les différentes tailles de cristaux observées.

Les DTC des cristaux de plagioclase et de feldspath potassique provenant des échantillons de South Mountain Batholith sont aussi courbées vers le haut. De plus, les longueurs caractéristiques indiquent deux différentes populations de tailles de cristaux, sauf pour les échantillons de leucogranite à muscovite des plutons phase 2 où les DTC sont linéaires. L'accroissement textural a formé les mégacristaux de South Mountain Batholith. Ceux-ci ont été produits par l'apport constant de nouveau magma dans les plutons, ce qui a ralentit la surfusion et a tamponné la température.

Table of Contents

List of Tables

List of Figures

Remerciements

La réalisation de cette thèse de doctorat n'aurait pas été possible sans l'aide et le support de nombreuses personnes. Tout d'abord, j'aimerais remercier Anthony Fowler et Michael Higgins pour leur disponibilité, leurs encouragements et leurs nombreux conseils scientifiques. J'aimerais aussi remercier Ilmari Haapala et Jarda Dostal pour m'avoir fait découvrir les roches de Eurajoki et de South Mountain lors de mon séjour en sol finlandais et néo-écossais. Il me faut également remercier George Mrazek pour la préparation des nombreuses lames minces et André Lalonde pour son support moral et ses encouragements. Enfin, je tiens à souligner l'appui et les encouragements soutenus d'Isabelle pendant les nombreuses années associées à ce projet, tout particulièrement lors de mes périodes de procrastination! J'ai, en bout de ligne, perdu mon pari : l'arrivée de notre petite Sarah aura précédé le dépôt de cette thèse de doctorat, mais quelle inspiration pour terminer!

Chapter 1

Introduction and theory

Introduction

One of the unresolved problems of Earth Sciences is the formulation of a complete model of the processes occurring in magma chambers. Theoretical and laboratory studies are useful but the scaling and complexity of the systems imposes severe constraints. Similarly observational techniques are constrained because the only way of doing them is through the study of the solidification products, rock, exhumed a long time after crystallization.

Rocks are generally studied quantitatively using chemical, isotopic and geophysical means, but generally only qualitatively in terms of their crystal sizes geometry and textures through the use of the optical microscope and petrological descriptions. However, one technique, Crystal size distributions (CSD), allows the quantification of some aspects of rock textures allowing for the formulation and testing of hypotheses about the crystallization conditions that led to the rock formation.

To date, most CSD studies of igneous rocks have been restricted to mafic volcanic and plutonic rocks (Cashman & Marsh, 1988; Jerram *et al.*, 2003; Armienti *et al.*, 1994; Higgins, 1991, 1998, 2000 and 2002b; Higgins & Roberge, 2003; Zieg & Marsh, 2002; Oze &Winter,

2005 and many other papers), whereas studies on felsic rocks are less common. Even in felsic rocks approximately two thirds of the studies reported in the literature have been done on volcanic rocks (Cashman, 1988 and 1992; Hammer *et al.*, 1999; Higgins, 1996; Castro et al., 2003; Gualda *et al.*, 2004; Bindeman, 2003; Bindeman & Valley, 2001; Mock & Jerram, 2005) while only about four studies have been done on plutonic rocks. These studies are: orthopyroxene and olivine in a syenite in Greenland (Hodson, 1998), clinopyroxene and magnetite in a syenite from Canada (Launeau & Cruden, 1998), potassic feldspar in a granodiorite from the United States (Higgins, 1999), orthoclase, plagioclase and quartz from a granite porphyry in Germany (Mock *et al.*, 2003).

As the reader can see, CSD work on plutonic felsic rocks is scarce and half of the studies were done on accessory minerals rather than rock-forming minerals. Thus little work has been done using this technique to give insight on the crystallization processes occurring in magma chambers.

Accordingly this dissertation documents extensive CSD work on plutonic felsic rocks from two well-known localities that have been well studied in terms of their chemical, isotopic and textural (to a lesser extent) properties. These are the Eurajoki stock in Finland and the South Mountain Batholith (SMB) in Nova Scotia, Canada. Eurajoki was chosen because it is a small rapakivi anorogenic granite showing evidence of interesting late stage processes, tin mineralization and where Haapala (1977, 1997) has done detailed work. SMB was chosen in order to do CSD on a larger batholithic mass, the whole batholith is easily accessible through

provincial roads and it was emplaced during the Acadian Orogeny. It also has tin mineralization and has been extensively studied. CSDs done by the author on rocks of these two localities are used with previous works done by others and other data generated during this study to quantify crystal sizes and to test hypotheses of crystal growth mechanisms in order to decipher the processes that likely occurred during magma chamber consolidation.

The Eurajoki stock is part of the 1570 Ma old Laitila rapakivi granite batholith (Vaasjoki, 1977) forming part of the anorogenic rapakivi granitic suite of Finland (1.65-1.54 Ga). These generally show a bimodal magmatic association and A-type geochemical and mineralogical characteristics (Haapala, 1997) and were formed by fractionation of alkali feldspars, quartz and clinopyroxene (Haapala & Rämö, 1992). Haapala (1977) showed that the Eurajoki stock is composed of several petrographically and distinct granite types (Väkkärä and Tarkki granites, details are given below). Greisen type Sn-Be-W-Zn mineralization is found as veins in the Tarkki granite and as veins, irregular lenses, and patches in the topaz-bearing granite (Väkkärä) (Haapala, 1997).

The South Mountain Batholith (SMB), which is part of the Appalachian Orogen and covers an area of approximately 7300 km^2 is located in southwestern Nova Scotia. The batholith was emplaced in the Meguma Terrane around 370 Ma (MacDonald *et al.*, 1992; Clarke & Halliday, 1980; Fairbairn *et al.*, 1964; Reynolds *et al.*, 1981; Reynolds *et al.*, 1987). The emplacement of the SMB occurred during the Acadian Orogeny, when the collision between

Gondwana and North America took place (Horne *et al.*, 1992; Benn *et al.*, 1997; Benn *et al.*, 1999).

The batholith was divided in 6 main rock types (biotite granodiorite, biotite monzogranite, muscovite-biotite monzogranite, coarse-grained leucomonzogranite, fine-grained leucomonzogranite and leucogranite) and 13 plutons (MacDonald *et al.,* 1992). The SMB is host to numerous polymetallic mineral deposits (Sn, W, U, Mo) and occurrences resulting from the deposition of late to post magmatic hydrothermal fluids (MacDonald *et al.,* 1992). Generally the mineral deposits are found in the leucogranites of the SMB. The best known one being the East Kemptville Sn-Cu-Zn-Ag deposit, found in the East Kemptville leucogranite (Davis Lake pluton).

In the following chapters, CSDs of these two localities will be presented after a short theory review.

Crystal size distribution (CSD) theory

A recent book by Higgins (2006) reviewed and compiled all work done on quantitative textural measurements in petrology. It offers, among other subjects, a detailed description of CSD theory, how to produce CSDs and how to interpret them. I will, in the current section, review CSD theory as it is described by Higgins (2006) and others.

CSD is one of the most commonly quantified aspects of rock texture. It measures the size distributions of crystals and/or grains in a rock and was introduced to igneous petrology starting with the works of Marsh and Cashman (Marsh, 1988; Cashman and Marsh, 1988). Although the technique stems from chemical engineering it was first pioneered in geology within metamorphic petrology on a study of garnets by Kretz (1966). Modern computer techniques, as demonstrated in this work, show that the technique can be practically applied to petrologic studies involving a significant number of specimens.

A wide range of processes may affect crystal or grain size distribution in igneous rocks, the most fundamental being the kinetics of nucleation and growth. These processes in themselves are complicated by feedbacks and by competition, for instance ripening, wherein the crystal population attempts equilibration so as to minimize the total energy of the population. Moreover, mechanical processes such as flow, sorting and compaction can modify the crystal population.

The fundamental functions that control kinetic processes and growth are nucleation rate expressed as a function of time $J(t)$, and the growth rate which is a function of time and crystal size $G(t,l)$. If these are known, then the evolution of the crystal size distribution with time $n(t,l)$ can be determined. Changes in intensive variables (generally temperature) force the system toward equilibrium thus increasing the total volume of crystals during cooling. Under plutonic conditions near to equilibrium conditions generally prevail such that the texture of the crystals responds to the change and strive to minimize the total energy of the

crystal population, unlike volcanic rocks where far from equilibrium textures may be preserved. Because rates of cooling are short relative to rates of diffusion, equilibrium is never attained and the final texture of igneous rocks generally reflects some combination of kinetic and "equilibrium" effects.

Kinetic processes

Nucleation

Atoms will spontaneously form clusters in magma or an aqueous solution to reduce energy by a process termed homogeneous nucleation. When the cluster exceeds a critical radius, it is energetically stable and a crystal nucleus is formed. Atoms will continue to be added to the nucleus in order to continue the reduction of energy in the system. Nucleation rate is closely related to the amount of undercooling. No nucleation occurs at the liquidus temperature; instead a finite amount of undercooling is required. Following this, the nucleation rate increases exponentially to a peak and diminishes with increased undercooling due to increasing viscosity. Nucleation can also occur on existing host grains or on defect structures within crystals. This process, termed heterogeneous nucleation, can occur at lower undercoolings than that necessary for homogeneous nucleation (McConnell, 1975).

Growth and solution

A crystal will grow if growth results in a reduction of the total energy of the system and similarly, a crystal will dissolve if the system's energy is increased. Growth is done by addition of atoms to the surface of a crystal. Thus all crystal growth and dissolution processes

require a departure from equilibrium, which in the case of temperature driven growth can be measured by the amount of undercooling. Because heat transfer is not the only driving mechanism for crystallization, the qualitative terms near equilibrium growth and far from equilibrium growth are used (Fowler & Roach, 1996). Near equilibrium silicate mineral growth is characterized by the formation of well faceted crystals and the growth rate is slow and largely controlled by interface attachment kinetics at defects on the crystal face (Fowler & Roach, 1996). Under far from equilibrium growth conditions the growth kinetics are dominated by the transfer rate of material to the crystal, not interface attachment kinetics (Fowler & Roach, 1996). Near equilibrium growth is most likely in plutonic conditions, while far from equilibrium growth is more likely in volcanic rocks formed in a rapidly cooled environment.

Primary textures

Crystal populations produced in a rock depend of the variation of the nucleation rate with time $J(t)$, the growth rate with time and crystal size $G(t,l)$. Since these are generally unknown, models and assumptions have to be made. One of the most common assumptions is that growth rate is independent of size (Higgins, 2006).

Steady-state crystallization models

An important type of steady-state reaction used in the chemical industry involves a constant input of reactant and output of products from a vessel termed a reactor. Depending on the reaction, crystallization may occur in the reactor, hence the output material will contain more

crystals than the input material. Randolph and Larson (1971) produced the first study of CSDs for such a system; which was then adapted for magmatic systems by Marsh (1988). One assumes that in the magmatic system, there is continuous feeding and extraction of magma from the chamber, which represents the reactor. In a steady-state model there is a linear relationship between the natural logarithm of the population density of crystals $n'_V(L)$ at size L and that size given by:

$$n'_V(L) = n'_V(0)e^{-L/G\tau} \qquad (1.1)$$

where $n'_V(L)$ is the population density of crystals for size L, $n'_V(0)$ is the final nucleation density, G is the growth rate and τ is the residence time in the reactor (Higgins, 2006). The characteristic length of a crystal C is defined by:

$$C=G\tau \qquad (1.2)$$

and can be estimated from plots (Figure 1.1). It is equal to the mean length of all the crystals in a straight CSD that extends from zero to infinite size. The plot of ln(population density) versus size (L) (Figure 1.1) is a straight line providing the steady state conditions were respected. The intercept is $\ln(n'_V(0))$ and the slope is -1/C. For steady-state systems the characteristic length equals the residence time multiply by the growth rate (Marsh, 1988). This crystallization model and CSDs can be used to predict crystal populations. For instance, if the residence time is constant but the nucleation density increases with undercooling, an array of parallel CSDs will be produced (Figure 1.2). Alternatively if the residence time is increased (Figure 1.2), size and C of the CSDs will increase.

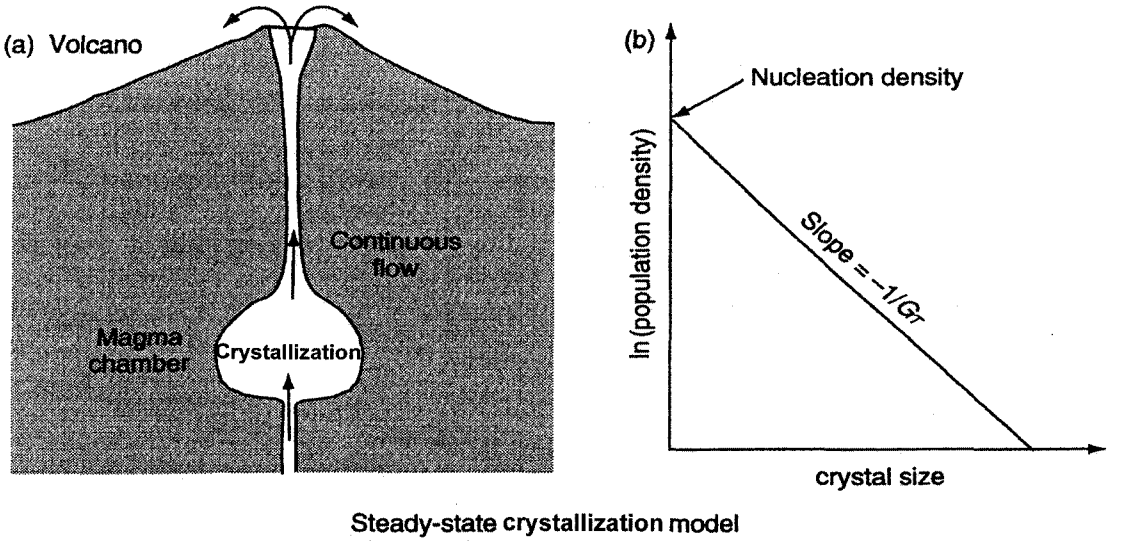

Figure 1.1: (a) A continuously erupting volcano is like a steady-state reactor (Marsh, 1988) (b) CSD of a phase in a magma chamber is a straight line. (Figure 3.5 from Higgins, 2006)

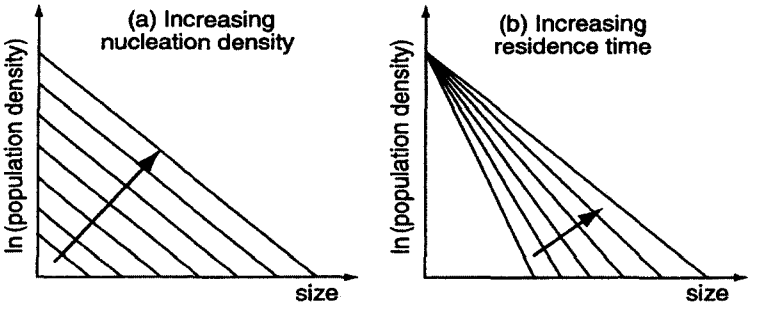

Figure 1.2: Theoritical dispersion of CSDs in a continuously fed crystallization system with (a) variable nucleation density and (b) residence time (Figure 3.6 from Higgins, 2006).

Batch crystallization: Marsh (1998) model

Marsh (1998) discovered that similar relationships exist under certain circumstances for closed-systems in addition to steady-state systems (Figure 1.3). In a closed system the

logarithmic-linear correlation is produced by an exponentially increasing nucleation density with time, as expected if the undercooling of the magma was increasing linearly. A characteristic length can be derived from the slope of the CSD but it does not have the clear physical meaning that the open system has.

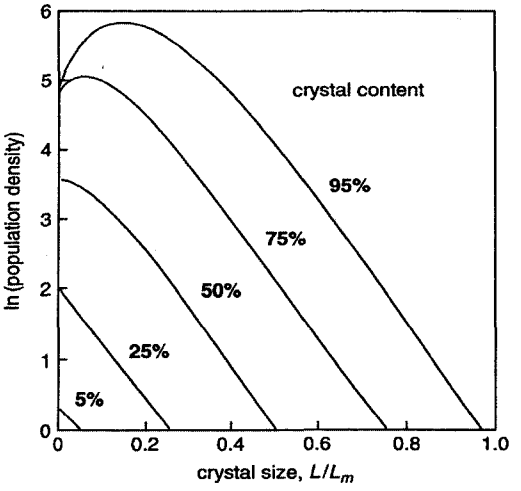

Figure 1.3: Development of closed-system CSDs with increasing crystal content. (Figure 3.7 from Higgins (2006) after Marsh (1998))

Mechanically modified textures

Mechanical processes can modify crystals population by the addition or subtraction of crystals and magma, by flow, separation or by changing the total mass of the system. Of course these mechanical processes are accompanied by chemical processes, however, the former are chiefly considered.

Compaction and filter pressing

Compaction or filter pressing of crystals or grains will cause pore fluid to be squeezed out and subsequently will change CSDs by elevating it at constant slope and increasing the intercept (Figure 1.4). It is possible that some of the finest grains may be removed with the fluid producing a lower population density for small CSD sizes. The same result will be produced by pressure-solution compaction (Meurer & Boudreau, 1998), where some grains will dissolve because they have higher surface energy. CSDs produced by this mechanism are similar to those produce by coarsening (Higgins, 1998), but the processes are not identical as crystals of all sizes can be dissolved by pressure solution.

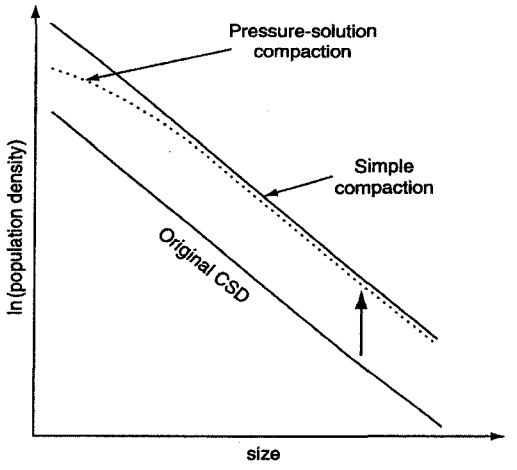

Figure 1.4: Simple compaction changes all the population density values evenly (Figure 3.8 from Higgins, 2006)

Crystal accumulation

Many different mechanisms can result in accumulation, meaning the process of separating crystals from magma. Some of theses mechanisms are: flowage differentiation, gravity separation and crystallization on conduit walls. It was suggested by Marsh (1998) that

accumulation of crystals by gravity would produce a curved CSD on a classical CSD diagram. Higgins (2002b) applied a model of crystal accumulation to plagioclase and olivine in a basaltic magma, showing that the resulting CSDs are equivalent to those produced by simple compaction (Figure 1.5).

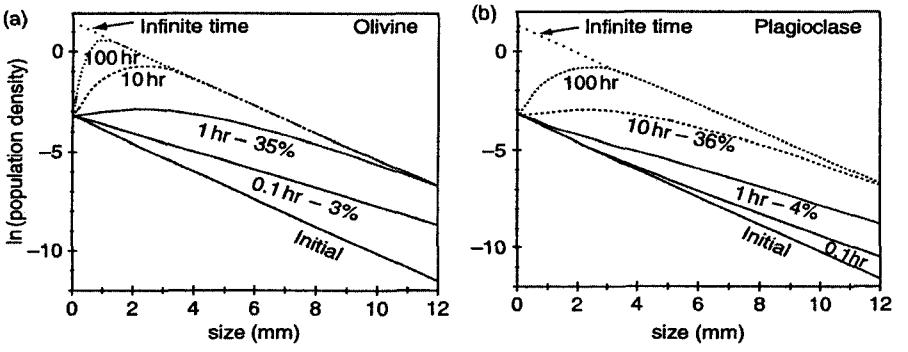

Figure 1.5: CSDs, from an initial straight CSD, evolution of accumulating plagioclase and olivine in a basaltic magma column (part of Figure 3.11 from Higgins, 2006).

Mixing of magmas and crystal populations

Mixing of magmas occurs frequently in many volcanic and plutonic rocks and this process can be seen on a CSD diagram. Higgins (1996) showed that addition of two straight CSDs, representing two different magmas, with contrasting slopes and intercepts yields a CSD with a steep slope at small sizes and a gentler slope at larger sizes. Summation of the two linear CSDs gives a curved CSD (Figure 1.6). Since the mixing of the two populations of crystals will not change the slope of their CSDs, Marsh's (1998) model predicted that the residence time can be determined for each population, but no meaning can be attached to the value of the intercept because it is lowered due to mixing.

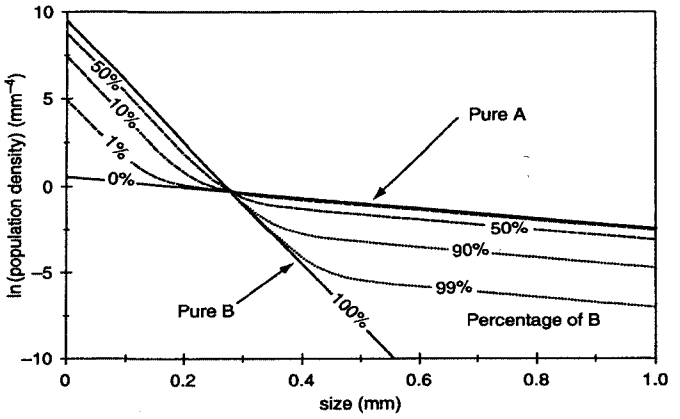

Figure 1.6: Addition of two linear CSDs (Figure 3.12 from Higgins, (2006) after Higgins, (1996)). The original slopes of the two components (A and B) are preserved for large and small crystals, but not their intercepts.

Textural effects of equilibration

In general crystal populations produced by nucleation, growth and/or modified by mechanical processes are not at equilibrium because they contain crystals with a wide range of sizes. Smaller crystals are less stable by virtue of the fact they have a higher surface area per unit volume. So a population will tend to produce large and equant crystals in order to minimize energy in the system. The size population, as represented by CSDs, will be affected by the solution of small crystals and the growth of larger ones.

The process of textural equilibration is commonly observed and appears to be an important process in the development of igneous rocks. It is referred to by many names for instance: coarsening (Higgins, 1998), Ostwald ripening (Voorhees, 1992), crystal aging (Boudreau, 1995) or annealing and fines destruction (Marsh, 1988). Consistent with Hunter (1992),

Higgins (1998, 1999, 2002b) and Higgins & Roberge (2003) the term coarsening will be used here.

In igneous systems, coarsening can only occur when the nucleation rate is small but the growth rate is large. This happens close to the liquidus of a mineral where material is transferred from grains smaller than a critical radius to the larger grains by diffusion (Figure 1.7). Coarsening will normally causes the smaller crystals to dissolve and the larger ones to grow.

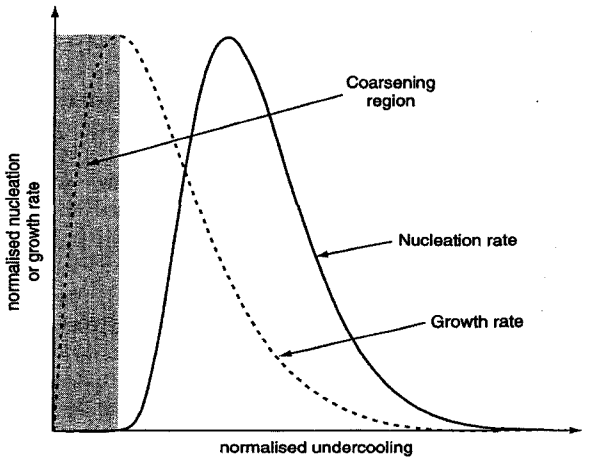

Figure 1.7: Coarsening occurs at low undercooling close to the liquidus (Figure 3.15 from Higgins, 2006).

Lifshitz-Slyozov-Wagner coarsening model

The Lifshitz-Slyozov-Wagner (LSW) coarsening model assumes that there is no interaction between crystals, but they "communicate" directly and instantaneously with a uniform liquid (Lifshitz & Slyozov, 1961). In this model, crystals below a critical radius are strongly resorbed and their material transferred to crystals slightly larger that the critical radius, while

the growth rate of even larger crystals tends to zero. On an initially straight CSD, LSW coarsening produces a progressive loss of very small crystals while the number of large crystals does not change (Figure 1.8 (a)). However, even if this theory gives good results for temporal development of textures, it doesn't yield CSDs corresponding to those of natural materials.

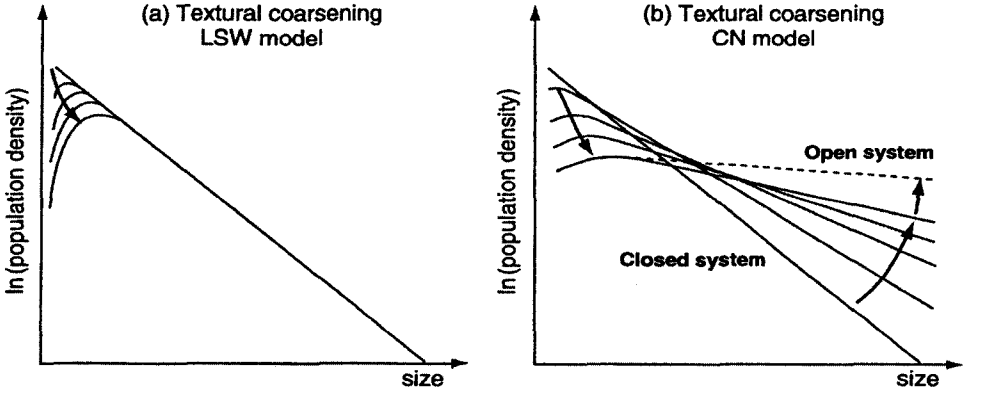

Figure 1.8: Modeling of the development of CSDs during LSW and CN coarsening (Figure 3.18 from Higgins, 2006 after Higgins, 1998)

Communicating neighbors coarsening model

A theory was proposed by DeHoff (1991) called communicating neighbors (CN) and was applied to plutonic rocks by Higgins (1998) because LSW theory could not model the observed CSDs. This theory is based on the fact that each crystal has its own growth rate, the position of each crystal is important during growth and hence the crystals "communicate" with each other by diffusion. CN theory is dependant on the distances to the neighboring crystals. According to the CN model, crystals below a critical radius are resorbed while the crystals larger than the critical radius will have their growth rate increased depending on undercooling. It supposes that a crystal only interacts with its neighbors, if a large crystal is

surrounded by small crystals then during textural coarsening the small crystals will dissolve, increasing the local concentration of the mineral component and allowing the large grain to grow (Higgins, 1998; Higgins & Roberge, 2003). If other large grains surround another large grain, there will be no dissolution and no grain growth. This process is not symmetrical around each crystal and can explain local variations observed. On a CSD diagram, a straight starting population will rotate (intercept lowers) because smaller crystals will be resorbed while larger ones will grow even more (Figure 1.8 (b)).

The simplest models of coarsening assume that the system is closed because all material produced by dissolving small crystals is precipitated on the larger crystals. However, the transfer of material is via a liquid phase and this can migrate into or out of a system implying that textural coarsening can be an open-system process (Higgins, 2006).

Closure in grain size distributions

The crystal or grain content of a rock cannot exceed 100% of crystal or grain concentration, even if closure for an individual phase occurs at less than 100%. For example, if a rock is made of 50% potassic feldspar and 50% quartz then closed-system processes cannot change the proportion of each phase, which is fixed at 50%. Closure must be considered in all CSDs studies, both of volcanic and plutonic rocks (Higgins, 2002a), because it is a way of insuring the accuracy of the transformation of 2D data to 3D and verifying that the CSD calculation reflects the actual proportion of crystals in the rock as estimated by petrological means.

For a population of crystals with constant shape, the volumetric proportion of phase *i*, V_i, can be calculated by integration of the volume of all the crystals (Higgins, 2006) following Higgins (2002a):

$$Vi = \sigma \int n'_{Vi}(L)\, L^3 dL \qquad (1.3)$$

Where σ is the shape factor of phase *i*, $n'_{Vi}(L)$ is the population density of crystals of phase *i* for size L. The shape factor is equal to the ratio of the actual volume of the grain divides by the volume of a cube that encloses the grain L^3. It can be expanded into a more applicable form as follows (Higgins, 2002a, 2006):

$$\sigma = (1-\Omega(1-\Pi/6))IS/L^2 \qquad (1.4)$$

where Ω is the roundness factor, which varies from 0 for rectangular parallelepipeds to 1 for a triaxal ellipsoid. S, I and L are the short, intermediate and long dimensions of the parallelepiped or ellipsoid respectively. The above equation should not be applied to crystals with concave surfaces or holes (Higgins, 2006).

For straight CSDs with intercept $n'_{Vi}(0)$ and characteristic length C (C= -1/slope) a simplified equation can be used (Higgins, 2002a):

$$V_i = 6\sigma n'_{Vi}(0) C^4_i \qquad (1.5)$$

A family of straight CSDs for 100% crystallized material defines a fan (Higgins, 2002a; Zieg & Marsh, 2002). Portions of this fan appear to describe rotation of the CSD around a point. The CSDs together outline a concave up envelope named closure limits where straight CSDs can only exist below this line (Figure 1.9 (c)).

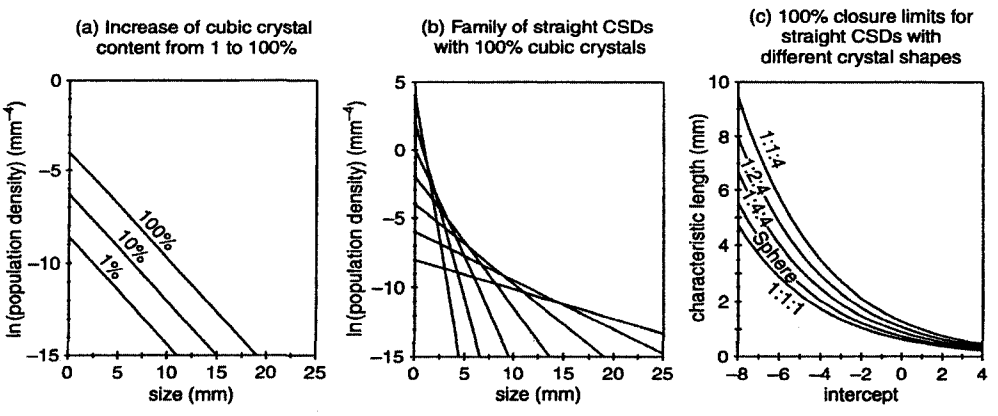

Figure 1.9: The closure problem in CSDs (Figure 3.24 from Higgins, 2006 after Higgins, 2002a). (a) A straight CSD has a volumetric phase proportion of 1% and if, for example, the intercept is increased by crystal growth and nucleation rate, then the crystal content will reach 100% and textural changes will stop. (b) A fan of straight-line CSDs with 100% crystals is tangential to a concave-up curve. (c) Straight CSDs can be represented by a point on a graph of characteristic length (-1/slope) against intercept. Slope and intercept values for material with 100% crystals proscribes a curve. CSDs can exist below, but not above this line. The position of the line differs for different shapes (Higgins, 2006).

Chapter 2

Methodology

Introduction

This chapter documents all the steps taken to acquire and process data necessary to do the research intended in this thesis. It covers the fieldwork, sample preparation, CSD calculations and electron microprobe measurements. All these technical steps allow for the interpretation of textures as documented in chapters 3 and 4.

Field work

Field work was necessary to obtain samples and to understand the geological context of the rocks used in the study of crystal size distribution (CSD) for the Eurajoki stock in Finland and the South Mountain Batholith (SMB) in Nova Scotia, Canada (see Figures 3.1 and 4.1 in next chapters). The time spent in the field was used to collect numerous samples and to investigate the relationships between the different lithological units.

Two weeks were spent in September 2000 investigating the Eurajoki stock. Thirteen samples were collected from the two granitic phases named Tarkki (5 samples) and Väkkärä (8 samples) granites. These granites and in particular their geochemistry have been extensively

studied by Haapala (1977, 1997). Approximately 50 kilos of samples were brought back to Ottawa for CSD analyses.

During summer of 2002, two weeks were spent in Nova Scotia investigating the different lithologies of the SMB. Twenty-seven samples (approximately 3 kilos each) were collected, reflecting all the major lithologies and mineral assemblages of the SMB. The samples were transported to Ottawa and classified as follows: 8 samples of biotite monzogranite, 3 of muscovite leucogranite, 2 of muscovite-biotite monzogranite, 4 of fine-grained leucomonzogranite, 5 of coarse-grained leucomonzogranite and 5 of biotite granodiorite. The names and classification of the units are based upon Macdonald *et al.* (1992) and Macdonald *et al.* (1994).

Sample Preparation

The samples were cut into ~3cm thick slabs so as to maximize surface area using a 30 cm and a 100 cm diameter diamond saw. When the thickness of the sample permitted, more than one slab was cut and used in the study (see Table 2.1).

Table 2.1: List of all the slabs and thin sections used in this study

Sample number	Rock Type	Number of slabs	Small thin section	Stained small thin section	Stained large thin section
Eurajoki					
00-GM-009	Väkkärä Granite	1	1	1	
00-GM-010	Väkkärä Granite	1	1		
00-GM-011	Tarkki Granite	2	1	1	
00-GM-012	Väkkärä Granite	2	1	1	
00-GM-013	Tarkki Granite	1	1	1	
00-GM-014	Tarkki Granite	1	1		
00-GM-015	Tarkki Granite	1	1		
00-GM-016	Tarkki Granite	2	1		
00-GM-017	Väkkärä Granite	2	1		
00-GM-018	Väkkärä Granite	3	1		
00-GM-019	Väkkärä Granite	1	1	1	
00-GM-020	Väkkärä Granite	1	1		
00-GM-021	Väkkärä Granite	1	1	1	
South Mountain Batholith					
02-GM-001	Biotite Monzogranite	2			1
02-GM-002	Coarse-grained Leucomonzogranite	1			1
02-GM-003	Fine-grained Leucomonzogranite	3			1
02-GM-004	Biotite Monzogranite	2			1
02-GM-005	Muscovite Leucomonzogranite	2			1
02-GM-006	Coarse-grained Leucomonzogranite	2			1
02-GM-007	Coarse-grained Leucomonzogranite	5			2
02-GM-008	Muscovite Leucomonzogranite	3			1
02-GM-009	Biotite Granodiorite	1			1
02-GM-010	Biotite Monzogranite	2			1
02-GM-012	Fine-grained Leucomonzogranite	2			1
02-GM-013	Biotite Monzogranite	2			1
02-GM-014	Biotite Monzogranite	2			1
02-GM-015	Fine-grained Leucomonzogranite	1			1
02-GM-016	Biotite Granodiorite	1			1
02-GM-017	Muscovite-Biotite Monzogranite	3			1
02-GM-018	Biotite Monzogranite	2			1
02-GM-019	Biotite Granodiorite	2			1
02-GM-020	Biotite Granodiorite	2			1
02-GM-021	Muscovite Leucomonzogranite	2			1
02-GM-022	Biotite Monzogranite	2			1
02-GM-023	Biotite Monzogranite	2			1
02-GM-024	Fine-grained Leucomonzogranite	2			1
02-GM-025	Coarse-grained Leucomonzogranite	2			1
02-GM-026	Coarse-grained Leucomonzogranite	3			1
02-GM-027	Muscovite-Biotite Monzogranite	2			1
02-GM-028	Biotite Granodiorite	1			1

Specimens were prepared for crystal size analysis using the following procedures. The slabs surfaces were sequentially polished, on a turntable using various sizes of grinding powder to remove all saw marks. Slabs were then placed in a 50% hydrofluoric (HF) solution for about one minute and rinsed with distilled water, before being placed in the sodium cobaltinitrite solution for about one minute (see Hutchison (1974) for details). After another rinse in distilled water, one could see that potassic feldspar crystals had taken a bright yellow color, whereas plagioclase crystals were white, and quartz crystals were gray (Figure 2.1). All slabs were then scanned on a flatbed scanner at a high resolution (450 dpi) and saved as TIFF files, for further manipulation.

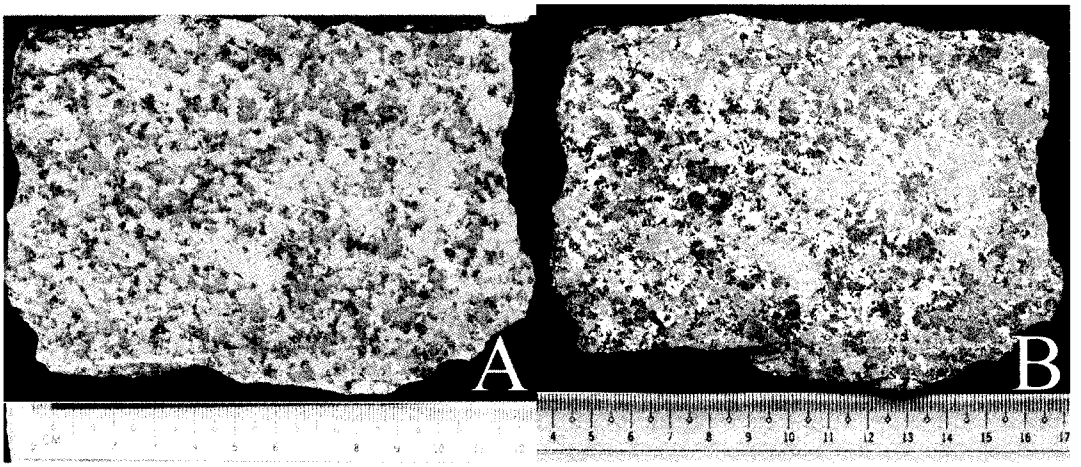

Figure 2.1: A) Example of a rock slab before staining. B) Same rock slab after staining with sodium cobaltinitrite. Sample 00-GM-017, Väkkärä Granite, Eurajoki.

For every sample of the two localities, 30 μm thick thin sections were made in the Earth Sciences department of the University of Ottawa. Two types of sections were produced: small polished sections (approximate size 4.5 cm per 2.5 cm) and large sections with no cover slip (approximate size 7.4 cm per 4 cm). For details on the number of sections produced, please refer to Table 2.1. All SMB sections were stained with cobaltinitrite, while

only 6 Eurajoki sections were stained because all the other sections had a cover slip. The staining of thin sections followed the principles laid down by Boone & Wheeler (1968), but with some minor adjustments. Sections were placed 2 cm above an HF solution and left to react with the HF fumes for a minute. After that, they were placed in a sodium cobaltinitrite solution for another minute. The sections were then rinsed with distilled water (Figure 2.2).

Following the staining, images of the sections were taken with a digital camera (Nikon Coolpix) at the University of Ottawa. For each Eurajoki section, 12 to 16 pictures were taken using a polarizing microscope so as to cover the whole area. For the relatively coarser SMB sections only 3 pictures were necessary as they were photographed directly with the camera. Two sets of pictures were taken for each section, one in plane-polarized illumination and one in cross-polarized illumination. The photographs were then assembled into mosaics of their respective whole thin sections using the software Adobe Photoshop©. These mosaics were used in the calculation of the CSDs.

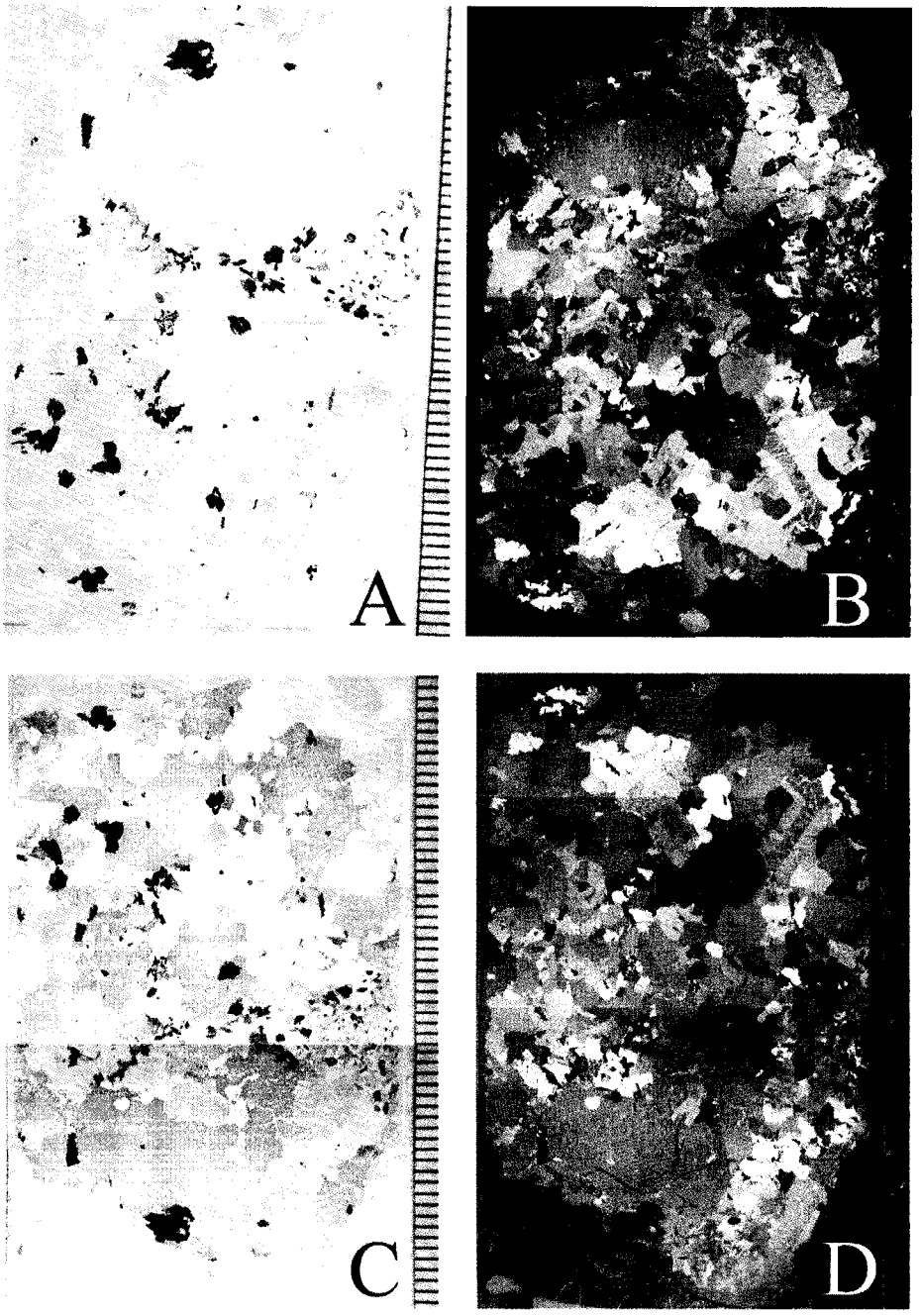

Figure 2.2: Example of pictures taken from thin section photomicrographs, sample 02-GM-003, South Mountain Batholith. Each bar of the ruler on the right side of each photo represents a millimeter. A) Thin section under plane-polarized illumination. B) Thin section under cross-polarized illumination. C) Stained thin section under plane-polarized illumination. D) Stained thin section under cross-polarized illumination.

How to calculate CSDs

As stated by Higgins (2002b), the CSD determination of crystals is a volumetric measure, but crystal sizes and numbers are typically measured on two-dimensional slices of rock. Therefore, the two-dimensional intersection data must be converted to three-dimensional CSDs, using a branch of mathematics called stereology. Several reviews and books on this subject have been made, mostly aimed at the biological sciences (Howard & Reed, 1998; Royet, 1991; Underwood, 1970) and some aimed toward geology (Cashman & Marsh, 1988; Peterson, 1996; Sahagian & Proussevitch, 1998).

For the calculation of CSD, the software *CSD corrections 1.3* was used (Higgins, 2000). This software estimates the third dimension of a crystal, as measured in two dimensions on a slab or thin section based on a modification of the method of Saltykov (1967). Because this method can only be used in its simplest form for isotropic fabrics (Higgins, 2000), Higgins developed a model based on a parallelepiped with an aspect ratio the same as that of the measured crystals. The model takes also into accounts for rounding of the crystals and the fabric of the rock.

CSD results are actually histograms but are usually represented as plots of $\ln(n_V(L))$ in mm^{-4} versus length (L) in mm (Higgins, 2000). The first value is the natural logarithm of the population density "nL" as represented by the number of crystals of a specific size in a specific "bin", while the second axis of the plot is the "bin size" i.e. the mean length "L"of the crystals in that interval. The software *CSD corrections 1.3* also provides the errors of

each point of the plot as calculated from the square root of the number of crystals in that size interval (Higgins, 2000).

In order to overcome stereological problems some parameters have to be considered before calculations can be made: length of major or minor axis in mm as measured on samples, total area in mm^2 where measurements were taken (area of slab, thin section, etc.), the shape of the crystals, roundness of crystals and the degree of foliation of the sample.

Lengths of major and minor axes of crystals are precisely measured using different techniques and on different materials (outcrop, rock slabs, thin sections). The methods used in this matter will be discussed later in the chapter. These measurements are the underpinning of the whole procedure and they are also used to estimate the shape of the crystals. Here, the method described in Higgins (1994) is employed. Essentially, he demonstrated that the mean aspect ratio of the crystals, short-intermediate-large (S:I:L) (three dimensions), can be estimated from the statistical distribution of intersection width/length ratios (W/L). W and L are measured in two dimensions and represent the small and longer lengths of a crystal. Hence the mode of (W/L) is equal to S/I and I/L is equal to the skewness of (W/L) plus 0.5. This shape is assumed to be the shape of every crystal in the sample. The roundness of crystals and the foliation of the rock are visually estimated and are also entered into the program *CSD corrections 1.3*. For igneous rocks, it is considered that the more a crystal is euhedral, the less round it is. The degree of foliation is also estimated from massive to

foliated. Accordingly, the degree of roundness and foliation are entered into the software as numbers varying between 0 and 1 based upon visual estimates.

Measurement of crystals intersections

Calculation of the CSD requires precise measurements of the sizes of crystals. Three media were used in this study: measurement directly on outcrop, measurement on slabs of rocks and measurement on thin sections. The measurements made on slabs and on thin sections can be done manually or automatically using a computer program. Manual measurements require the tracing of every crystal perimeter using a digitalizing tablet or a drawing computer program from photos of the thin section or the slab, whereas automated measurements use functions built into a computer programs to recognized the different colors of the crystals after staining. In order to avoid tedious and error-prone manual digitizing automated techniques were developed.

Measurement on outcrops

If crystals boundaries can be seen on outcrops, it is possible to measure crystals sizes directly in the field with a scale. This method was only used once in our study, because most of the outcrops we visited, the crystal sizes were too small or the outcrops were insufficiently large making the observation of megacrysts, if they existed, improbable. This method was used in Finland, at outcrop 00-GM-011, located in a quarry exposing megacrystic granite. These

crystals were usually elongated, showing a rectangular form. The long and short axes of the crystals (or of the rectangular shape) were measured and used to calculate CSDs.

Only 31 crystals were measured in 11 m^2 area in the field, but the accuracy was great and errors were minimal (see Chapter 3), making this method one of the most reliable and accurate. Unfortunately, this method could not be used again because the ideal exposure and grain size conditions were only found once, in a quarry.

Measurements on rock slabs

After the slabs were prepared, as described earlier, they were placed on a flatbed scanner and scanned at a resolution of 450 dpi. The resulting images were then automatically digitized using the commercial software Adobe Photoshop©. Since the minerals composing the rocks have different colors due to the staining, it was easy to separate them into different files because the software can extract all pixels having the same color, for instance yellow for potassic feldspar. A second file containing only those pixels was constructed. We ended up with 3 files: one containing the potassic feldspar distribution data, one of plagioclase and the last one containing all other minerals. The 2 files containing the feldspars were then "cleaned" by erasing all pixels that did not represent crystals. This is called cleaning the noise and can be done using the functions in Adobe Photoshop©. In some cases it was necessary to repeat this process 2 or 3 times.

Nonetheless, after cleaning, some of the images of discrete but close-neighbouring crystals showed them to be attached to one and other. Consequently it was necessary to manually separate them by comparing the file with the slab in order to determine the crystal boundaries. Usually, this was done rapidly because most of the images of close-neighbour crystals were attached together only by small lines, easily recognized and erased. Before any further manipulations, the files were converted to binary color image (black and white) using Adobe Photoshop© (Figure 2.3 B).

The sizes of the crystals extracted previously (as data files and images) were simply measured by a computer program rather than a ruler. NIH (United States National Institute of Health) Image was selected because it is a widely available public domain image processing and analysis program for Macintosh computers. The software is available at http://rsb.info.nih.gov/nih-image/. It draws a virtual ellipse over each crystal-image that has the same moment of inertia as the crystal, and then measures the long and short axis of this ellipse. Thus for every crystal, two measurements are produced, the short and long axes. To ensure accurate results in NIH Image, a scale has to be entered into the software. The scale is set by accurately measuring, with a ruler, one large crystal of the slab. It was noticed that during the process, small crystals were commonly either enlarged or reduced by the computer manipulations. The effect introduces significant error for small crystals (5mm) whereas for larger crystals the effect is negligible due to size.

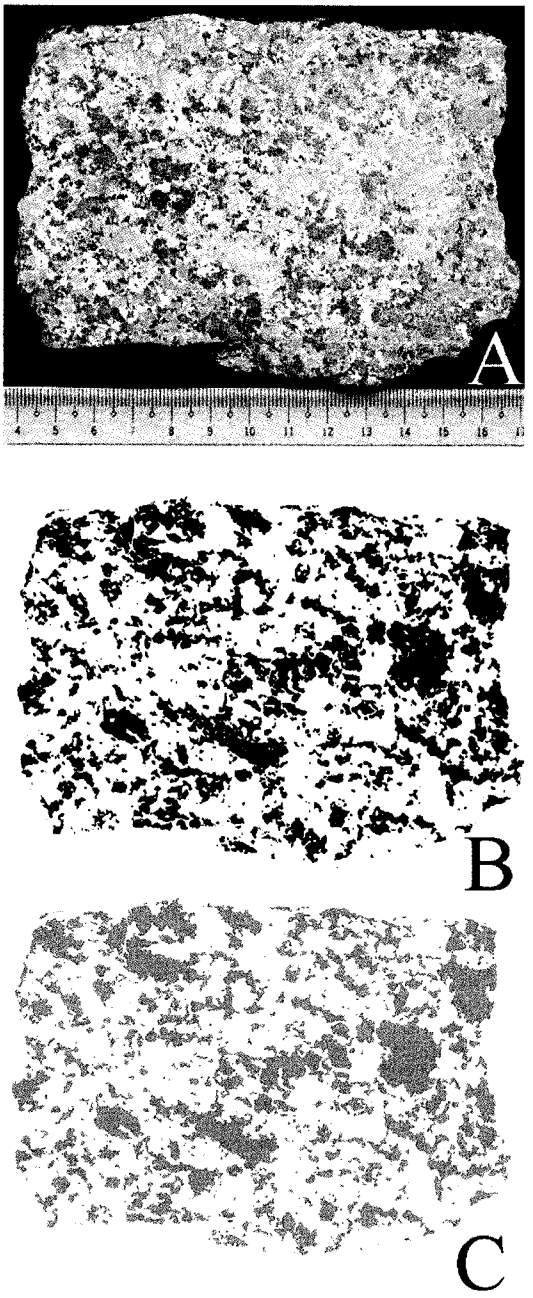

Figure 2.3: A) Stained slab of sample 00-GM-017. B) Same slab after manipulations done in Adobe Photoshop© to extract the potassic feldspars now seen in black. C) Slab after manipulations in NIH Image, where crystals sizes have been measured. Notice that NIH Image does not take into account holes in crystals and fill them. Field of view of each image is the same, 13.5 cm.

Accordingly, to be certain that noise was not been introduced and interpreted as small crystals, the crystals smaller than 5 mm were not measured (Figure 2.3 C). Measurements done in NIH Image are subsequently used to calculate the shape of the crystals and the CSD.

Reproducibility and errors

The method of gathering data for rock slabs described earlier yielded reproducible results. The CSD of the slab 00-GM-017 was done 3 times, using the same methods and manipulations, to compare the results. Table 2.2 documents the number of crystals measured for different sizes intervals, for each of the three analyses.

Table 2.2: Intersection widths distribution of potassic feldspars crystals in sample 00-GM-017

Sample number	00-GM-017 dup	00-GM-017 dup 2	00-GM-017 dup 3
Upper size limit (mm)	# of crystals	# of crystals	# of crystals
10	7	9	5
6.31	21	15	19
3.98	74	59	52
2.51	99	96	73
1.59	80	110	92
1	58	96	108
0.631	21	149	126
0.398	10	108	55
0.251	2	11	2

Results (Table 2.2 and Figure 2.4) are similar for the three analyses, except for the results from crystals of size 1 mm and under. As shown in Figure 2.4, the 3 CSD curves for sample 00-GM-017 are similar for the points greater than 5 mm. The values of the points and the slope and the general trend of the curves are all similar. However, below 5 mm, one of the curves differs from the other two. Similar results were obtained for other samples. As stated previously, the computer noise produced during the manipulations creates artifacts interpreted as small crystal and it is difficult to separate small crystals from large ones of the rock slabs because crystal boundaries are not always clear. Accordingly, we used thin sections to measure the sizes of the small crystals and joined those results to the slabs results (see below).

The advantage of using this automatic method, rather than manually tracing the contour of every crystal, is the saving in time. A slab, of any reasonable size, can be processed in an hour or less and for many different crystal types, compared to manual digitizing crystals wherein a slab analysis can take up to a day's work for one mineral type, and the quality of the determination is very much dependent on the care exercised by the operator.

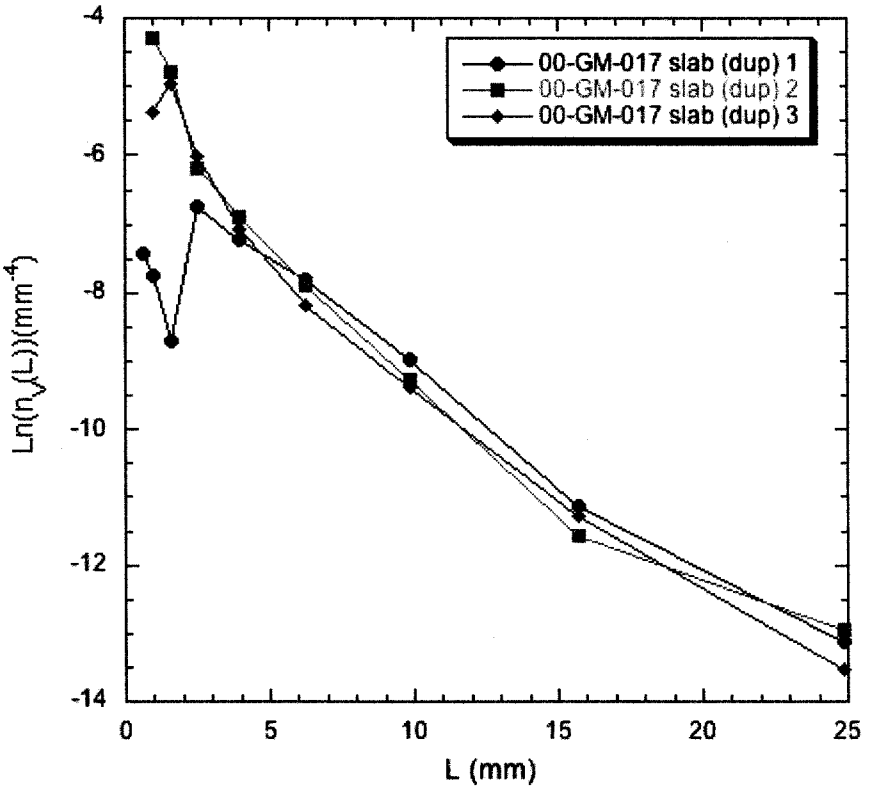

Figure 2.4: CDSs of the 3 analyses of a slab of sample 00-GM-017 from the Väkkärä granite. Note artifacts for crystal sizes smaller than 5 mm.

Measurements on thin sections

For thin sections made from the same samples as the slabs, two different techniques were used: manual digitalization and automated digitalization of every crystal. The automated work was done on some thin sections stained with cobaltinitrite and some that were not. Thin sections of Eurajoki were processed with all the techniques: manual digitalization, automated digitalization and automated digitalization of stained thin sections. Thin sections of SMB rocks were all stained and done by automation in the same way the slabs were treated.

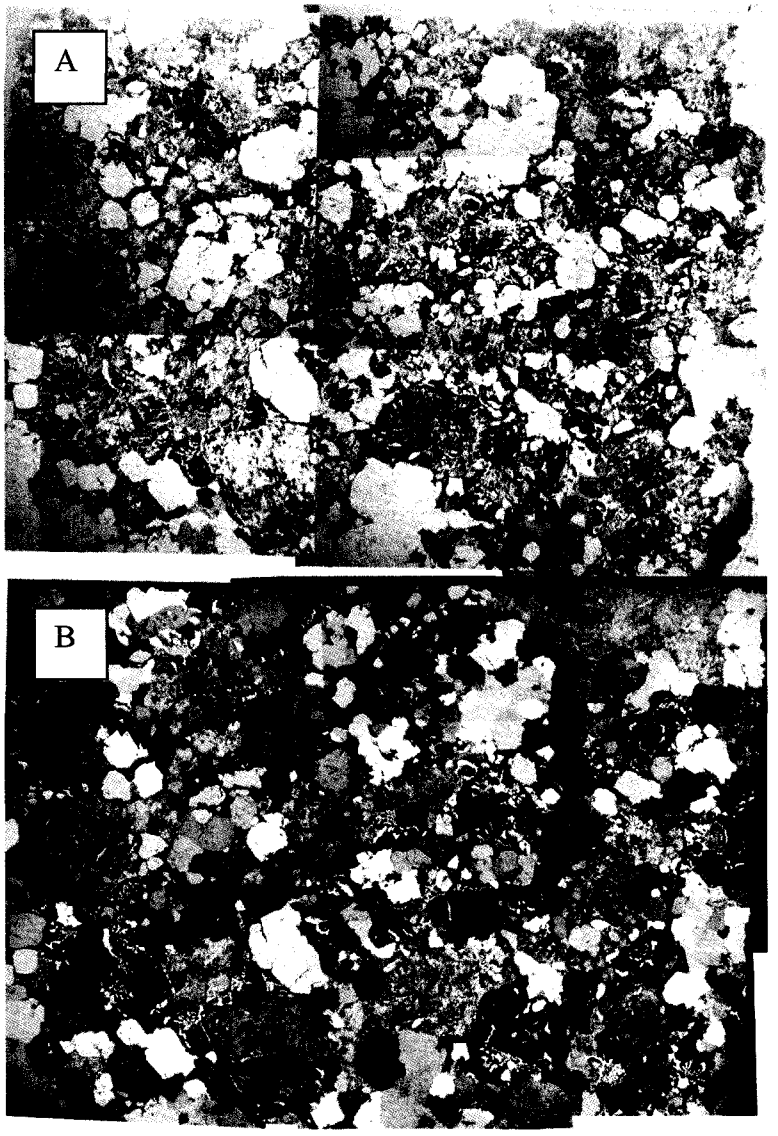

Figure 2.5: Photo mosaic of thin section 00-GM-010 from Eurajoki. Notice how the feldspars are cloudy. (Field of view is 3.5 cm). (A) Normal View. (B) Cross-polar

The mosaics of the pictures taken from the thin sections (Figure 2.5) were then processed to take out only the geometric data of potassic feldspar crystals. The stained thin sections were dealt with in the same manner as the slabs using Adobe Photoshop©. The other thin sections mosaics were treated differently. In some cases, contours of potassic feldspar crystals were

manually traced in Adobe Illustrator© and in other cases, the digitization was automated using the fact that feldspar crystals from Eurajoki are grey and cloudy while plagioclase and quartz crystals are clear in thin sections.

Figure 2.6 shows images produced using the manually and automated methods of digitalizing the thin section 00-GM-010 from Eurajoki. The two methods yield similar measurements as shown in Table 2.3, but more crystals were measured using the manual method. This is due to the fact that the automatic method does not always separate crystals, producing a few larger crystals than the manual technique.

CSD curves of sample 00-GM-010 produced with both methods are very similar (Figure 2.7), the shape and slope of both curves are the same, except for the last point (at 17 mm), which has a higher value for the automatic in comparison to the manual method. This illustrates a factor that must be accounted for when using the automatic method, i.e. the tendency to create larger "crystals" than really exist. Staining the thin sections for feldspars greatly eliminates this problem because potassic feldspars perimeters are contrasted from other minerals; hence this method was mostly used. Experience shows that if in a CSD curve the points representing the larger crystals do not conform with the trend of the smaller ones, careful examination of the results are necessary prior to assigning any geological interpretation. This problem is nicely eliminated (at some scales) by our technique of combining slabs and thin sections, because the small crystals in slabs represent larger crystals in a thin section.

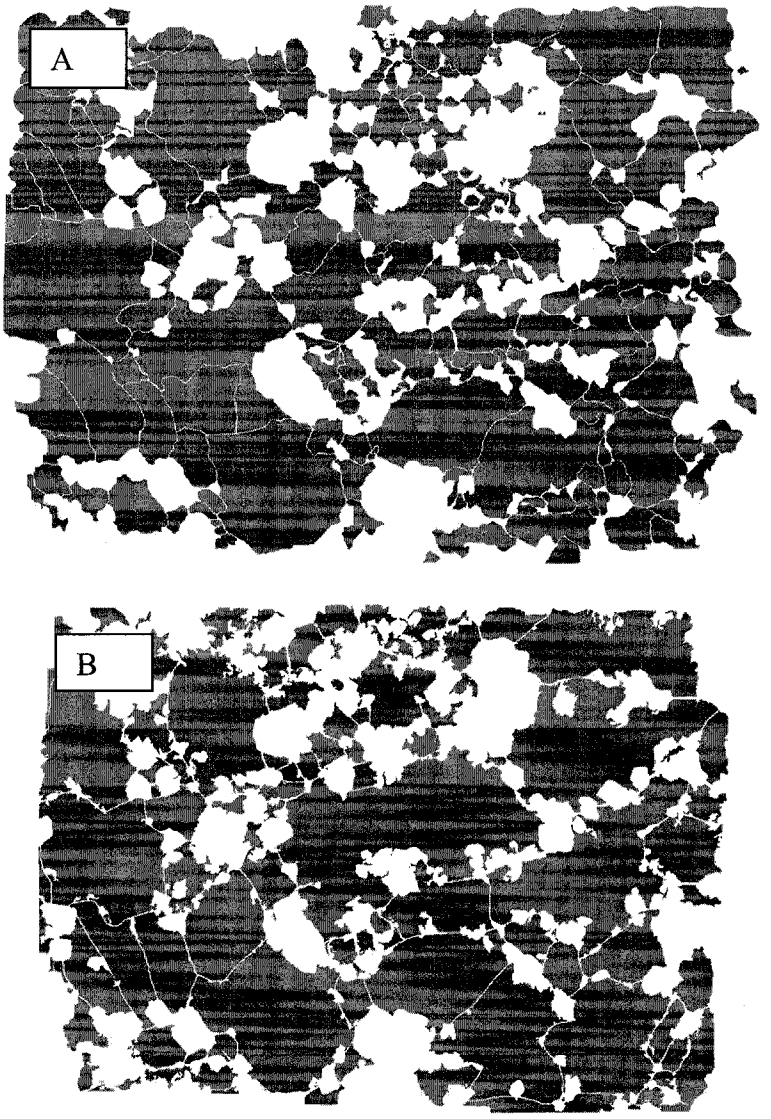

Figure 2.6: Examples of the 2 methods of digitalizing thin sections (field of view is 3.5 cm). (A) Manual digitalization of thin section 00-GM-010. (B) Automated digitalization of the same section. Notice the larger crystals in section B and that there are less crystals.

Table 2.3: Results of the 2 methods of measuring crystals in thin sections.

Sample number	00-GM-010 Manual digitalization	00-GM-010 Automated digitalization
Upper size limit (mm)	# of crystals	# of crystals
6.31	3	11
3.98	11	5
2.51	24	15
1.59	36	20
1	45	22
0.631	30	11
0.398	16	9
0.251	8	5
0.158	4	6
0.1	1	8
0.0631	1	6
Total # of crystals	179	118
Area (mm^2)	884	884

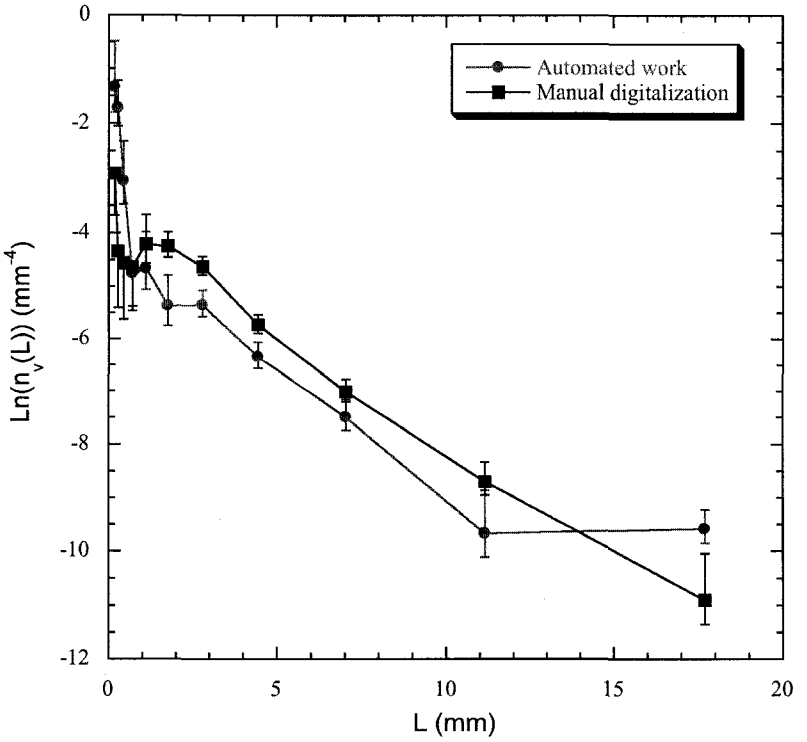

Figure 2.7: CSDs curves of thin section 00-GM-010 (Väkkärä granite) using both methods of digitalization.

Presentation of results

For most of the samples, more than one CSD determination has been calculated using slabs and/or thin sections. For a better understanding and more clarity of the CSDs, it is better if all the results of one sample are combined into one CSD curve. In Figure 2.8, this method is illustrated. To form the curve presented in Figure 2.8 B, the data from the thin section for points smaller than 6 mm, were combined with those between 6 and 15 mm from the slab 00-GM-017 2. The cut off point between slabs and thin sections is always around 5 mm because below that point, data obtained from slabs are not very accurate as shown previously, and above 5 mm results obtained from thin sections lose accuracy because there are only a few

crystals. All samples from Eurajoki and SMB were processed the same way, so as to yield one integrated CSD curve for each specimen. In a simplified way we threshold the data at 5 mm, omit some data for smaller crystals from the slabs and larger crystals from thin sections and then integrated the two sets.

Combination curves are then used to calculate slope and intercept that can be used to compare different rock types and interpret textures. The shape of these combination curves are also used to interpret the geological cooling history of the rocks.

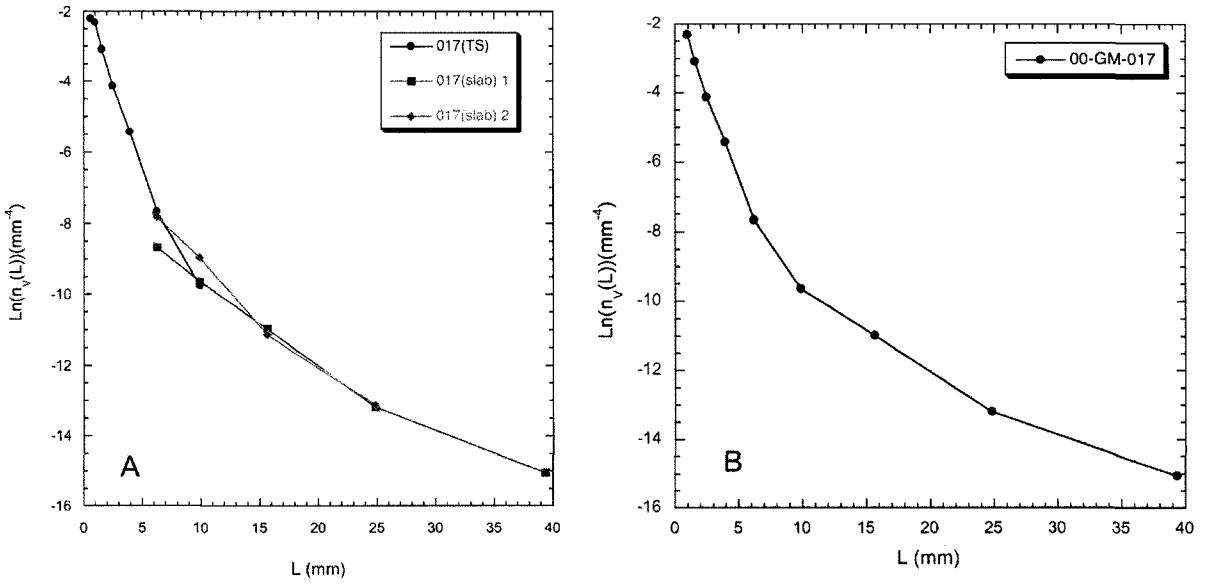

Figure 2.8: (A) All CSDs done on sample 00-GM-017 from the Väkkärä granite of Eurajoki, 1 thin section (TS) and 2 slabs. (B) Combination of theses 3 CSDs curves into one.

Electron microprobe

The electron microprobe used is an automated Camebax MBX, running under Henderson automation and Cameca PAP matrix correction software, equipped with 4 wavelengths dispersive X-ray spectrometers (WDX) for quantitative analyses and an energy dispersive spectrometer Kevex Si (EDX) for rapid qualitative analyses. Digital imaging techniques utilizing backscattered electron Bausch and Lomb 4 quadrant solid state detector and quad summing amplifier (BSE), secondary electron (SE), and cathodo-luminescence (CL) detectors were also used. All this equipment is located in the Earth Sciences department at Carleton University and was used during 3 days in March 2001 under the supervision of Mr. Peter Jones.

The electron microprobe was used to characterize some of the textures found in the Eurajoki granites, mainly the graphic and myrmekitic textures. The results and findings will be discussed in the next chapter.

Conclusion

Automation of data collection using NIH and Adobe Photoshop was discussed. Automated techniques can yield spurious data due to noise for small crystal sizes. A simple method of thresholding and combining data collected at the macroscopic and microscopic scales yields CSD curves over a large scaling range. Further it obviates the data depopulation at large

crystal sizes encountered in thin sections and noise-induced errors encountered for small crystal sizes in rock-slabs.

All the data acquired by using the methods described here will be used in the next chapters to interpret textures found in granite from Finland and Nova Scotia, Canada.

Chapter 3

Eurajoki stock

Introduction

In this chapter feldspar CSDs will be used to understand how the Eurajoki stock solidified and to identify the most important processes leading to the textural development during solidification. The CSD results complement the mineralogy, structural and geochemical works done herein, and by others, and yields a better understanding of this granitic intrusion.

Local geology and previous work

The Eurajoki stock (57 km^2) is a satellite of the 1570 Ma old Laitila rapakivi granite batholith, which covers approximately 1800 km^2 (Vaasjoki, 1977). They (Figure 3.1) form part of the anorogenic rapakivi granitic suite of Finland (1.65-1.54 Ga), which generally shows a bimodal magmatic association and A-type geochemical and mineralogical characteristics (Haapala, 1997). The emplacement of the rapakivi granites is related to mantle upwelling and extensional tectonics caused by mafic underplanting following the Svecofennian orogeny (Haapala & Rämö, 1992; Korja *et al.*, 1993). Nd isotopes suggest that the rapakivi granites were derived from a single 1.9 Ga intermediate source, probably the Svecofennian crust and were formed by fractionation of alkali feldspars, quartz and clinopyroxene (Haapala & Rämö, 1992).

Haapala (1977) showed that the Eurajoki stock is composed of several petrographically distinct granite types (Figure 3.1). The Tarkki granite is a homogeneous medium grained rock with scarce potassic feldspar megacrysts (3-6 cm) biotite-hornblende (±fayalite) granite, that makes up the marginal section of the Eurajoki stock (Haapala, 1997). A younger phase, the Väkkärä granite makes up the internal part of the stock. Haapala (1977) showed that the Väkkärä granite is an intrusive complex composed of three granite types: A contact type composed of fine grained granite in contact with the Tarkki granite, a homogeneous medium grained biotite granite with sparse alkali feldspar megacrysts, and a texturally heterogeneous topaz-bearing granite. Haapala (1977) did not observe contacts between the different members of the Väkkärä granite due to the lack of outcrops in some areas. However it is assumed that the types are genetically closely related to each other and the following order of formation is proposed by Haapala (1977, 1997): biotite granite contact type – biotite granite even-grained type – porphyritic and coarse grained topaz-bearing type.

The Tarkki granite is cut by fine grained porphyry dykes, some of which are topaz-bearing, as well as by intermediate dark porphyry dykes which represent hybrids between mafic and felsic magmas (Haapala, 1977, 1997). Greisen type Sn-Be-W-Zn mineralization is found as veins in the Tarkki granite and as veins, irregular lenses, and patches in the topaz-bearing granite (Haapala, 1997). The Tarkki granite is also cut by an olivine diabase of 1250 Ma (Happala, 1977).

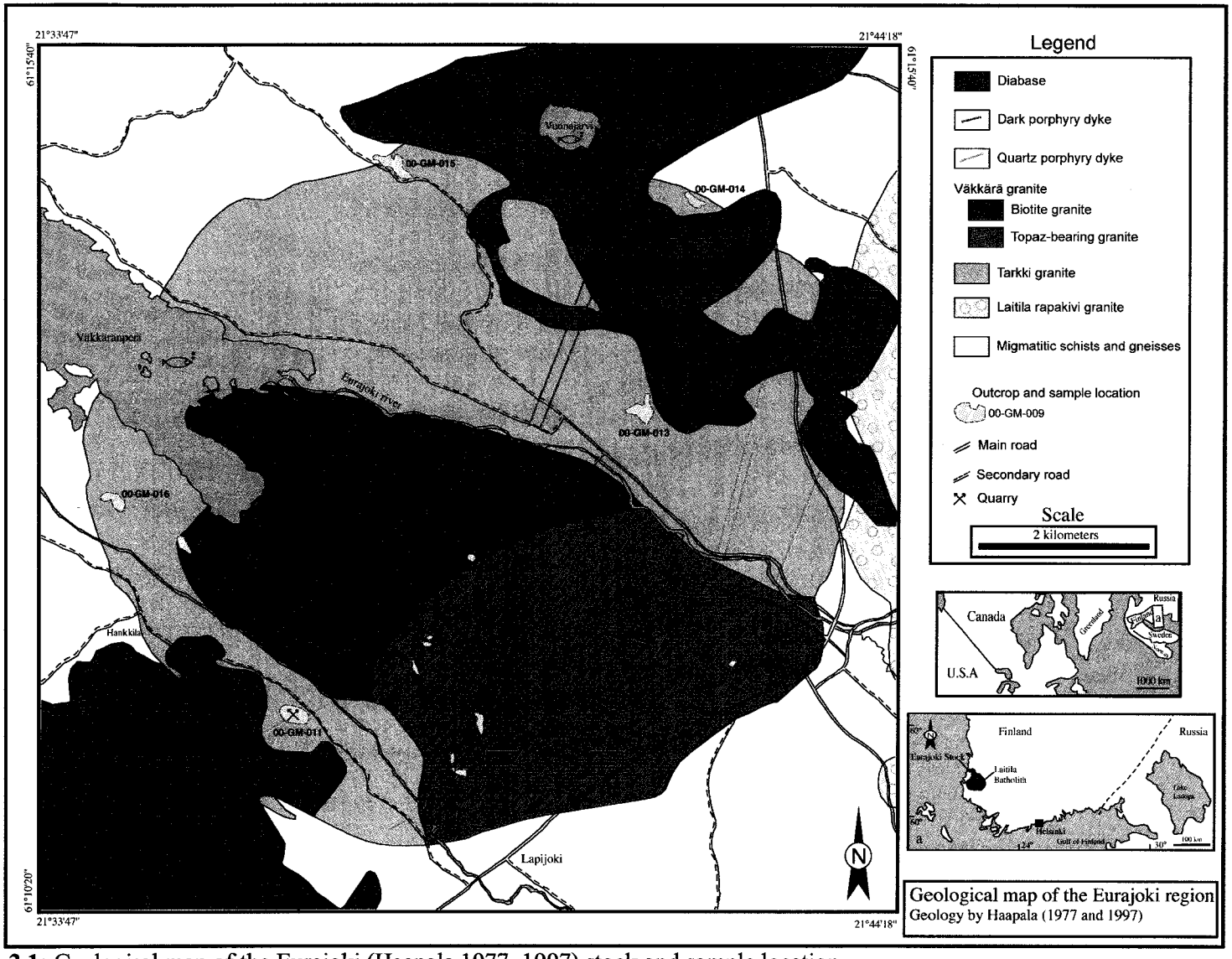

Figure 3.1: Geological map of the Eurajoki (Haapala 1977, 1997) stock and sample location.

Detailed description of the units in large part summarized from the work of Haapala (1977, 1997) and Haapala & Thomas (2000)

Tarkki granite

This is a homogeneous, reddish gray, equigranular, medium grained massive granite with sparcely distributed ovoids (3-6 cm) of alkali feldspars (Figure 3.2 A) and plagioclase mantled alkali feldspars. The major minerals constituents are alkali feldspar, quartz, more or less sericitised plagioclase and partly chloritised biotite and hornblende, all having an apparent average grain size of 2-4 mm. The accessory minerals are: fayalite (Figure 3.2 C) (altered to iddingsite and grunerite), ilmenite, apatite, zircon, fluorite, magnetite and pyrite. The alkali feldspar generally shows a faint perthitic texture, but some crystals or parts of crystals appear homogeneous. The plagioclase is heavily sericitized, but in the less altered crystals a zonal structure is still visible. The amphibole is a hornblende, which has been altered along mineral margins and fractures into biotite, which also occurs as independent flakes. The biotite has itself been replaced by green chlorite. The fayalite has commonly been replaced by iddingsite and is often surrounded by a thin seam of grunerite. The alteration phenomena have been caused partly by fluids related to the Tarkki granite itself, and partly by fluids emanating from the younger Väkkärä granite. In the Tarkki granite, feldspars and quartz form two types of intergrowth: micrographic and myrmekite. The micrographic texture (Figures 3.2 B and 3.5) is usually of the radiating fringe or insular type, but can also be vermicular and cuneiform (Haapala, 1977). The core is usually alkali feldspar, but can sometimes be plagioclase. A very pronounced micrographic texture occurs at the contact

against the younger diabase. Rims or grain rows of myrmekite and sodic plagioclase occur in many samples of the Tarkki granite. Myrmekite and sodic plagioclase usually form thin rims between plagioclase and alkali feldspars or two alkali feldspar grains. The width of the rims is usually about 50 μm or less.

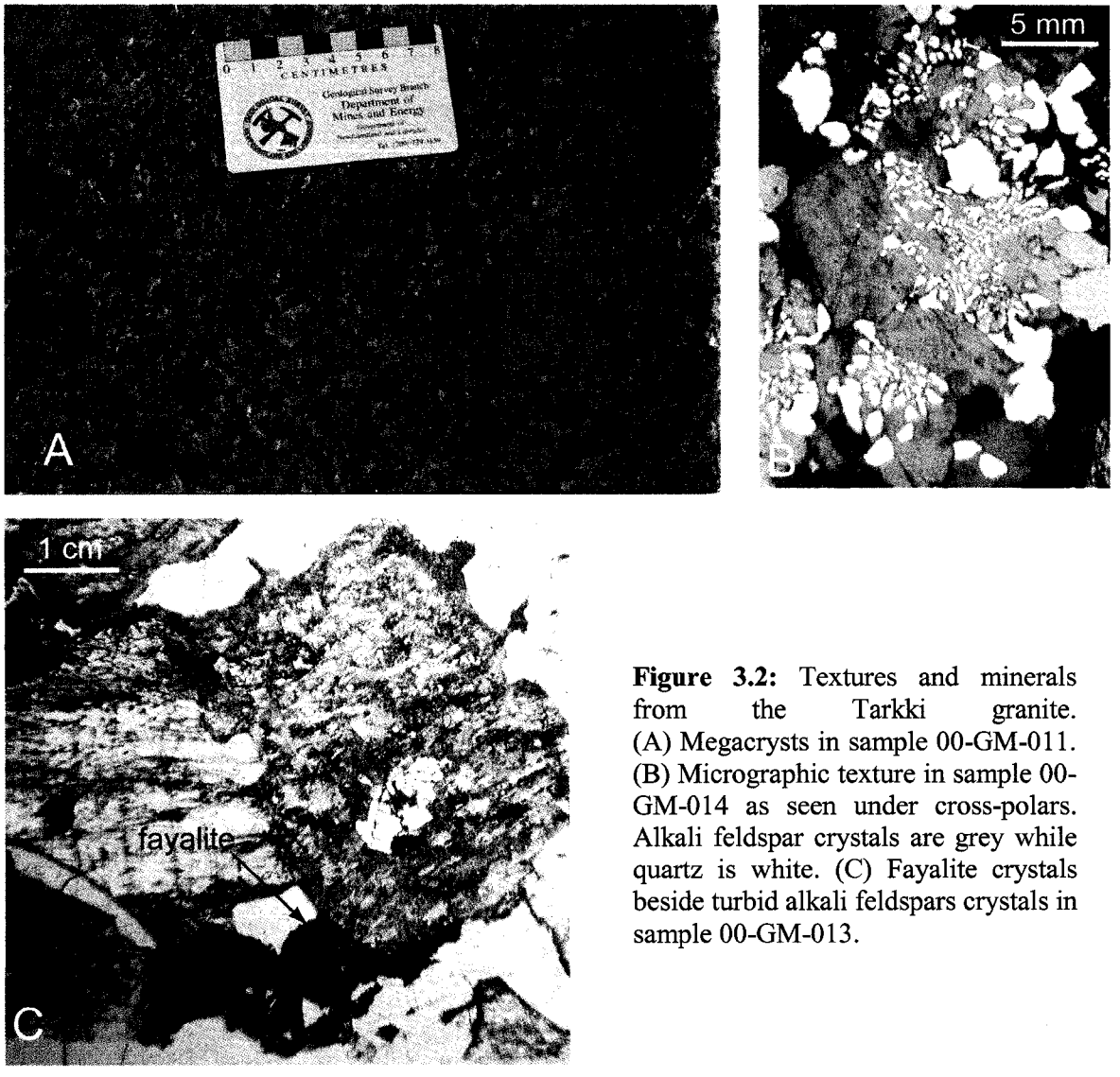

Figure 3.2: Textures and minerals from the Tarkki granite. (A) Megacrysts in sample 00-GM-011. (B) Micrographic texture in sample 00-GM-014 as seen under cross-polars. Alkali feldspar crystals are grey while quartz is white. (C) Fayalite crystals beside turbid alkali feldspars crystals in sample 00-GM-013.

Väkkärä granite

Biotite granite

This granite can be subdivided in two: contact type with the Tarkki granite and even-grained type.

Contact Type

The contact type granite has a sharp contact against the Tarkki granite, contains fragments of it and has apophyses projecting into it. It has a reddish-gray or gray color and is composed of angular or corroded porphyritic alkali feldspar, plagioclase and quartz (1-10 mm) in a fine-grained groundmass of the same minerals plus biotite. The groundmass also contains the following accessory minerals: zircon, ilmenite, anatase, monazite, apatite, xenotime, magnetite and secondary fluorite. Quartz and alkali feldspar commonly form micrographic textures of the radiating type at the edges of the K-feldspar phenocrysts. A more irregular micrographic intergrowth occurs sometimes in the groundmass and in some cases the quartz crystals are optically continuous from one grain to another without any changes in crystallographic orientations. The phenocryst alkali feldspars (5 cm) and those of the groundmass are typically perthitic.

Even-Grained type

The even-grained granite (Figure 3.3 A) is light red in colour, medium grained, hypidiomorphic-granular and contains alkali feldspar, quartz, plagioclase and biotite as its main constituents. It has zircon, ilmenite, anatase and monazite as accessory minerals, and

very small amounts of secondary topaz and cassiterite. The alkali feldspars are typically somewhat larger than the other minerals. Quartz grains are partially euhedral, but are commonly anhedral between alkali feldspar grains. Quartz also appears as euhedral or irregular inclusions or as micrographic intergrowths (radiating fringes) in alkali feldspar (Figure 3.6). Plagioclase usually has euhedral outlines against alkali feldspar. Two generations of biotite are present. Flakes of dark red-brown biotite or its alteration products are in part euhedral and a second generation is represented by anhedral aggregates of less altered biotite. The alkali feldpar is perthitic and contains many inclusions of quartz. The plagioclase is sericitized and to a small extent fluoritized.

Porphyritic and coarse-grained topaz bearing granite

This granite is red in colour and has markedly variable texture. In general it is porphyritic with 1-3 cm long alkali feldspar and 0.5-1 cm quartz megacrysts in a medium to fine grained groundmass (Figure 3.3 B). Locally it can be sub-equigranular fine-grained or coarse-grained. The alkali feldspar is usually perthitic (Figure 3.6 D) and granophyric texture is locally present. Quartz occurs in two generations, as euhedral early grains and as anhedral late grains. Biotite occurs in the matrix as pale brown to pale greenish brown, anhedral flakes filling the space between the main minerals. Topaz and fluorite (Figure 3.6 A and C) occur commonly and account for as much as 3% of the rock. Topaz crystallized after the feldspars but before late quartz. Topaz grains are subhedral and show crystal faces against late quartz. Other accessory minerals are monazite, bastnäsite, xenotime, zircon, ilmenite, cassiterite, columbite and thorite (Haapala, 1977). Microscopic and centimeter long miarolitic cavities

filled with clay minerals are common, indicating the existence of a separate fluid phase and shallow depths of emplacement. This granite is characterized by textures indicating subsolidus reactions: exsolution, recrystallization and mineral alterations.

Quartz porphyry dikes

Quartz porphyry dikes are only found in the Tarkki granite and their widths are between 1 and 15 m. They are red in color and show a darker chilled margin against the country rock in which an indistinct flow banding and mineral parallelism is often visible. It consists of megacrysts of perthitic microcline, albite and quartz in an aphanitic groundmass of the same constituents. Mica, chlorite, topaz, cassiterite, apatite and fluorite are also found in small amounts. The grain size of the groundmass is typically about 0.2 mm, whereas the grain size of the alkali feldspars megacrysts is on the order of 2-3 cm and increases toward the dike centre. It is possible that some of the quartz porphyry dikes are apophyses of the Väkkärä granite.

Dark porphyry dikes

These are composed of corroded altered calcic plagioclase megacrysts (1-3 cm) in a groundmass composed of plagioclase, biotite, hornblende, alkali feldspar, quartz, apatite, sericite, epidote, titanite, oxides, sulphides, carbonate and zircon. The colour of these dikes is dark gray to nearly black.

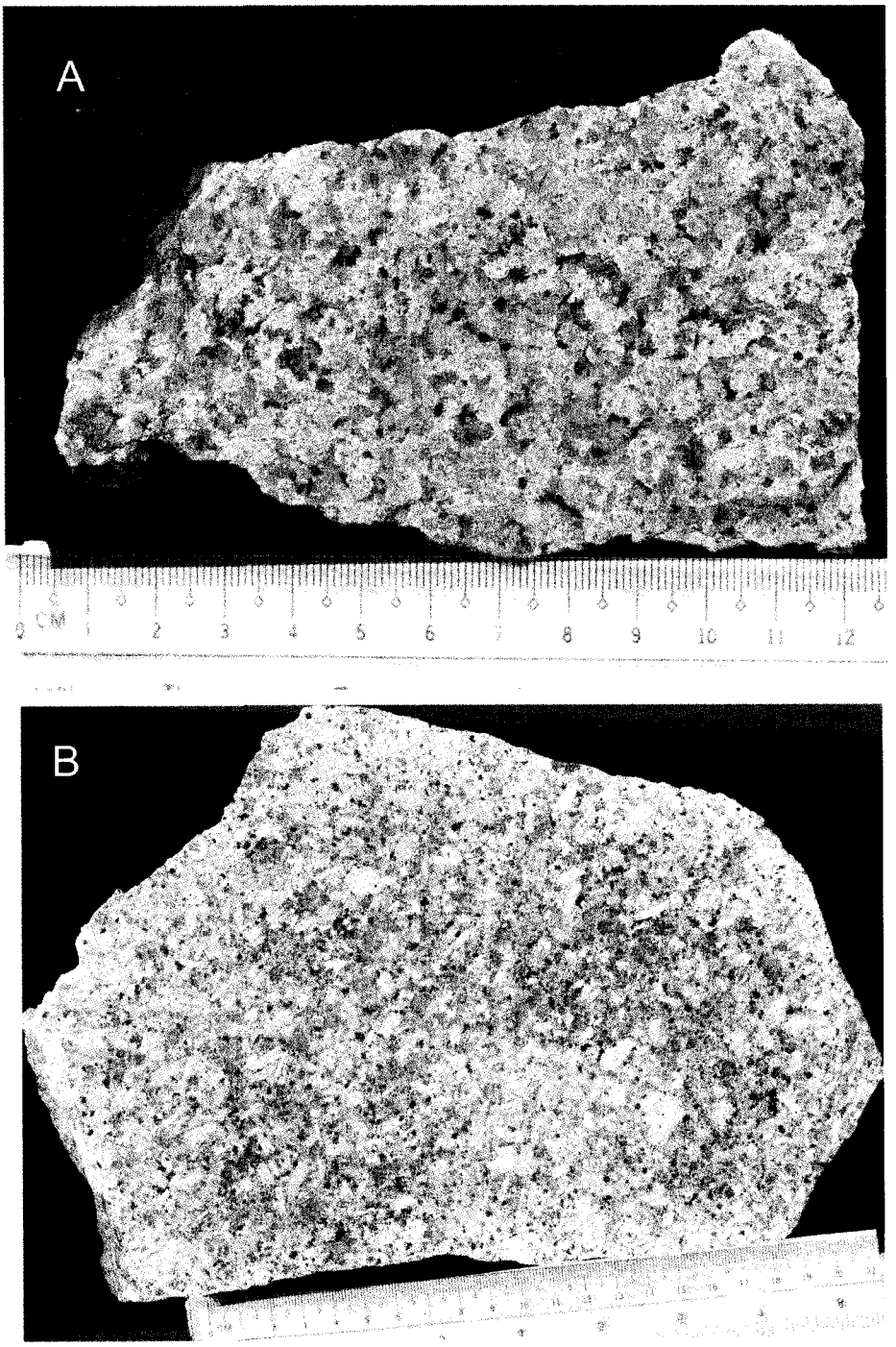

Figure 3.3: (A) Even-grained biotite granite (sample 00-GM-010). (B) Porphyritic and coarse-grained topaz bearing granite (sample 00-GM-012).

Sampling strategy

Sampling of the Eurajoki stock was done during a two-week period in the summer of 2000. The sampling sites were chosen (see Figure 3.1) to be representative of all the granitic phases in the area. Unfortunately other than a granite quarry, the flatness of the terrain, the thick layer of unconsolidated sediments and the dense forest left very few well-exposed outcrops in the area to be studied. Accordingly most samples were taken from road cuts and are described in Appendix A.

Electron Microprobe data

An electron microprobe (EMP) was used to accumulate mineral compositional data of feldspars, identify some minerals, and confirm the identities of others that were tentatively classified using a polarizing microscope. In the following section, results for feldspars chemical analyses and photomicrographs are presented. All the EMP data are presented in Appendix B. The microprobe work confirmed macroscopic and microscopic descriptions made earlier and presented in Appendix A.

A total of 84 chemical analyses were done using the EMP, 39 analyses of minerals from the Tarkki granite and 45 analyses of minerals from the Väkkärä granite. All theses analyses were made on feldspars except for 2 analyses of mica (annite variety), 1 of chlorite (diabantite variety) and 2 of olivine (fayalite variety) in the Tarkki granite (see Appendix B).

All feldspars analyses were plotted on an Orthoclase-Albite-Anorthite ternary diagram (Figure 3.4).

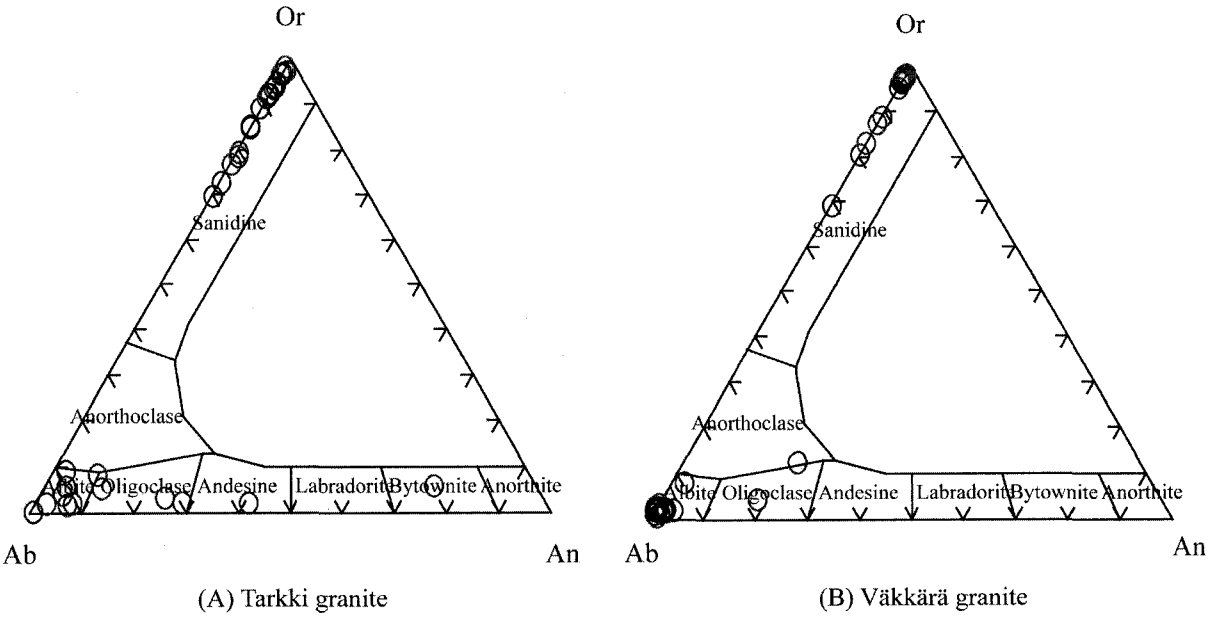

Figure 3.4: Classification of feldspars based on EMP data.

Generally all feldspars crystals encountered in this study can be classified as either potassic-rich feldspar or pure albite. Some plagioclase crystals in the Tarkki granite contain calcium to the extent that bytownite was locally identified Figure 3.4(A), but the majority of the feldspars are alkaline.

The electron microprobe was also used in back-scatter SEM mode to image textures encountered in the Eurajoki rocks. For the Tarkki granite, granophyric texture is a striking feature that can be seen in many samples. Two of theses microphotographs are shown in

Figure 3.5. In these pictures, quartz crystals are radiating in circular pattern from a potassic feldspar crystal.

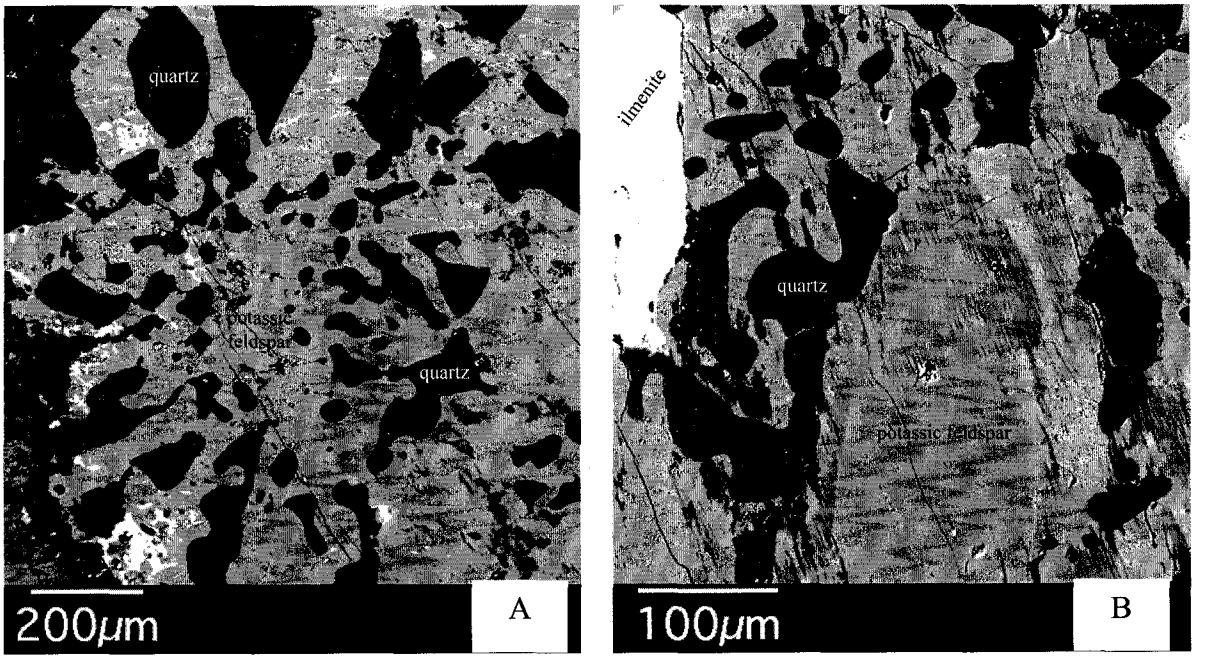

Figure 3.5: Tarkki granite - (A) Backscatter image from sample 00-GM-014 where quartz crystals (black) form a radiating pattern around a potassic feldspar crystal (light gray). (B) Backscatter image from sample 00-GM-016 where quartz crystals (black) form a radiating pattern around a potassic feldspar crystal (light gray). The feldspar crystal is partly turbid. An ilmenite crystal is visible in the top left corner.

In the Väkkärä granite, textures and mineral assemblage are different to those of the Tarkki granite. Four images are shown in Figure 3.6 to demonstrate two of the more common textures, perthite and granophyric and two other pictures to illustrate topaz crystals in the granite.

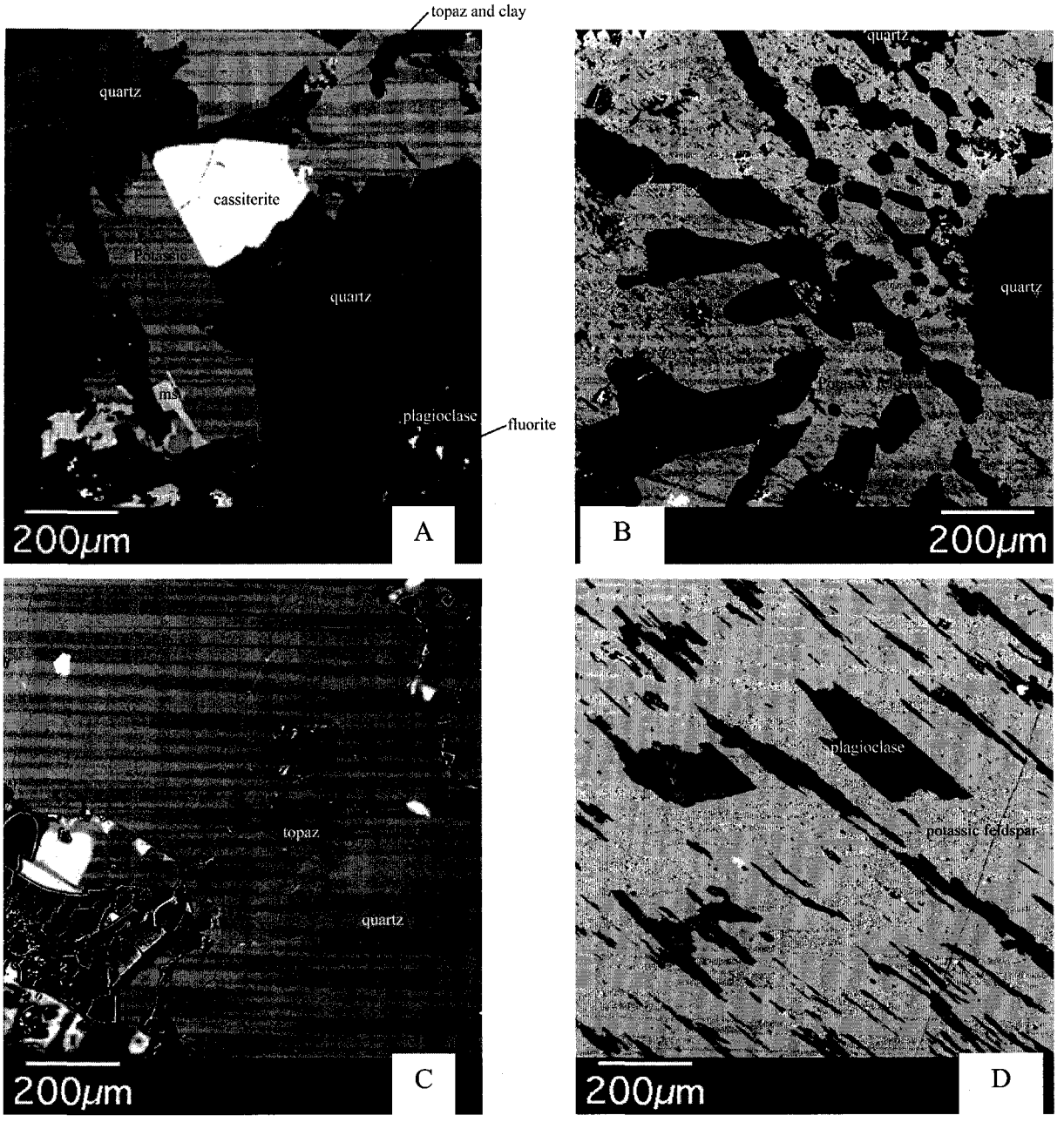

Figure 3.6: Väkkärä granite - (A) Image from sample 00-GM-009 where cassiterite is visible and some fluorine minerals to the right of the image (topaz and fluorite). (B) Image from sample 00-GM-010 quartz crystals (black) form a radiating pattern around a central quartz crystal. (C) Image from sample 00-GM-017 a euhedral topaz crystal is included in a quartz crystal. (D) Image from sample 00-GM-017 perthitic texture is visible as an exsolution of albite from potassic feldspar.

The textures seen in the Eurajoki stock (graphic, granophyric, perthitic and myrmekitic) suggest that there was an increase of fluid phase activity towards the end of crystallization. That fluid phase, following a period of near equilibrium growth, caused a saturation in volatile phases, producing an effective undercooling and a rapid growth of crystals.

Quantitative textural studies

The CSD of crystals is a volumetric measure, but crystal sizes and numbers were measured in two dimensions as described previously (see chapter 2) for every sample of the Eurajoki stock, hence the raw data must be corrected. The program *CSDCorrections 1.2* (Higgins, 2000) was used to calculate potassic feldspar CSDs in rocks from the Eurajoki stock. The overall shape (Short:Intermediate:Long dimensions) of the crystals was estimated from the statistical distribution of intersection width/length ratios (W/L) measured in two dimensions (Higgins, 1994), using the formulas S/I=mode(W/L) and I/L=skewness(W/L)+0.5. This was done for every sample and the mean, 1:1.7:3.1, was taken as the shape of the crystals. All samples had angular crystals (no rounding) and no obvious foliation.

Results obtained using the techniques described in chapter 2 and the software CSD Corrections are presented in Table 3.1 and 3.2. These tables contain the results of all the measurements done at different scales (outcrop, slabs, thin sections) and are used to plot the CSDs. The CSD data were then plotted following the method of Marsh (1988) (Figure 3.7).

During the computation bin-size was adjusted so that there were adequate numbers of crystals in each size interval so as to avoid depopulation particularly for large crystals. This also ensures that the total number of bins is low and hence that the errors introduced during the data conversion from 2D to 3D are minimized. There were no empty bins and those with only one or two crystals and those having small size intervals with very large uncertainties were removed from the CSD diagrams, as they are imprecise. The errors as calculated by CSD Corrections, for other data points are small (typically less than 8%) and have been omitted for clarity in all figures.

All Tarkki granite CSDs have a maximum population density at sizes between 0.6 and 0.9 mm while CSDs of Väkkärä have a maximum population density at sizes between 0.4 and 1.3 mm (Figure 3.7). To the left of the maximum (lower size limit) there are no measurements because it represents the limit of the measurement techniques and not necessarily the smallest crystals in the rocks. For both granites, the parts of the CSDs to the right of the maximum have a negative slope and are slightly concave upwards.

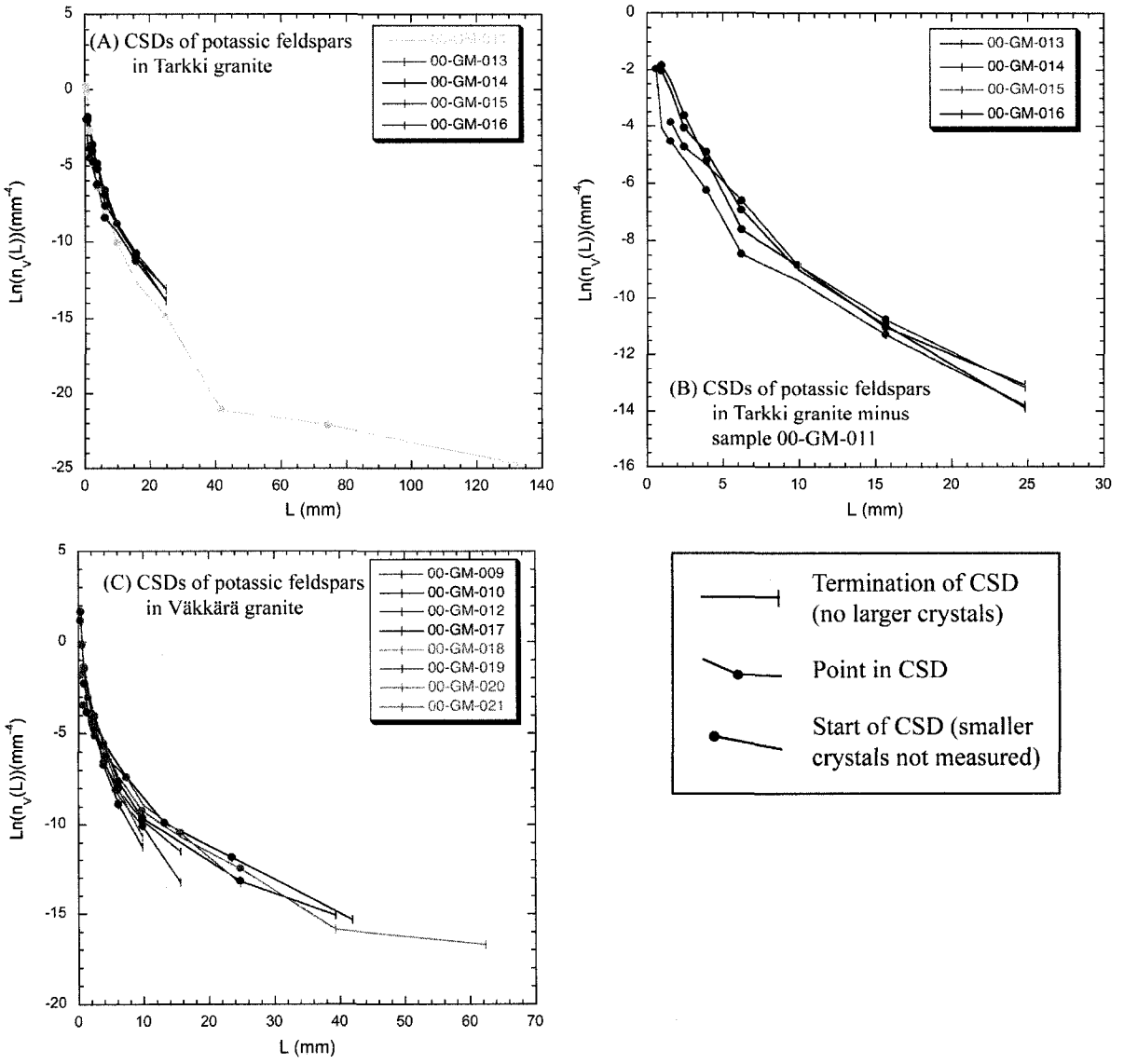

Figure 3.7: CSDs of potassic feldspars in the Eurajoki stock. (A) Potassic feldspars crystals of the 5 samples from Tarkki granite as measured on outcrop, rock slabs and thin sections. (B) Same figure as (A) but without sample 00-GM-011 for more clarity. (C) Potassic feldspars crystals of the 8 samples from Väkkärä granite as measured on rock slabs and thin sections.

Table 3.1: Intersection width distributions of potassic feldspar crystals in Tarkki granite

Sample number	00-GM-011	00-GM-011	00-GM-011	00-GM-013	00-GM-013	00-GM-014	00-GM-014	00-GM-015	00-GM-015	00-GM-016	00-GM-016
Type of sample	outcrop	rock slab	stained thin section	rock slab	stained thin section	rock slab	thin section	rock slab	thin section	rock slab	thin section
Upper size limit (mm)											
56.20	3										
31.60	13										
17.80	14										
10.00	0	4		4		6		5		2	
6.31		15		19		19		22		15	
3.98		79		52		67		60		43	
2.51		235		55		94		42	28	51	20
1.59		477	20	77	15	99	46		42		62
1.00			22		18		92		35		63
0.63			25		15		131		34		95
0.40			23		11		103		22		84
0.25			40		27		40				49
0.16			36		44		12				11
0.10			4								
Total	30	810	170	207	130	285	424	129	161	111	384
Area measured (mm2)	11600000	30942	748	10008	735	7627	884	6820	884	5600	884

Table 3.2: Intersection width distributions of potassic feldspar crystals in Väkkärä granite

Sample number	00-GM-009	00-GM-009	00-GM-012	00-GM-012	00-GM-017	00-GM-017	00-GM-018	00-GM-018	00-GM-019	00-GM-019	00-GM-020	00-GM-020	00-GM-021	00-GM-021
Type of sample	rock slab	stained thin section	rock slab	stained thin section	rock slab	thin section	rock slab	thin section	rock slab	stained thin section	rock slab	thin section	rock slab	stained thin section
Upper size limit (mm)														
25.10							2							
15.85					3		2							
10.00					8		21				2			
6.31			10		29		52		3		14			
3.98	7		23		46		89		28		29		8	
2.51	31		47		51	10	89	13	60		29	19	45	
1.59	107		50	7		37		33	102	18		21	155	22
1.00	256	24		12		57		64		35		32		49
0.63		77		10		68		70		68		32		84
0.40		110		30		63		61		96		19		117
0.25		165		89		38		46		141		13		172
0.16		120		247		5		31		126				
0.10				109				42		23				
0.06								35						
Total	401	496	130	504	137	278	255	395	193	507	74	136	208	444
Area measured (mm2)	9250	759	6600	500	11177	884	14545	884	11697	875	3263	884	5988	718

Since all CSDs are curved it is not appropriate to estimate slopes and intercepts. Initially the curves were fit with polynomial expressions but it became difficult to attach a physical meaning to the results. Because the rocks are composed of phenocrysts within a groundmass it was decided to treat the data of each rock as two linear line segments. This way of presenting the data does not imply that the rocks were formed by mixing, only that the CSDs can be decomposed into two straight CSDs. Thus the CSD curves were separated in two, at the point of flexure, and a linear regression yielding a slope and intercept for each segment was attained. The linear regressions are named groundmass and phenocrysts, the former for the smaller and larger crystals sizes respectively. Points in each CSD are separated into these 2 groups. The point of separation (crystal size) was chosen for each sample in a way to attain the highest degree of confidence for each regression line (phenocrysts and groundmass), and in most case the separation was usually done at 5 mm. By separating the results in this manner, it is possible to respect the crystal distribution and obtain regression lines having a significant goodness of fit ($R>0.95$) with a linear model.

This CSDs separation is presented in Figures 3.8 and 3.9. The blue and green lines are linear regression curves of the phenocrysts and groundmass. However in order to attain a complete view of the results at all scales they were combined into amalgamated CSD plots as shown in Figure 3.8 for the Tarkki granite, and in Figure 3.9 for the Väkkärä granite. In theses figures, the third curve (red) was obtained by summing the regression line of the phenocrysts and groundmass. This represents the model CSD of each sample and makes for easy comparison of samples. The addition was made:

Total (red line): Ln (population density) = Ln (exp(phenocrysts regression line)+exp(groundmass regression line)) (a)

If we use sample 00-GM-013 as an example, where the formulas of the regression lines are of the type y=slope*x+intercept (as calculated by the software Kaleidagraph to minimize errors):

Phenocrysts regression line: ln (population density)= -5.8-0.3(size) (b)

Groundmass regression line: ln (population density)= -2.5-1.1(size) (c)

Where size is a variable between the smallest and the largest values of sizes measured and calculated for the CSD, for our example size varies from 0.62 to 24.84 mm

If we put (b) and (c) into (a):

Ln (population density) = Ln (exp(b)+exp(c))

This is how the red curves in Figures 3.8 and 3.9 are obtained. These curves were also used to obtain Figure 3.10 as it is easier to compare one to another. The compilation of the CSDs (Figure 3.10) shows that all CSDs lie in a single curved band and that CSDs of Tarkki are less curved than CSDs of Väkkärä.

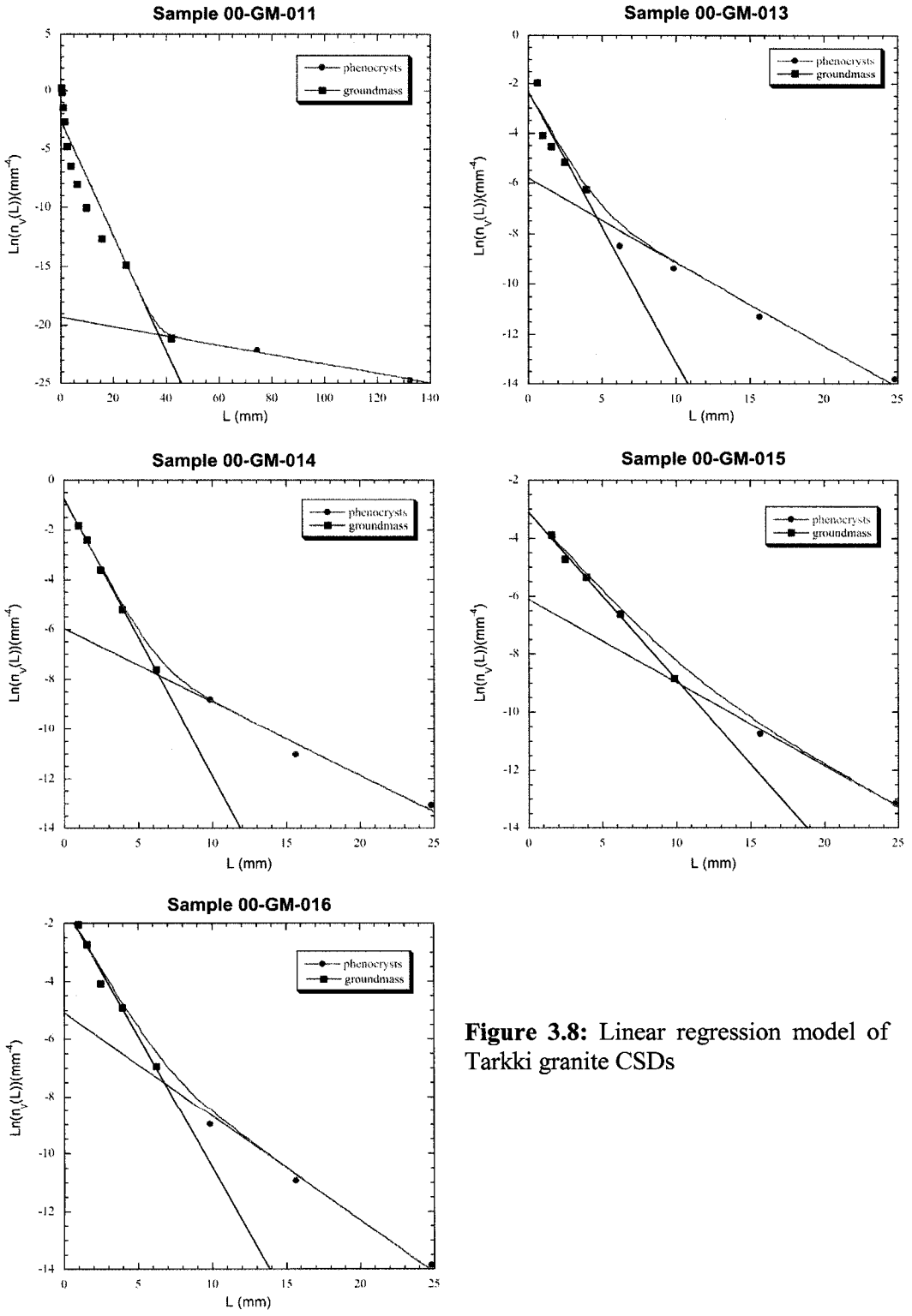

Figure 3.8: Linear regression model of Tarkki granite CSDs

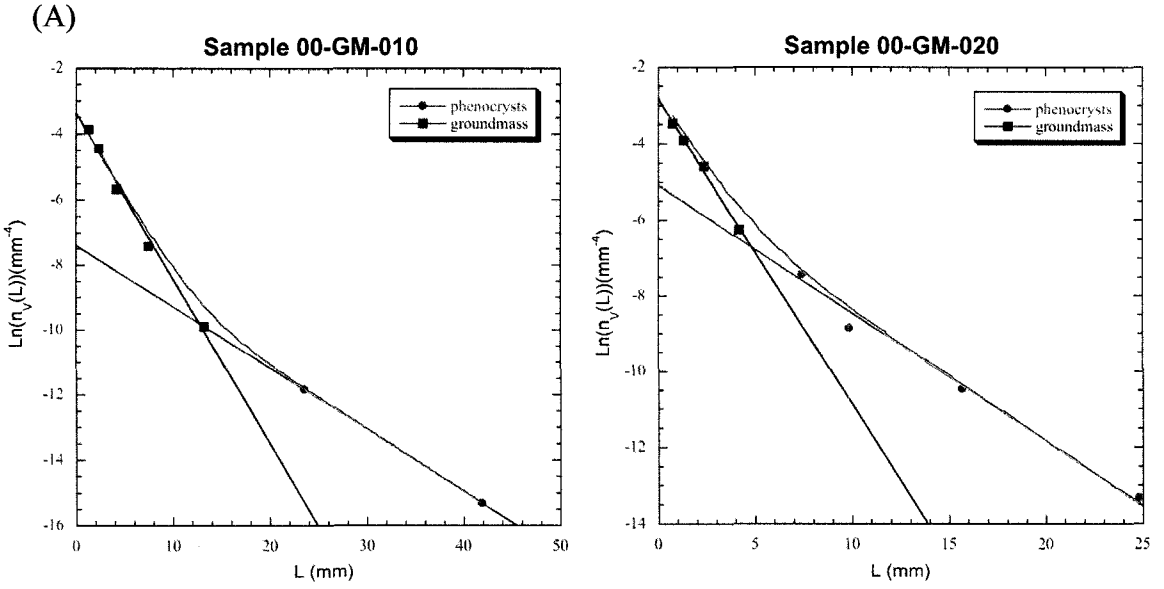

Figure 3.9: Linear regression model of Väkkärä granite CSDs. (A) Biotite granite. (B) Porphyritic and coarse-grained topaz bearing granite.

(B)

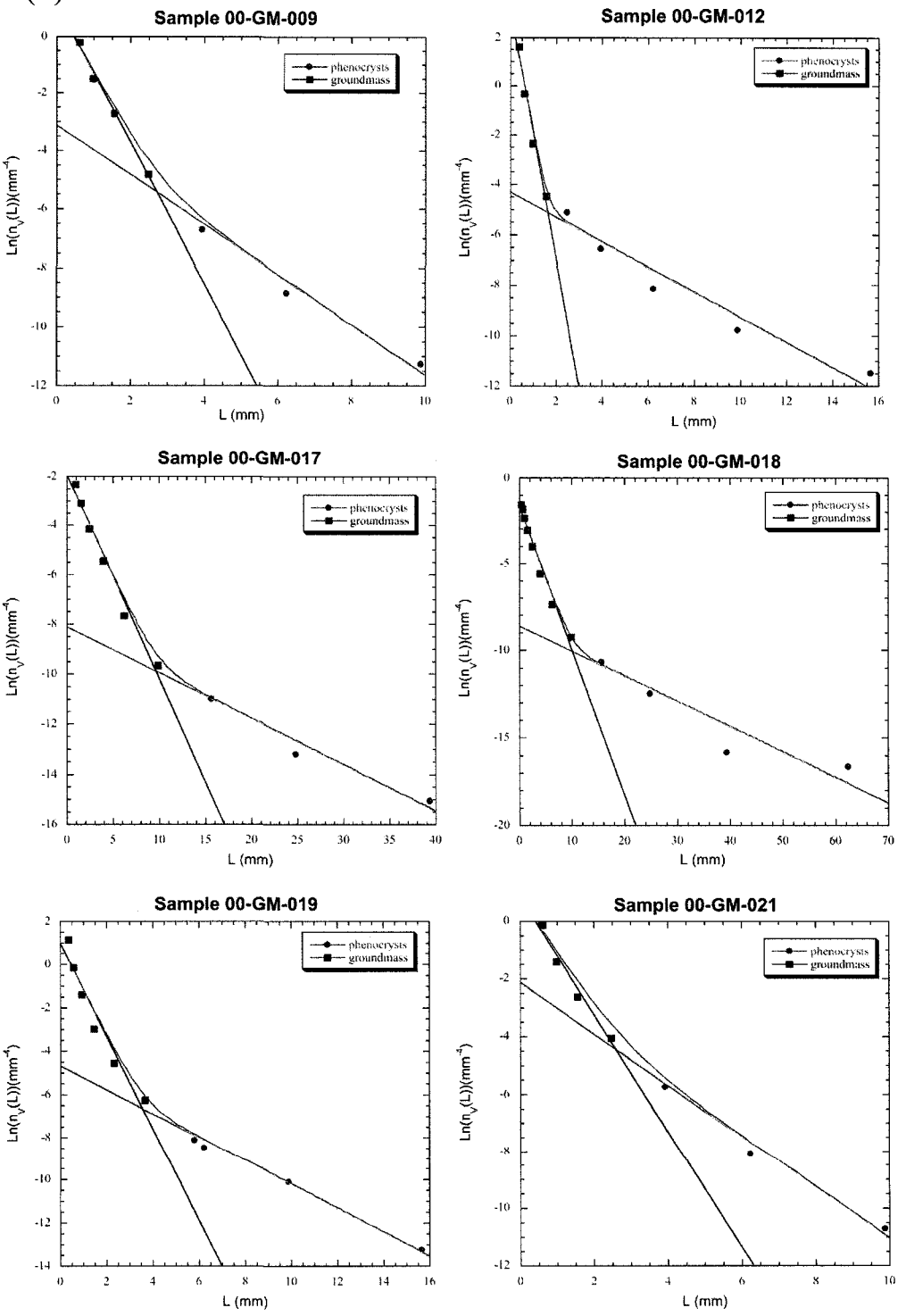
Sample 00-GM-009
Sample 00-GM-012
Sample 00-GM-017
Sample 00-GM-018
Sample 00-GM-019
Sample 00-GM-021
phenocrysts
groundmass
Ln(n_v(L))(mm^-4)
L (mm)

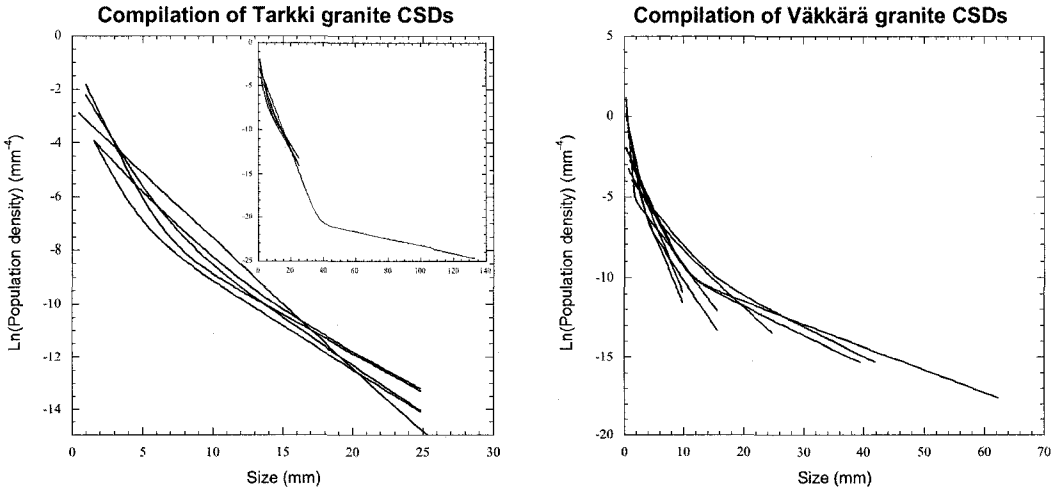

Figure 3.10: Compilation of CSDs calculated from addition of the linear regressions curves.

Since linear regression were done on both part of the CSDs, the slope and intercept could be estimated with relative confidence. So for each sample two points were obtained. The characteristic length of the CSD was calculated from the slope:

Characteristic length = -1/slope (Marsh, 1988)

A histogram of characteristic length (CL) has been plotted in Figure 3.11(A). In the Tarkki granite, CL of the groundmass is between 0 and 2 mm and the CL of the phenocrysts is between 2 and 4 mm. There is also, at 24 mm, a CL represented by the megacrysts in sample 00-GM-011. The CL of the Väkkärä granite groundmass is the same as the Tarkki groundmass, whereas the CL of the phenocrysts ranges between 1 and 8 mm with gaps between 4 and 6 mm and between 6 and 8 mm. The CL of phenocrysts overlaps the CL of the

groundmass and is not continuous indicating an evolution of texture in the Väkkärä granite because it means that nucleation was stopped at one point and crystals were growing without new crystals forming.

The characteristic length has been plotted against the intercept in Figure 3.11 (B) and (C). The 100% closure limit, which means that no CSD should represent more than 100% crystals, was calculated as described by Higgins (2002a) for an ellipsoid of the same dimensions (1:1.7:3.1) as used in the data reduction. In the Tarkki granite, the phenocrysts and groundmass data are grouped into 2 separated clusters of points, except for sample 00-GM-011 phenocrysts. All data points are close to, but beneath the closure limit. Since the 2 clusters are close to one and other, it means that the CSDs do not have a very high curvature. All CSD's of Tarkki granite are quite uniform, except for 00-GM-011, possibly because it was sampled from a quarry, which permitted the observation of megacrysts sparsely dispersed through the granite at this location. The small outcrops at other sampling localities may not have exposed such megacrysts.

In contrast the Väkkärä granite data points are not separated into 2 clusters, but show a linear correlation, with increasing characteristic length, going from groundmass to phenocrysts. The phenocrysts' data range from a value of 1.5 mm up to 7 mm in a linear manner and points follow very closely the curve defined by closure limit. There seems to have been an evolution of the texture in the Väkkärä granite, because the samples with the higher values of

characteristic length are also those containing the most topaz crystals. In general values of characteristic length are higher for the Väkkärä granite than the Tarkki granite.

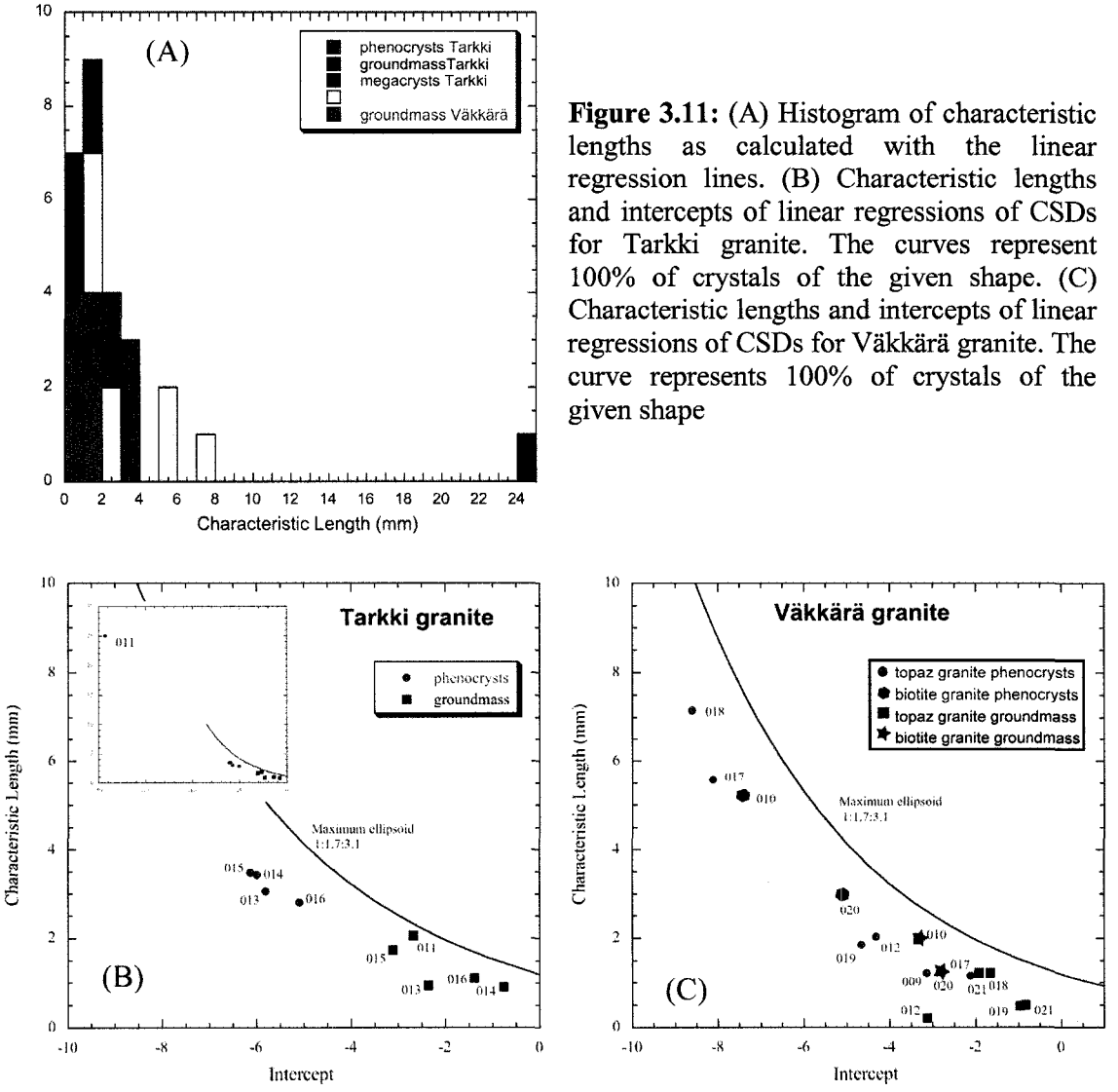

Figure 3.11: (A) Histogram of characteristic lengths as calculated with the linear regression lines. (B) Characteristic lengths and intercepts of linear regressions of CSDs for Tarkki granite. The curves represent 100% of crystals of the given shape. (C) Characteristic lengths and intercepts of linear regressions of CSDs for Väkkärä granite. The curve represents 100% of crystals of the given shape

Discussion of the results

Crystal size distributions

The Tarkki granite is homogeneous and is the older component of the Eurajoki stock. It is mostly composed of alkali feldspars and quartz with sparsely distributed megacrysts of alkali feldspars. Locally quartz and feldspar are intergrown to form micrographic and/or granophyric texture. CSDs of Tarkki granite (Figures 3.7 and 3.10) show a straight trend with their right side slightly concave up if sample 00-GM-011 is not taken into account (Figure 3.7B). The CSD of sample 00-GM-011 is different because it was possible in the quarry to see and measure sparsely distributed (3 to 5 cm long) megacrysts. The CSD for smaller grains is similar to the CSDs of the other samples (Figure 3.7A), but it is strongly concave up for larger grains. These megacrysts were not seen in other outcrops but it is reasonable to assume that they are dispersed within the Tarkki granite, as Haapala (1977) stated that megacrysts are sparsely distributed and separated by several meters.

The Väkkärä granite is composed of three components: the biotite granite in contact with the Tarkki granite, the even-grained biotite granite and the porphyry topaz-bearing granite. Contact relationships between these 3 types are unknown due to lack of outcrop but they are assumed to be gradational between one and other. Petrology and chemistry show that they are closely related. Väkkärä granite is mostly composed of alkali feldspar and quartz and shows perthitic and granophyric textures. Haapala (1997) states that the biotite granite is temporally and compositionally intermediate between the Tarkki granite and the topaz-

bearing granite, but is part of the Väkkärä. CSDs of Väkkärä granite (Figures 3.7C and 3.10) have a pronounced concave up curvature, except for sample 00-GM-009, 00-GM-010 and 00-GM-020 where the curvature is not as pronounced compared to other samples of this granite. This could be explained by the fact that samples 010 (contact type facies) and 020 (even-grained facies) are part of the biotite granite, while all other samples come from the topaz-bearing granite.

Solidification of the Eurajoki stock, Tarkki and Väkkärä granites, must have started with nucleation and growth of crystals likely producing initial linear CSDs. Theorical studies (Marsh, 1988, 1998) and field studies (Higgins, 1999; Mock *et al.*, 2003) suggest that initial CSDs for simple steady-state dynamics with linearly increasing undercooling should be straight lines on a conventional CSD plot (Figure 3.12A) for closed and open systems (Figure 1.3 and 1.4). However an initial straight CSD may be modified, as described in chapter 1, by geological processes.

Since CSDs of Tarkki and Väkkärä granites are not straight but concave up, let's take a look at some geological processes that could give rise to the measured CSDs and discuss them in light of the geochemical and other petrologic data accumulated.

Compaction and filter pressing will push the CSD upward, increasing the intercept but the slope will remain constant (Figure 1.4) (Higgins, 2006). It can also remove some of the finest crystals with the magma. CSDs measured in the Eurajoki stock do not show evidence of this

process because the process changes the population density evenly without bending the CSDs. The petrology of the Väkkärä granite indicates that there was magma present with the crystals until the late stage of solidification; there is no foliation something that is commonly produced by compaction and filter pressing.

Accumulation of crystals in the magma chamber under the influence of gravity will skew the right side of the CSD upwards (Higgins, 2002b; Marsh, 1998) (Figure 1.5 and 3.12B). This has been observed in layered rocks of Kiglapait (Higgins, 2002b) because larger crystals are accumulated in some specific layers while smaller ones are removed by physical process in the magma chamber such as convection currents or crystal settling by gravity. At Eurajoki, this cannot be applied because the megacrysts in Tarkki granite and phenocrysts in Väkkärä are sparsely distributed, are not found in specific layers or in layered rocks and because the viscosity of felsic magmas is likely too high to support convection or crystal settling (see below).

Fractional crystallization is another process considered to be a prevalent magma chamber differentiation process and it will skew the right side of the CSD (Figure 3.12B and E) downward because it removes the larger crystals from the crystallization site. This process does not seem to happen at Eurajoki because none of the CSDs are curved downward and again is unlikely due to the high viscosity of silica-rich magmas.

Physical mixing of magmas can also produce a CSD curved concave up (Figure 1.6). The mixing of almost any crystal population with straight CSDs will produce a concave-up curve. (Higgins, 1996, 2006; Armienti *et al.,* 1994). Field observations, petrology and chemistry do not show any evidence of magma mixing at Eurajoki, because the granite is homogeneous and there is no evidence of different magmas mingling.

Another important natural process that can modify CSDs significantly is textural coarsening if undercooling remains small for a period of time. Two, of many different theories, have been described in chapter 1 (Figure 1.8) and have been developed to explain textural coarsening in geological systems: the Lifshitz-Slyozov-Wagner theory (LSW) (Lifshitz & Slyozov, 1961) that does not take into account diffusion and the Communicating Neighbors (CN) (DeHoff, 1991) theory that does. The CN theory can explain the right part of the observed CSDs at Eurajoki and has been supported by studies of plutonic rocks (Higgins, 1998, 1999, 2002b).

Tarkki granite CSDs conform to a textural coarsening model (Figure 3.12). In addition, the correlation between characteristic length and intercept for phenocrysts (Figures 3.11 and 3.12) conforms to a CN model, but not completely because the left parts of the CSDs do not fan around a small size. As seen in Figure 3.11, there are two distinct populations of crystals and there is only a small difference between phenocrysts and groundmass crystal characteristic lengths. This small difference indicates coarsening between groundmass and phenocrysts, but not a long coarsening period, except for sample 00-GM-011. The

megacrysts in the granite found at location 00-GM-011 and reported elsewhere by Haapala (1977) may be a first generation of crystals formed in the magma chamber. The relation between them and the other crystals (phenocrysts and groundmass) is not easy to decipher with only one sample.

The right part of Väkkärä granite CSDs follows the CN coarsening model (Figure 3.12) and the correlation between characteristic lengths and intercept (Figures 3.11 and 3.12) of the CN textural coarsening model, but the left side does not fan around a small size as predicted by the CN model. The results obtained for the Väkkärä granite show coarsening between groundmass and phenocrysts, as shown in Figure 3.12, phenocrysts and groundmass show a linear correlation between them. This implies coarsening in the melt producing the granite.

However the CN coarsening model cannot alone explain CSDs measured at Eurajoki because in the model, which is a closed system model, fine crystals are depleted on the final CSD (Figures 1.8 and 3.12 D) because they are consumed to produce larger crystals. As observed (Figures 3.7 and 3.10) in Eurajoki CSDs, the smallest crystals are present in the granites and are an important part of the crystal population. This can possibly be explained by the fact that Eurajoki components were formed in an open-system environment and new material was brought to the magma chamber.

A concave up CSDs, as is observed at Eurajoki, can also be obtained by changing the crystallization conditions in the magma chamber, but since there is no evidence from

petrographic (e.g. mineral zoning, sieve textures, resorption textures, reaction rims) or chemical analyses of the magmatic conditions having changed, it will be assumed in the following models that they were largely unchanged. Of course it is often difficult to observe changing crystallization conditions because only the final product of crystallization can be studied.

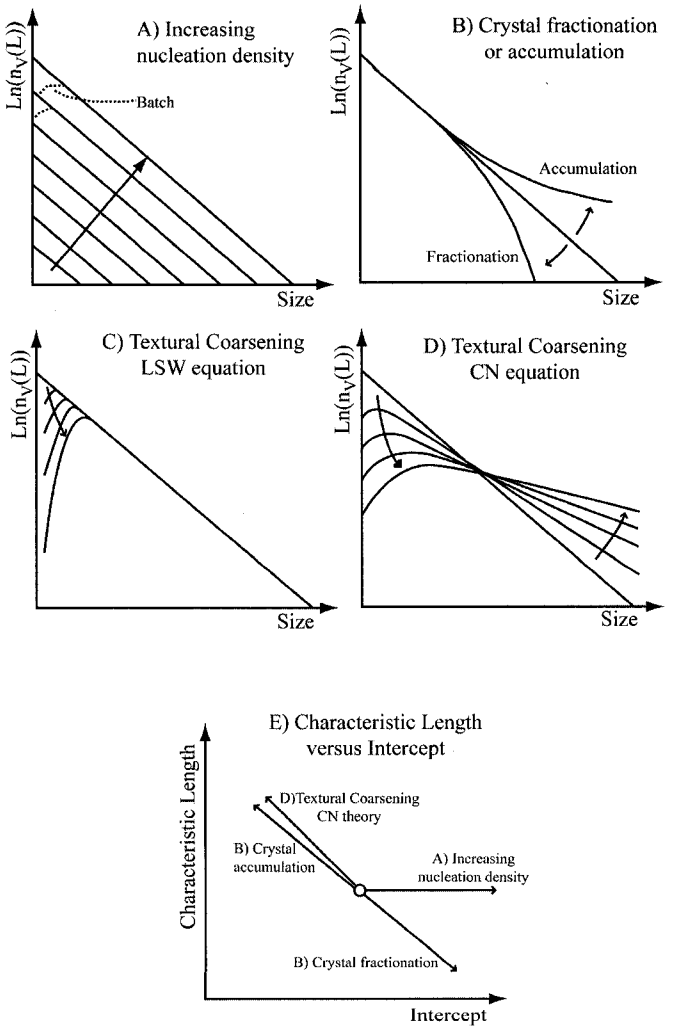

Figure 3.12: Schematic crystal size distributions from Chapter 1 except for figure (E). (A) Open or closed systems with increasing nucleation density (Marsh, 1988, 1998). (B) Accumulation or fractionation of crystals (Marsh, 1988). (C) Textural coarsening following the LSW theory (Lifshitz & Slyozov, 1961; Higgins, 1998). (D) Textural coarsening following the CN theory (Dehoff, 1991; Higgins 1998). (E) Summary of CSD models in terms of characteristic length versus intercept (Higgins, 1999).

Tarkki granite potassic feldspars growth model

It was previously demonstrated that textural coarsening was likely an important process in the formation of the Tarkki granite, but before coarsening can begin, initial nucleation and growth of crystals must occur at depth (Figure 3.13) close to where the magma was produced or during ascent to the magma chamber.

Haapala (1977) reports that a fine grained chilled contact of the Tarkki granite against other, older rocks, is lacking and that the country rock was hot because either the Tarkki granite was a relatively deep intrusion or, due to the heating effect of the contemporaneous Laitila rapakivi intrusion (Figure 3.1). Therefore it is expected that undercooling was slight and existent heat buffered the temperature in the Tarkki granite slowing nucleation to a minimum but permitting growth of the crystals nucleated previously. This is the first phase of cooling (Figure 3.13) and was likely of sufficient duration to induce coarsening in the chamber resulting in the megacryst formation. Following this phase it is interpreted that the degree of undercooling increased due to magma ascent or degassing in the chamber or simply because coarsening did not produce enough latent heat to keep the temperature near the liquidus. The increase in undercooling increased the nucleation and growth rates. Megacrysts continued to grow but slower than during the coarsening period, making a large size difference between two crystals populations (Figure 3.13).

The presence of phenocrysts in the granite indicates another period of near-liquidus-temperature growth and coarsening. Since the curvature of CSDs is not as pronounced as seen in Figure 3.11 there is not a large size difference between phenocrysts and groundmass, the second period of coarsening must have been relatively short. It is interpreted as a return to conditions similar to those existing during megacryst growth.

This second period of coarsening could have simply have arisen as heat produced by the release of latent heat of crystallization from nucleation and growth was unable to escape and undercooling was stalled, thus the temperature was buffered. This suppressed nucleation of new crystals promoting grain size coarsening. A loss of pressure, volatiles or simply because of uplift, since it is an open-system, could have restarted nucleation and growth in the magma chamber producing the last part of the CSDs curves (Figure 3.13). The loss of volatiles can be corroborated by the fact that the Tarkki granite lack cavities (no accumulation of fluids or volatiles) and has very faint perthitic texture (Haapala, 1977) and granophyric texture can be produced by near to equilibrium growth followed by late stage volatile saturation triggering rapid growth. These are features typical of a chamber not saturated with water.

Other textures such as micrographic and granophyric, seen in the granite could also be form by reheating from diabase (Haapala, 1977), while myrmekite could be formed from exsolution or metasomatic replacement. Also, late stage activity of volatiles (alteration of mafic minerals, sericitization) is caused partly by deuteric fluids from Tarkki and partly from fluids produced by the crystallizing Väkkärä granite.

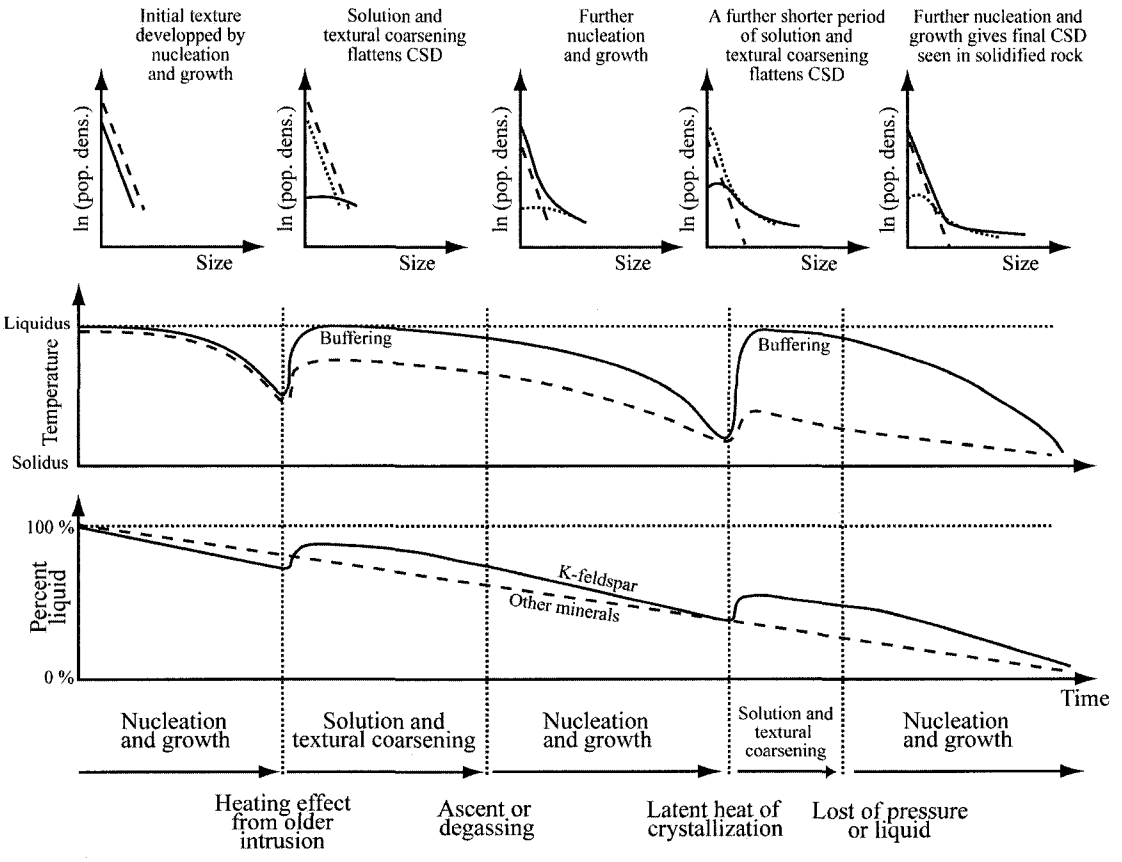

Figure 3.13: Dynamic model for the development of textures in the Tarkki granite. Potassic feldspar model is compared to the theorical model of other minerals.

Väkkärä granite potassic feldspars growth model

It was previously demonstrated that textural coarsening is an important process in the formation of the Väkkärä granite, but before coarsening can begin, initial nucleation and initial growth of crystals must occur at depth (Figure 3.14) in the conduits bringing the magma from its origin to the magma chamber higher in the crust.

Based on field relationships, Haapala (1977) reports that the Tarkki granite was already cooled and fractured when the Väkkärä granite was emplaced. He also documents that they

crystallized under different conditions and from different magmas. If the Tarkki granite was already cooled, it could not have helped produce a low undercooling, by keeping heat inside the Väkkärä and inducing textural coarsening as interpreted from the CSDs. The coarsening process must have been taken place in the Väkkärä without help from other igneous bodies or from older metamorphic rocks (Figure 3.1). However, crystallization of the biotite granite, that does not show textural coarsening (Figure 3.7), may have helped to produce a low undercooling in the middle of the Väkkärä intrusion (the topaz granite) and have provided an ideal environment for coarsening.

The warm external part of the intrusion (biotite granite and external part of the topaz bearing granite) would have thermally insulated the interior. Thus latent heat would not have been rapidly diffused from the middle of the intrusion due to the small temperature gradient. Undercooling was minimized and temperature buffered by the release of latent heat of crystallization. This condition suppressed nucleation and promoted grain size coarsening.

In order to have ripening or coarsening, conditions in the magmatic chamber have to be such that heat escapes very slowly. In general, heat can escape from a pluton by convection, diffusion (conduction), or by advection of groundwater.

Conduction can be assessed by the heat equation of Fourier:

$$\Delta Q/\Delta t = -kA(\Delta T/\Delta x) \qquad (3.1)$$

where $\Delta Q/\Delta t$ is the amount of heat transferred over time, and k is the material thermal conductivity, A is the end surface area and $\Delta T/\Delta x$ is the thermal gradient. In order to maximize heat flow and cooling and therefore undercooling, a large temperature gradient is required which under plutonic conditions is unlikley.

Cooling by advection of meteoric water through fractures may also serve to cool intrusive bodies. Here the rate-limiting factor is the permeability of the intrusive and host rock. Given that the Eurajoki was likely intruded at a depth of at least 10 km (Haapala & Rämö, 1992), it is expected that the permeability of the surrounding host rocks was low. Obviously granites do not have significant matrix permeability and fractures must provide channels for fluid flow. Inspection of quarry faces and the very fact the granite is quarried show that the granites are not well fractured precluding significant cooling by advection of groundwater.

By calculating Rayleigh number, using the following formula, it is possible to estimate if convection was the principal heat loss process in Eurajoki plutons:

$$Ra = (g\alpha\Delta T L^3)/\kappa\nu \qquad (3.2)$$

where g is the gravitational constant (980.7 cm/s^2), α is the coefficient of thermal expansion, ΔT is the temperature difference, L is the thickness, ν is the kinematic viscosity and κ is thermal diffusivity.

Although we calculated critical Rayleigh numbers above and below the threshold for free convection there is so much uncertainty in the selection of the parameters that the results are

not useful. Depending on the scale of the intrusion and the viscosity selected our results varied over 10 orders of magnitude. The Ra number is critically dependent upon the characteristic length scale and uncertainty exists whether granites are emplaced as dykes or diapirs (Clemens, 1998). Hence to evaluate the possibility of convective cooling we defer to the field observations. The process is discounted because there is no evidence of flow banding or crystal alignment as seen in mafic intrusive bodies.

Thus it is most likely that thermal convection and advection heat transport mechanisms were minimal at Eurajoki and that heat loss was dominated by diffusion producing a small undercooling and coarsening of feldspars.

Because the curvature of the CSDs is pronounced (as seen in Figure 3.11), there is a large gap in size between phenocrysts and groundmass, meaning that the period of coarsening must have been relatively long. The high characteristic length of the topaz granite crystals translates to even more coarsening, as shown on the Figure 3.12 (E). Remember, the topaz granite formed after the biotite granite that surrounds it. The biotite granite may served as an insulator between the topaz granite and the Tarkki granite, so that heat was not lost quickly and temperature was buffered. The middle of the Väkkärä granite, the topaz granite, stayed warm, cooling was at is slowest, nucleation was nil, and the coarsening of the crystals occurred, while in the biotite granite, heat was rapidly loss to the cool walls of the Tarkki granite, nucleation rate was relatively high, growth rate was moderate such that crystals

remained relatively small, coarsening almost nil, and the CSDs following almost a straight line as predicted by Marsh (1988, 1998).

In the topaz granite, a loss of pressure, volatiles or simply uplift, restarted nucleation and growth by resuming rapid undercooling, giving the final crystals as illustrated by the "groundmass" CSD. Haapala (1997) reported that the late-stage magmatic topaz crystals crystallized in response to a loss of pressure and this same event could have halted coarsening in the granite, resumed rapid effective undercooling, and restarted nucleation and crystallization of feldspar. Other minerals produced by magmatic processes were not affected by slowing of the undercooling recorded by feldspars because their liquidi are not at the same temperature. Unfortunately there are not enough crystals of other minerals to do a relatively precise CSD, except perhaps quartz that forms around 20% of the minerals.

Haapala (1977, 1997) noticed the presence of a late fluid phase and subsolidus reaction that produced cavities and pegmatite. Some topaz crystals were also produced during the late-stage of solidification, probably by metasomatism (Haapala, 1997), rather than by igneous process.

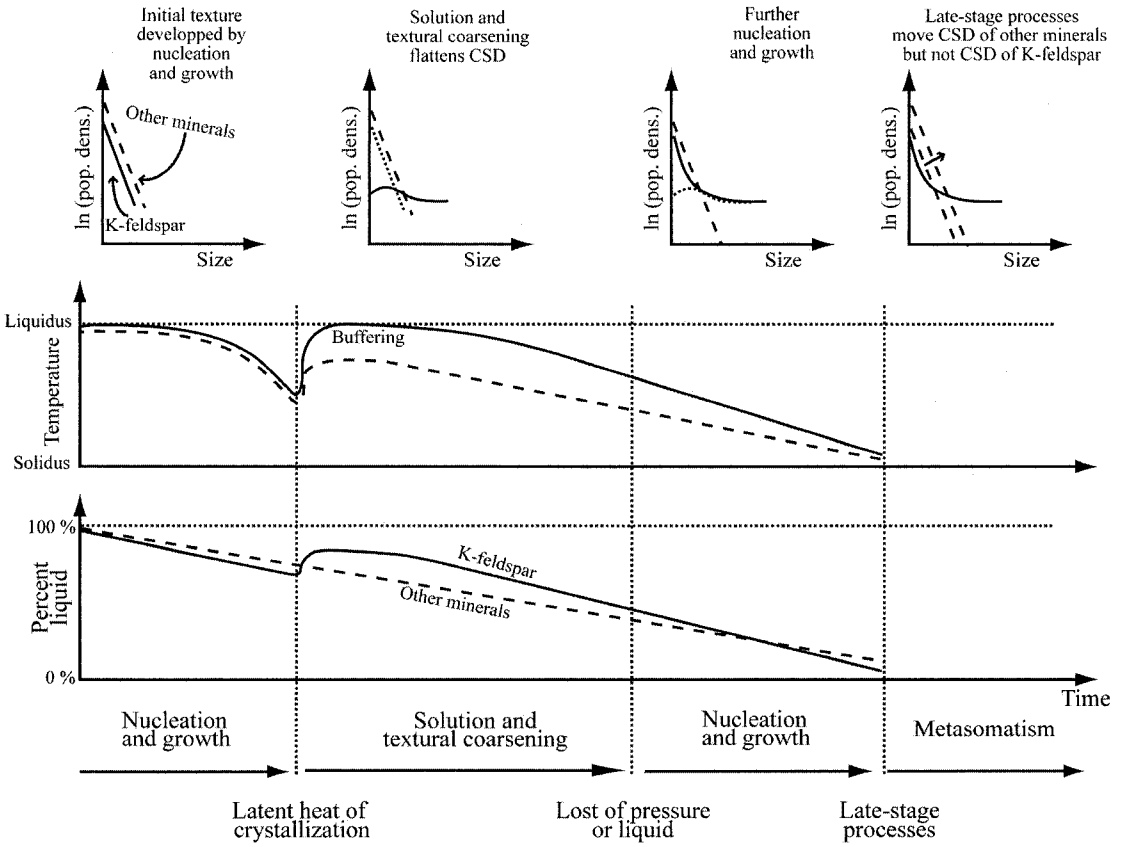

Figure 3.14: Dynamic model for the development of textures in the Väkkärä granite. Potassic feldspar model is compared to the theorical model of other minerals.

Conclusion

Quantitative textural analysis of a series of samples from the Eurajoki stock indicate that the potassic feldspar crystals have been texturally coarsened. Coarsening followed in part the communicating neighbours model of Dehoff (1991). This process accounts for the size variation of the feldspars in the stock.

In the Tarkki granite, two distinct episodes, of textural coarsening have occurred to produce the megacrysts and phenocrysts. These episodes of coarsening, the last one relatively short, were possibly due to the presence of the still hot Laittila Batholith which slowed undercooling in the granite and buffered temperature near the liquidus of potassic feldspar.

In the Väkkärä granite, textural coarsening also played a role in producing the textures. Some parts of the granite, mainly the biotite granite, show little evidence of textural coarsening. Because it was in contact with Tarkki granite that was already cooled when the Väkkärä granite was emplaced, no process slowed undercooling and produced conditions required for textural coarsening. However, in the middle part of the granite, the topaz bearing granite, there is evidence of textural coarsening. The biotite granite played a role of insulator and helped retain the latent heat of the topaz-bearing granite, slowing undercooling and buffering the temperature near the liquidus of potassic feldspar.

Chapter 4

South Mountain Batholith

Introduction

In this chapter, CSDs will be used to understand how the South Mountain Batholith solidified and to identify the most important texture-forming processes involved during solidification. CSD results will complement the mineralogy, structural geology, and geochemical work done by others, thus giving a better understanding of the intrusion.

Local geology and previous work

The South Mountain Batholith (SMB) is located in southwestern Nova Scotia, covers approximately 7300 $km^{2,}$ and is part of the Appalachian Orogen. The batholith was emplaced in the Meguma Terrane around 370 Ma (MacDonald *et al.*, 1992; Clarke & Halliday, 1980; Fairbairn *et al.*, 1964; Reynolds *et al.*, 1981; Reynolds *et al.*, 1987). It is overlain by coarse - clastic terrestrial sedimentary rocks (Bell & Blenkinshop, 1960; Howie & Barss, 1975) and/or ground moraine made of unconsolidated deposits (MacDonald *et al.*, 1992).

The emplacement of the SMB occurred during the Acadian Orogeny, when the collision between Gondwana and North America took place (Horne *et al.*, 1992; Benn *et al.*, 1997;

Benn *et al.*, 1999), thus producing a syntectonic granite batholith emplaced within an active contractional orogen (Benn *et al.*, 1999). The SMB has a tabular shape, with elongated root zones that represent magma feeder zones (Benn *et al.*, 1999), consistent with the transport of granitic magma in dykes that may have exploited a major Acadian shear zone (Benn *et al.*, 1999).

Geological mapping of the SMB started with the work of Fairbault (1908) and continued with mapping by Fairbault (1924), Taylor (1969), Smitheringale (1973), Charest (1976), Smith (1974), McKenzie & Clarke (1975) and Keppie (1979). Typically these publications were the result of reconnaissance mapping and therefore covered large regions, however some were very detailed and restricted to small areas.

MacDonald *et al.* (1992) provides the most detailed and recent mapping of the whole SMB (Figure 4.1). The batholith was divided into 6 main rock types (biotite granodiotite, biotite monzogranite, muscovite-biotite monzogranite, coarse grained leucomonzogranite, fine-grained leucomonzogranite and leucogranite) on the basis of modal proportions of quartz, alkali feldspar and plagioclase (Streckeisen, 1975), grain size, texture and accessory minerals. Also, several small bodies (<100 m^2 – 1 km^2) of fine grained, often porphyritic, granodiorite and monzogranite containing a high percentage of biotite, and commonly, metasedimentary xenoliths, termed mafic porphyry were mapped (MacDonald *et al.*, 1992).

MacDonald et al. (1992) outlined 13 plutons (Table 4.1) that comprise the SMB (MacDonald *et al.*, 1994). These plutons were further divided into 2 stages: The early stage 1 (Scrag lake, Little Round Lake, Cloud Lake, Salmontail Lake and Five Mile Lake plutons) is mostly comprised of biotite granodiorite, biotite monzogranite and minor fine-grained leucomonzogranite, and; the late stage 2 plutons (Davis Lake, Kejimkujik, Morse Road, West Dalhousie, East Dalhousie, New Ross, Big Indian Lake and Halifax) are composed mostly of two-mica monzogranite, coarse- and fine grained leucomonzogranite, and leucogranite. Some of the observations and differences between the 2 stages are: stage 2 plutons invariably intrude stage 1 plutons; stage 1 plutons are elliptical in shape while stage 2 plutons are more circular; prominent primary flow features (schlieren, parallel alignment of megacrysts/xenoliths) are common in stage 1 plutons whereas they are variably developed in stage 2 plutons (Figure 4.2) (MacDonald *et al.*, 1992).

Granodiorite and biotite monzogranite units are generally medium to coarse grained with or without megacrystic textures, and contain biotite, metasedimentary xenoliths and traces of muscovite and cordierite (MacDonald *et al.*, 1994). Muscovite-biotite monzogranite units are medium to coarse grained with megacrystic or seriate textures, and contain biotite, muscovite, traces of cordierite and some metasedimentary xenoliths (MacDonald *et al.*, 1994). Coarse-grained leucomonzogranite units are medium to coarse grained with megacrystic or seriate textures, and contain biotite, muscovite traces of cordierite and andalusite plus some metasedimentary xenoliths (MacDonald *et al.*, 1994). Fine-grained leucomonzogranite units are fine to medium grained with porphyritic or equigranular

textures, containing biotite, muscovite traces of cordierite and andalusite and some metasedimentary xenoliths (MacDonald *et al.*, 1994). Muscovite leucogranite units are fine to medium grained with porphyritic, equigranular or pegmatitic textures, containing muscovite, topaz, traces of biotite, cordierite and andalusite (MacDonald *et al.*, 1994).

Petrographic differences noted throughout the SMB define a sequence from least evolved granodiorite to most evolved leucogranite, in the sense of differentiation (MacDonald *et al.*, 1992). Biotite with inclusions of apatite and zircon decreases from >25% within granodiorite units to nil in leucogranite units, whereas muscovite has an opposite trend (MacDonald *et al.*, 1992). Muscovite generally occurs as anhedral grains replacing potassic feldspars in granodiorite units, and as euhedral to subhedral magmatic grains in fine-grained leucomonzogranite and leucogranite units (MacDonald *et al.*, 1992). Alkali feldspar is invariably perthitic (Figure 4.2E), dominantly so in granodiorite and monzogranite units, whereas in leucogranite units the alkali feldspar is rarely perthitic (MacDonald *et al.*, 1992). Plagioclase is typically either normally or reverse zoned in granodiorite and biotite monzogranite (Figure 4.2) units and unzoned in leucogranite units (MacDonald *et al.*, 1992). Subhedral to euhedral magmatic topaz is restricted to leucogranite rocks (MacDonald *et al.*, 1992; Kontak, 1990).

Table 4.1: Summary of selected features of Phase 1 and Phase 2 plutons (modified from MacDonald *et al.*, 1992).

A) Early Stage 1 Plutons

PLUTON NAME	ROCK TYPES (% of Pluton)	ZONING	SHAPE	FAULT BOUNDED	PRIMARY FEATURES
Scrag Lake	BMG(79); BGD(21)	N and R	elongate	partially	well developped megacryst alignment
Little Round lake	BMG(100)	R	elongate	partially	well developped megacryst alignment
Cloud lake	BMG(95); BGD(5)	none	elongate	partially	pervasive developped megacryst alignment
Salmontail Lake	BMG(91); BGD(8); FGLMG(1)	N	elongate	partially	weakly developped megacryst alignment
Five Mile Lake	BGD(100)	R	elliptical	partially	moderate megacryst alignment

B) Late Stage 2 Plutons

PLUTON NAME	ROCK TYPES (% of Pluton)	ZONING	SHAPE	FAULT BOUNDED	PRIMARY FEATURES
Davis Lake	CGLMG(93); FGLMG(3); BMG(1); BGD(1); MBMG(1); LG(<1)	N	circular and elongate	partially	well developped megacryst alignment
Kejimkujik	MBMG(100)	none	roughly circular	no	no consistent alignment
Morse Road	CGLMG(85); MBMG(15)	none	roughly circular	no	no consistent alignment
West Dalhousie	MBMG(100)	none	roughly circular	partially	well developped megacryst alignment
East Dalhousie	CGLMG(52); FGLMG(34); ULG(10); MBMG(4)	none	narrow dike-like	predominantly	locally-developped megacryst alignment
Big Indian lake	CGLMG(81); FGLMG(17); BMG(2)	none	circular/irregular	partially	no consistent alignment
New Ross	CGLMG(59); FGLMG(28); MBMG(12); ULG(2)	N and R	roughly circular	partially	megacryst alignment defines weakly-developed circular patterns
Halifax	CGLMG(38); MBMG(33); BMG(13); FGLMG(12); BGD(4)	N and R	roughly circular	no	megacryst alignment defines weakly-developed circular patterns

Rock Types: BGD-biotite granodiorite; BMG-biotite monzogranite; MBMG-muscovite-biotite monzogranite; CGLMG-coarse-grained leucomonzogranite; FGLMG-fine-grained leucomonzogranite; ULG-ultra-leucogranite; LG-leucogranite
Zoning: N-normal; R-reverse

The SMB is host to numerous polymetallic mineral deposits (Sn, W, U, Mo) and occurences resulting from the deposition of late to post magmatic hydrothermal fluids (MacDonald *et al.*, 1992). Most of the mineral deposits are found in the leucogranites of the SMB, with the best known one being the East Kemptville Sn-Cu-Zn-Ag deposit, found in the East Kemptville leucogranite, with reserves estimated at 56 millions tons and an average grade of 0.165% of Sn (Kontak, 1990). The mineralization at East Kemptville is modeled as a product of fractional crystallization of fluorine-rich melt generated by crustal anatexis. The muscovite and topaz crystallized under magmatic conditions and the magma did not reach fluid saturation (Kontak, 1990). Mineralization in the other leucogranites may represent localized concentrations of components from a volatile rich fluid phase (Clarke *et al.*, 1993).

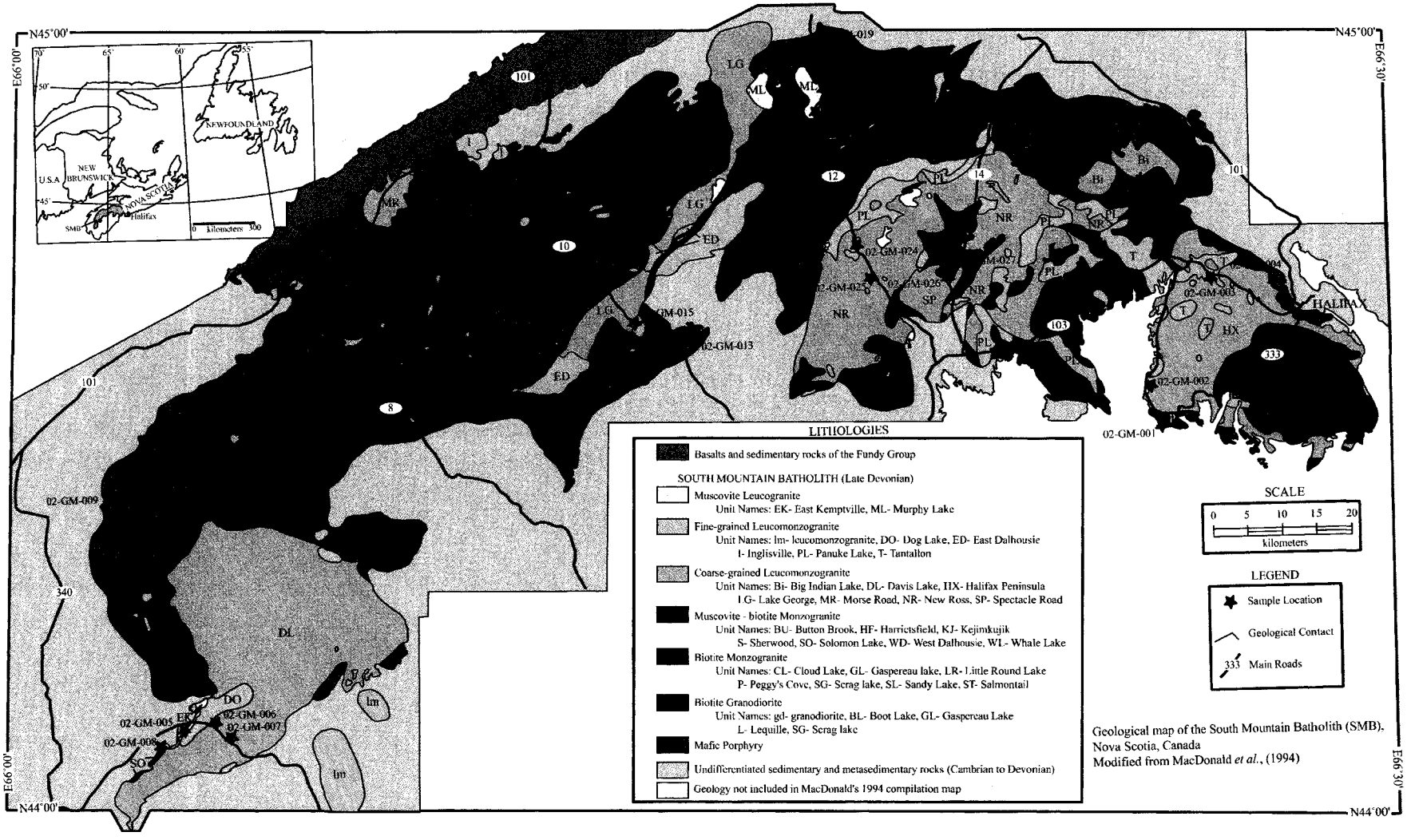

Figure 4.1: Geological Map of the South Mountain Batholith after MacDonald *et al.,* (1994)

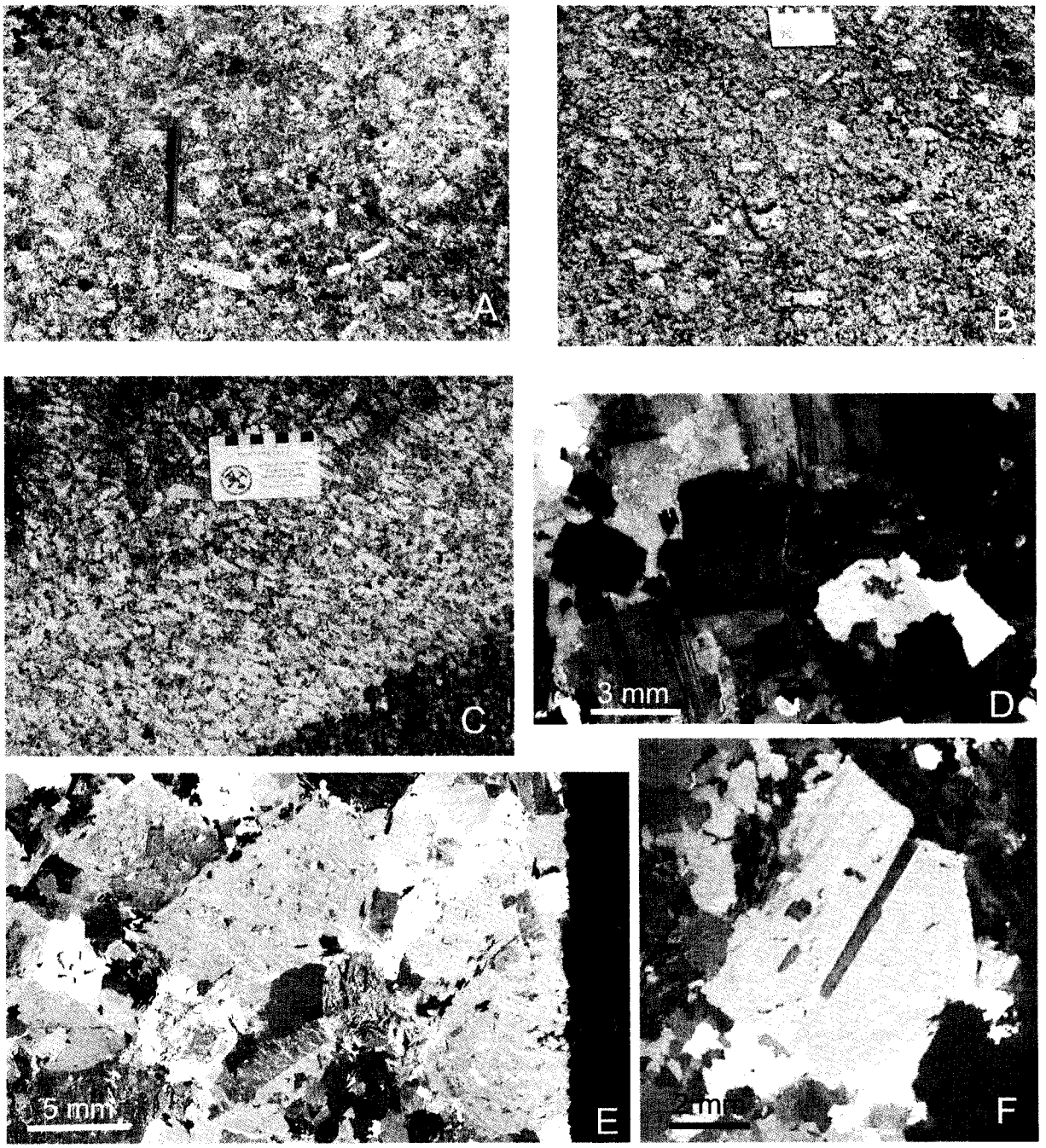

Figure 4.2: (A) Euhedral feldspar megacrysts in outcrop 02-GM-003 from Tantallon Pluton (late stage 2 plutons). (B) Aligned megagrysts in biotite monzogranite (02-GM-010) from Scrag Lake Pluton (Early stage 1). (C) Aligned megagrysts in muscovite-biotite monzogranite (02-GM-017) from West Dalhousie Pluton (Late stage 2). (D) Plagioclase zoning in sample 02-GM-012 from a fine-grained leucomonzogranite from an unnamed pluton. (E) Perthitic texture in potassic feldspar in muscovite-biotite monzogranite (02-GM-017) from West Dalhousie Pluton. (F) Plagioclase zoning in sample 02-GM-019 from a biotite granodiorite from Gaspereau Lake pluton.

Sampling strategy

Sampling in the South Mountain Batholith was done over a two-week period in the summer of 2002. The sampling sites were chosen (see Figure 4.1) to be representative of all the granitic phases in the area. Due to the large area covered by the SMB most specimens were taken from roadcuts along major roads traversing the batholith and are described in Appendix C. This strategy also allowed for examination of fairly large outcrops in several dimensions and enabled the sampling of large fresh blocks.

Quantitative textural studies

The CSD of crystals is a volumetric measure, but crystal sizes and numbers were measured in two dimensions as described previously (see chapter 2) for every sample of the South Mountain Batholith, hence the raw data must be inverted. The program *CSD Corrections* 1.3 (Higgins, 2000) was used to calculate potassic and plagioclase feldspar CSDs. The overall shape (Short:Intermediate:Long dimensions) of the crystals was estimated from the statistical distribution of intersection width/length ratios (W/L) measured in two dimensions (Higgins, 1994), using the formulas S/I=mode(W/L) and I/L=skewness(W/L)+0.5. This was done for every sample and the mean, 1:1.9:2.7 for potassic feldspar and 1:1.8:2.9 for plagioclase feldspar crystals, was taken as the shape of the crystals. All samples had angular crystals (no rounding) and no obvious metamorphic foliation. In the field, megacrysts alignment was

observed at some outcrops, but this was not obviously seen in the samples, so all samples were assumed to have no foliation when CSDs were calculated.

Results obtained with *CSD Corrections* are presented in Table 4.2 to 4.5, these tables contain the results of all the measurements done at different scales (slabs, thin sections). The CSD data were then plotted following Marsh (1988) (Figure 4.3 to 4.5). During computation with *CSD Corrections*, the bin size interval was chosen so that each size interval was reasonably populated. This also ensured that the total number of bins was low and hence that the errors introduced during the data conversion from 2D to 3D were minimized. There were no bins without crystals. Large size intervals with only one or two crystals and small size intervals with very large uncertainties were removed from the CSD diagrams, as they are imprecise. The errors as calculated by *CSD Corrections*, in other points are small relative to the data points of the plots, and have therefore error-bars have been omitted so as to reduce clutter in all CSD plots.

South Mountain Batholith - potassic feldspar stage 1														
Rock Type	Biotite granodiorite	Biotite granodiorite	Biotite granodiorite	Biotite granodiorite	Biotite granodiorite	Biotite granodiorite	Biotite granodiorite	Biotite granodiorite	Biotite granodiorite	Biotite granodiorite	Biotite monzogranite	Biotite monzogranite	Biotite monzogranite	Biotite monzogranite
Pluton Name	Scrag Lake	Scrag Lake	Scrag Lake	Scrag Lake	Gaspereau Lake	Gaspereau Lake	Gaspereau Lake	Gaspereau Lake	Unnamed granodiorite	Unnamed granodiorite	Peggy's Cove	Peggy's Cove	Sandy Lake	Sandy Lake
Sample number	*02-GM-009*	*02-GM-009*	*02-GM-016*	*02-GM-016*	*02-GM-019*	*02-GM-019*	*02-GM-020*	*02-GM-020*	*02-GM-028*	*02-GM-028*	*02-GM-001*	*02-GM-001*	*02-GM-004*	*02-GM-004*
Type of sample	rock slab	stained thin section	rock slab	stained thin section	rock slab	stained thin section	rock slab	stained thin section	rock slab	stained thin section	rock slab	stained thin section	rock slab	stained thin section
Upper size limit (mm)														
39.80														
25.10											1			
15.90	1				2				1		1	1	1	
10.00	4				5		3		4	1	15	4	9	1
6.31	4	2	1		23		18	1	32	3	53	5	19	1
3.98	33	8	6		50		56	8	83	13	72	3	54	3
2.51	115	5	13		77	1	103	17	142	13	95	5	102	4
1.59	229	7	18		114	10	186	42	172	13	173	12	231	8
1.00	179	20	27		85	12	155	56	136	12	280	9	440	12
0.63	10	31	63		7	19	6	109	6	19	145	22	265	17
0.40		38	89	3	1	41		146		49		54	1	24
0.25		79	124	4		60		210		62		153		31
0.16		11	24	20		17		25		6		85		5
0.10				31				1						
0.06				101										
0.04				54										
0.03				50										
0.02				2										
Total	575	201	365	265	364	160	527	615	576	191	835	353	1122	106
Area measured (mm2)	27060	1809	9733	1867	22725	1720	24676	2240	27478	1920	34439	1822	42882	1576

Table 4.2: Intersection widths distributions of potassic feldspar crystals in stage 1 plutons from the South Mountain Batholith

South Mountain Batholith - potassic feldspar stage 1												
Rock Type	Biotite monzogranite	Biotite monzogranite	Biotite monzogranite	Biotite monzogranite	Biotite monzogranite	Biotite monzogranite	Biotite monzogranite	Biotite monzogranite	Biotite monzogranite	Biotite monzogranite	Biotite monzogranite	Biotite monzogranite
Pluton Name	Scrag Lake	Scrag Lake	Little Round Lake	Little Round Lake	Little Round Lake	Little Round Lake	Cloud Lake	Cloud Lake	Salmontail	Salmontail	Salmontail	Salmontail
Sample number	02-GM-010	02-GM-010	02-GM-013	02-GM-013	02-GM-014	02-GM-014	02-GM-018	02-GM-018	02-GM-022	02-GM-022	02-GM-023	02-GM-023
Type of sample	rock slab	stained thin section	rock slab	stained thin section	rock slab	stained thin section	rock slab	stained thin section	rock slab	stained thin section	rock slab	stained thin section
Upper size limit (mm)												
39.80												
25.10	3				3		1				4	
15.90	10		1		3		9		1		8	
10.00	18	3	0		18		12		6		15	1
6.31	34	3	4		52		18	1	28	2	24	3
3.98	34	2	13	2	124	10	68	2	89	8	31	0
2.51	100	4	33	4	182	12	133	6	225	20	44	3
1.59	219	6	198	20	286	29	403	24	470	36	109	13
1.00	338	11	545	68	261	34	397	54	320	35	134	18
0.63	246	23	404	118	21	62	49	78	23	67	11	35
0.40	23	61	8	162		70		109		88		44
0.25		84		222		93		141		120		70
0.16		8		45		21		26		16		127
0.10		1		2						2		38
0.06												2
0.04												
0.03												
0.02												
Total	1025	206	1206	643	950	331	1090	441	1162	394	380	354
Area measured (mm2)	36327	1975	31964	1859	39025	1705	36747	1660	37746	1760	40925	1829

Table 4.2 (continued): Intersection widths distributions of potassic feldspar crystals in stage 1 plutons from the South Mountain Batholith

South Mountain Batholith - plagioclase feldspar stage 1															
Rock Type	Biotite granodiorite	Biotite granodiorite	Biotite granodiorite	Biotite granodiorite	Biotite granodiorite	Biotite granodiorite	Biotite granodiorite	Biotite granodiorite	Biotite granodiorite	Biotite granodiorite	Biotite monzogranite	Biotite monzogranite	Biotite monzogranite	Biotite monzogranite
Pluton Name	Scrag Lake	Scrag Lake	Scrag Lake	Scrag Lake	Gaspereau Lake	Gaspereau Lake	Gaspereau Lake	Gaspereau Lake	Unnamed granodiorite	Unnamed granodiorite	Peggy's Cove	Peggy's Cove	Sandy Lake	Sandy Lake
Sample number	02-GM-009	02-GM-009	02-GM-016	02-GM-016	02-GM-019	02-GM-019	02-GM-020	02-GM-020	02-GM-028	02-GM-028	02-GM-001	02-GM-001	02-GM-004	02-GM-004
Type of sample	rock slab	stained thin section	rock slab	stained thin section	rock slab	stained thin section	rock slab	stained thin section	rock slab	stained thin section	rock slab	stained thin section	rock slab	stained thin section
Upper size limit (mm)														
39.80														
25.10			1											
15.90	3		2				1		1		1		1	
10.00	27	1	7	1	19	1	10		21	3	5		14	
6.31	84	4	22	6	69	6	29	1	62	6	30	9	59	4
3.98	118	8	32	16	88	8	64	5	82	8	78	11	98	5
2.51	121	7	66	25	76	15	150	22	104	15	124	25	145	15
1.59	150	15	90	36	141	27	223	53	120	10	180	24	206	17
1.00	149	14	130	45	98	29	147	69	89	25	237	35	106	19
0.63	18	38	91	51	6	44	9	81	2	49	128	60	4	31
0.40		55	4	89		54		112		69	1	97		53
0.25		115		103		91		151		101		108		109
0.16		32		16		17		21		14		14		15
0.10		1				1								1
0.06														
0.04														
0.03														
0.02														
Total	670	290	445	388	497	293	633	515	481	300	784	383	633	269
Area measured (mm2)	27060	1809	9733	1867	22725	1720	24676	2240	27478	1920	34439	1822	42882	1576

Table 4.3: Intersection widths distributions of plagioclase feldspar crystals in stage 1 plutons from the South Mountain Batholith

South Mountain Batholith - plagioclase feldspar stage 1												
Rock Type	Biotite monzogranite	Biotite monzogranite	Biotite monzogranite	Biotite monzogranite	Biotite monzogranite	Biotite monzogranite	Biotite monzogranite	Biotite monzogranite	Biotite monzogranite	Biotite monzogranite	Biotite monzogranite	Biotite monzogranite
Pluton Name	Scrag Lake	Scrag Lake	Little Round Lake	Little Round Lake	Little Round Lake	Little Round Lake	Cloud Lake	Cloud Lake	Salmontail	Salmontail	Salmontail	Salmontail
Sample number	02-GM-010	02-GM-010	02-GM-013	02-GM-013	02-GM-014	02-GM-014	02-GM-018	02-GM-018	02-GM-022	02-GM-022	02-GM-023	02-GM-023
Type of sample	rock slab	stained thin section	rock slab	stained thin section	rock slab	stained thin section	rock slab	stained thin section	rock slab	stained thin section	rock slab	stained thin section
Upper size limit (mm)												
39.80												
25.10							1					
15.90	6		1				9		1			
10.00	22		4	1	19		14	1	8		17	
6.31	63	4	45	3	61	1	42	3	54	2	64	
3.98	113	4	122	13	125	6	123	10	147	11	136	9
2.51	102	7	242	11	220	14	218	20	299	36	241	21
1.59	171	15	402	36	371	29	390	40	405	52	293	32
1.00	236	8	429	57	253	31	283	63	252	55	199	36
0.63	127	15	141	76	14	70	22	112	7	62	18	54
0.40	3	46	3	94		114		141		93		38
0.25		88		174		193		218		143		57
0.16		13		37		52		25		19		66
0.10								1		1		20
0.06												1
0.04												
0.03												
0.02												
Total Area measured (mm2)	843	200	1389	502	1063	510	1102	634	1173	474	968	334
	36327	1975	31964	1859	39025	1705	36747	1660	37746	1760	40925	1829

Table 4.3 (continued): Intersection widths distributions of plagioclase feldspar crystals in stage 1 plutons from the South Mountain Batholith

South Mountain Batholith - potassic feldspar stage 2														
Rock	Muscovite-biotite	Muscovite-biotite	Muscovite-biotite	Muscovite-biotite	Coarse-grained	Coarse-grained	Coarse-grained leuco-	Coarse-grained leuco-	Coarse-grained leuco-	Coarse-grained leuco-	Coarse-grained leuco-	Coarse-grained leuco-	Coarse-grained leuco-	Coarse-grained leuco-
Type	*monzogranite*	*monzogranite*	*monzogranite*	*monzogranite*	*leucomonzogranite*	*leucomonzogranite*	*monzogranite*	*monzogranite*	*monzogranite*	*monzogranite*	*monzogranite*	*monzogranite*	*monzogranite*	*monzogranite*
Pluton Name	West Dalhousie	West Dalhousie	Sherwood	Sherwood	Halifax Peninsula	Halifax Peninsula	Davis Lake	Davis Lake	Davis Lake	Davis Lake	New Ross	New Ross	Spectacle Road	Spectacle Road
Sample number	02-GM-017	02-GM-017	02-GM-027	02-GM-027	02-GM-002	02-GM-002	02-GM-006	02-GM-006	02-GM-007	02-GM-007	02-GM-025	02-GM-025	02-GM-026	02-GM-026
Type of sample	rock slab	stained thin section	rock slab	stained thin section	rock slab	stained thin section	rock slab	stained thin section	rock slab	stained thin section	rock slab	stained thin section	rock slab	stained thin section
Upper size limit (mm)														
39.80									3					
25.10	1		1		2				12					
15.90	9		14	2	6		9		20		6		3	
10.00	49	2	22	0	19	1	8		39	2	21	1	30	
6.31	110	7	39	3	58	2	33	3	59	2	65	2	42	3
3.98	72	3	65	11	67	9	73	6	59	7	97	7	79	2
2.51	45	9	91	7	134	29	147	7	89	13	128	13	155	4
1.59	62	12	165	11	188	26	228	4	171	21	138	14	301	10
1.00	73	4	122	9	109	28	365	14	264	34	79	20	318	11
0.63	8	10	6	51	9	53	196	25	170	38	8	20	208	21
0.40		26		84		43	3	75	9	68		48	10	21
0.25		74		149		56		99		124		94		35
0.16		34		37		10		10		26		36		7
0.10		2								1				
0.06														
0.04														
0.03														
0.02														
Total	429	183	525	364	592	257	1062	243	895	336	542	255	1146	114
Area measured (mm2)	39849	1559	30798	1705	30169	1720	32171	1610	52511	3391	28000	1977	39306	1674

Table 4.4: Intersection widths distributions of potassic feldspar crystals in stage 2 plutons from the South Mountain Batholith

South Mountain Batholith - potassic feldspar stage 2													
Rock Type	Fine-grained leuco-monzogranite	Fine-grained leuco-monzogranite	Fine-grained leucomonzogranite	Fine-grained leucomonzogranite	Fine-grained leuco-monzogranite	Fine-grained leuco-monzogranite	Fine-grained leuco-monzogranite	Fine-grained leuco-monzogranite	Muscovite leucogranite	Muscovite leucogranite	Muscovite leucogranite	Muscovite leucogranite	Muscovite leucogranite
Pluton Name	Tantallon	Tantallon	Unnamed leucomonzogranite	Unnamed leucomonzogranite	East Dalhousie	East Dalhousie	Panuke Lake	Panuke Lake	East Kemptville	East Kemptville	East Kemptville	Murphy Lake	Murphy Lake
Sample number	02-GM-003	02-GM-003	02-GM-012	02-GM-012	02-GM-015	02-GM-015	02-GM-024	02-GM-024	02-GM-005	02-GM-008	02-GM-008	02-GM-021	02-GM-021
Type of sample	rock slab	stained thin section	rock slab	stained thin section	rock slab	stained thin section	rock slab	stained thin section	stained thin section	rock slab	stained thin section	rock slab	stained thin section
Upper size limit (mm)													
39.80			1										
25.10	5		2										
15.90	16		4		5		4			4			
10.00	44	1	13	3	33	1	31			27		1	
6.31	103	16	33	1	60	4	41	3		61		2	
3.98	152	21	59	2	57	5	56	2		150	6	11	
2.51	190	32	93	6	35	12	67	5	1	211	10	63	8
1.59	284	45	130	9	40	13	117	6	20	407	31	362	33
1.00	323	47	128	9	92	11	79	17	48	284	12	467	82
0.63	157	78	13	21	62	24	12	25	97	16	41	35	142
0.40	2	119		45	1	57		50	107		42		180
0.25		143		90		95		89	130		59		196
0.16		21		22		18		11	11		19		42
0.10				1							1		
0.06													
0.04													
0.03													
0.02													
Total	1276	523	476	209	385	240	407	208	414	1160	221	941	683
Area measured (mm2)	60357	1646	26227	1836	18120	1744	25113	1998	1865	33447	1532	31550	1680

Table 4.4 (continued): Intersection widths distributions of potassic feldspar crystals in stage 2 plutons from the South Mountain Batholith

South Mountain Batholith - plagioclase feldspar stage 2														
Rock	Muscovite-biotite	Muscovite-biotite	Muscovite-biotite	Muscovite-biotite	Coarse-grained	Coarse-grained	Coarse-grained leuco-	Coarse-grained leuco-	Coarse-grained leuco-	Coarse-grained leuco-	Coarse-grained leuco-	Coarse-grained leuco-	Coarse-grained leuco-	Coarse-grained leuco-
Type	monzogranite	monzogranite	monzogranite	monzogranite	leucomonzogranite	leucomonzogranite	monzogranite	monzogranite	monzogranite	monzogranite	monzogranite	monzogranite	monzogranite	monzogranite
Pluton Name	West Dalhousie	West Dalhousie	Sherwood	Sherwood	Halifax Peninsula	Halifax Peninsula	Davis Lake	Davis Lake	Davis Lake	Davis Lake	New Ross	New Ross	Spectacle Road	Spectacle Road
Sample number	02-GM-017	02-GM-017	02-GM-027	02-GM-027	02-GM-002	02-GM-002	02-GM-006	02-GM-006	02-GM-007	02-GM-007	02-GM-025	02-GM-025	02-GM-026	02-GM-026
Type of sample	rock slab	stained thin section	rock slab	stained thin section	rock slab	stained thin section	rock slab	stained thin section	rock slab	stained thin section	rock slab	stained thin section	rock slab	stained thin section
Upper size limit (mm)														
39.80														
25.10									4					
15.90							2		3		4			
10.00	5		6	3			8	1	23	2	6		13	3
6.31	10		42	5	1		29	1	28	6	30	2	62	3
3.98	50	7	87	10	5		68	15	67	16	77	6	135	12
2.51	120	13	187	19	11		110	15	105	19	160	14	197	19
1.59	285	28	241	12	19		267	26	250	48	191	16	319	19
1.00	191	49	125	29	19		470	33	328	42	106	16	297	29
0.63	11	64	4	83	11	1	281	80	185	84	11	41	76	32
0.40		80		149	6	6	12	175	6	164		53	5	47
0.25		116		204		40		113		269		109		66
0.16		49		37		83				72		27		18
0.10		1				96				1		1		
0.06						286								
0.04						104								
0.03						17								
0.02														
Total Area measured (mm2)	672 39849	407 1559	692 30798	551 1705	72 30169	633 1720	1247 32171	459 1610	999 52511	723 3391	585 28000	285 1977	1104 39306	248 1674

Table 4.5: Intersection widths distributions of plagioclase feldspar crystals in stage 2 plutons from the South Mountain Batholith

South Mountain Batholith - plagioclase feldspar stage 2													
Rock Type	Fine-grained leuco-monzogranite	Fine-grained leuco-monzogranite	Fine-grained leucomonzogranite	Fine-grained leucomonzogranite	Fine-grained leuco-monzogranite	Fine-grained leuco-monzogranite	Fine-grained leuco-monzogranite	Fine-grained leuco-monzogranite	Muscovite leucogranite	Muscovite leucogranite	Muscovite leucogranite	Muscovite leucogranite	Muscovite leucogranite
Pluton Name	Tantallon	Tantallon	Unnamed leucomonzogranite	Unnamed leucomonzogranite	East Dalhousie	East Dalhousie	Panuke Lake	Panuke Lake	East Kemptville	East Kemptville	East Kemptville	Murphy Lake	Murphy Lake
Sample number	02-GM-003	02-GM-003	02-GM-012	02-GM-012	02-GM-015	02-GM-015	02-GM-024	02-GM-024	02-GM-005	02-GM-008	02-GM-008	02-GM-021	02-GM-021
Type of sample	rock slab	stained thin section	rock slab	stained thin section	rock slab	stained thin section	rock slab	stained thin section	stained thin section	rock slab	stained thin section	rock slab	stained thin section
Upper size limit (mm)													
39.80													
25.10													
15.90	2		1										
10.00	13	1	29	3	3					2			
6.31	89	1	60	3	19	7	18			25	9		
3.98	132	12	97	14	47	20	52	12	1	79	9	6	
2.51	247	9	105	8	85	20	114	11	13	174	9	20	9
1.59	358	6	129	18	133	37	203	17	46	334	15	98	40
1.00	325	11	85	11	182	32	139	33	91	504	18	117	114
0.63	186	19	6	22	89	68	12	40	119	201	26	8	160
0.40	5	41		58	3	125		67	157	8	40		152
0.25		84		102		165		105	140		65		220
0.16		24		15		32		24	34		20		36
0.10													2
0.06													
0.04													
0.03													
0.02													
Total Area measured (mm2)	1357 60357	208 1646	512 26227	254 1836	561 18120	506 1744	538 25113	309 1998	601 1865	1327 33447	211 1532	249 31550	733 1680

Table 4.5 (continued): Intersection widths distributions of plagioclase feldspar crystals in stage 2 plutons from the South Mountain Batholith

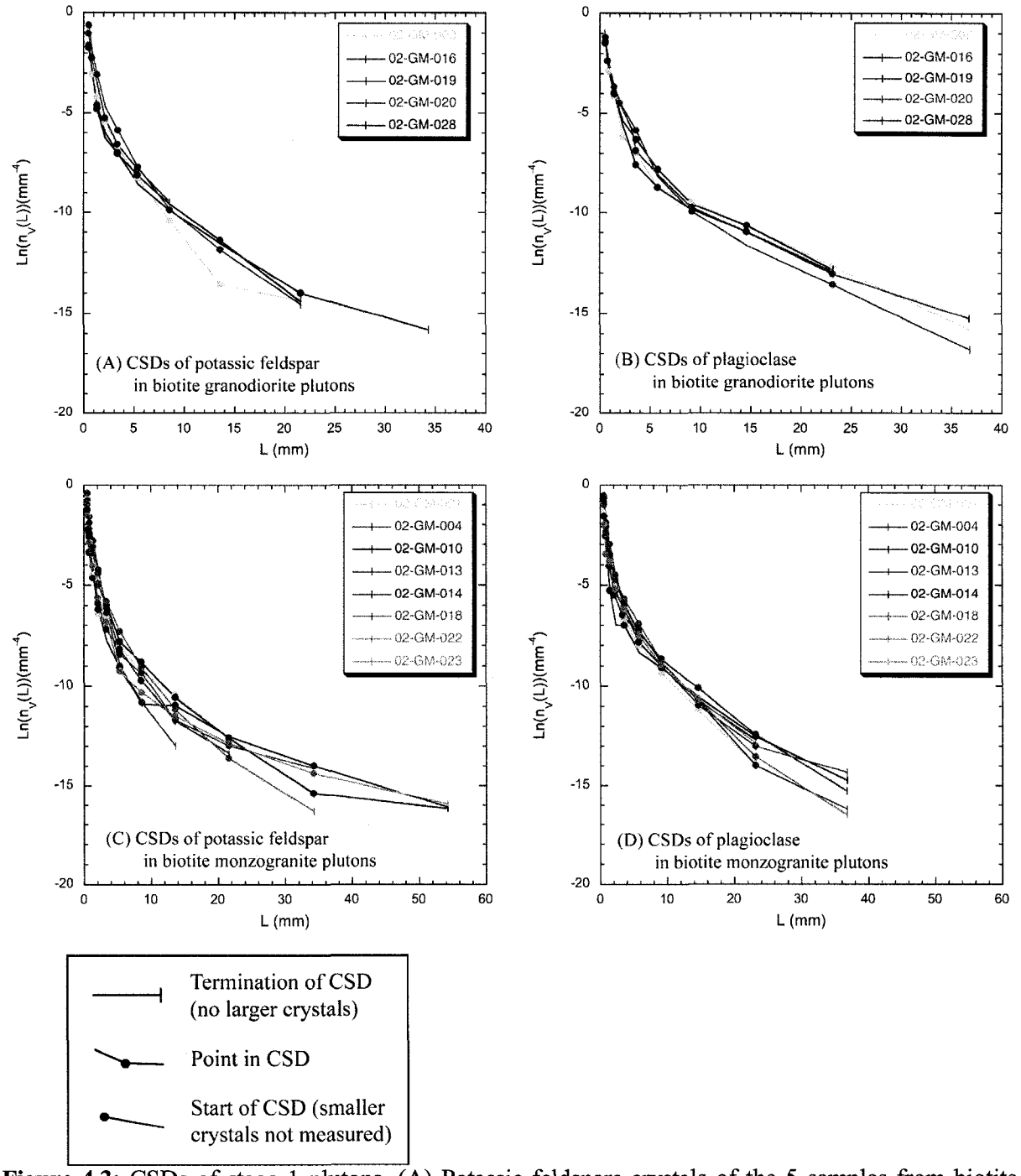

Figure 4.3: CSDs of stage 1 plutons. (A) Potassic feldspars crystals of the 5 samples from biotite granodiorite plutons as measured on rock slabs and thin sections. (B) Same specimens as (A) but for plagioclase crystals. (C) Potassic feldspars crystals of the 8 samples from biotite monzogranite plutons as measured on rock slabs and thin sections. (D) Same specimens as (C) but for plagioclase crystals.

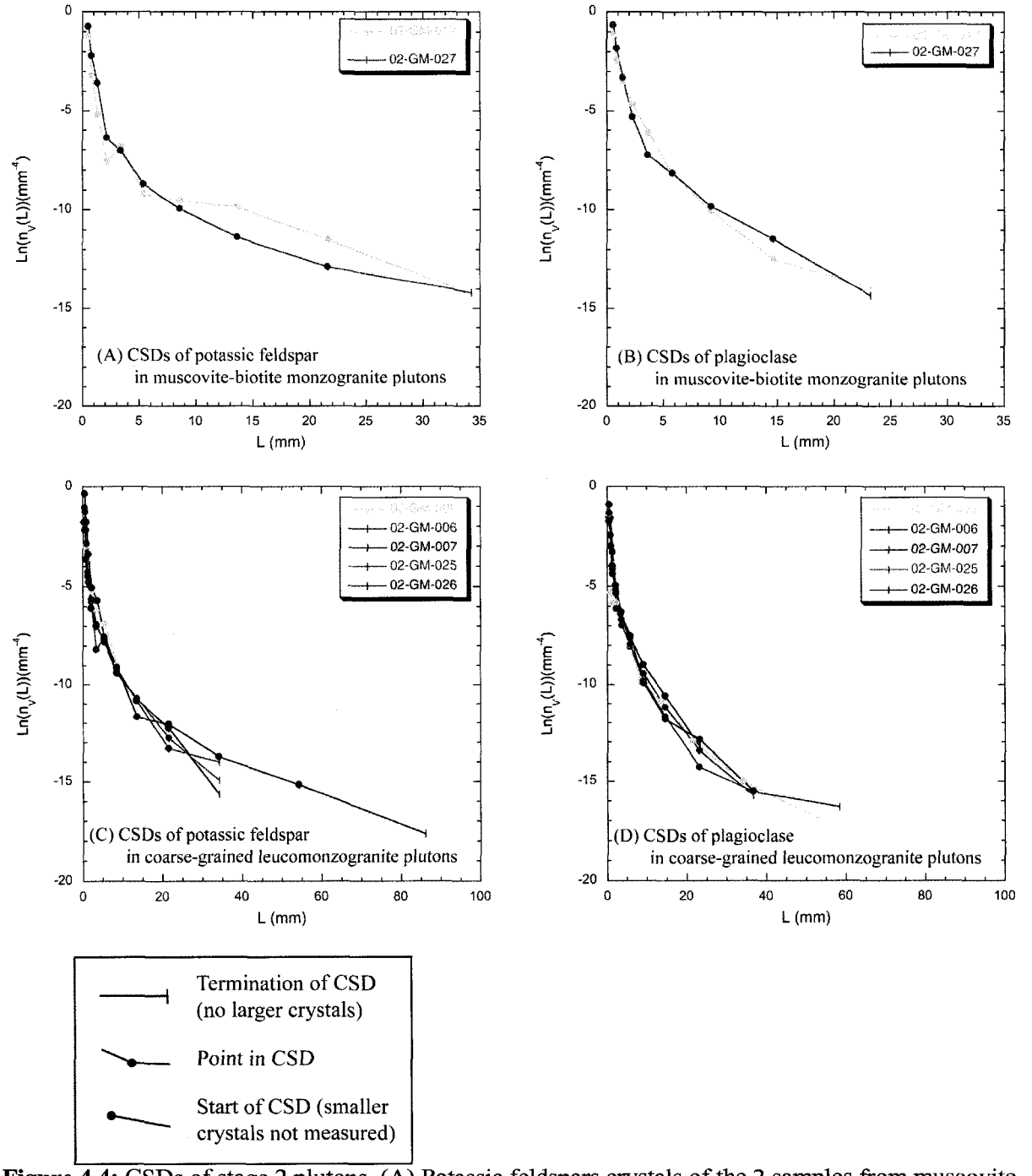

Figure 4.4: CSDs of stage 2 plutons. (A) Potassic feldspars crystals of the 2 samples from muscovite-biotite monzogranite plutons as measured on rock slabs and thin sections. (B) Same specimens as (A) but for plagioclase crystals. (C) Potassic feldspars crystals of the 5 samples from coarse-grained leucomonzogranite plutons as measured on rock slabs and thin sections. (D) Same specimens as (C) but for plagioclase crystals.

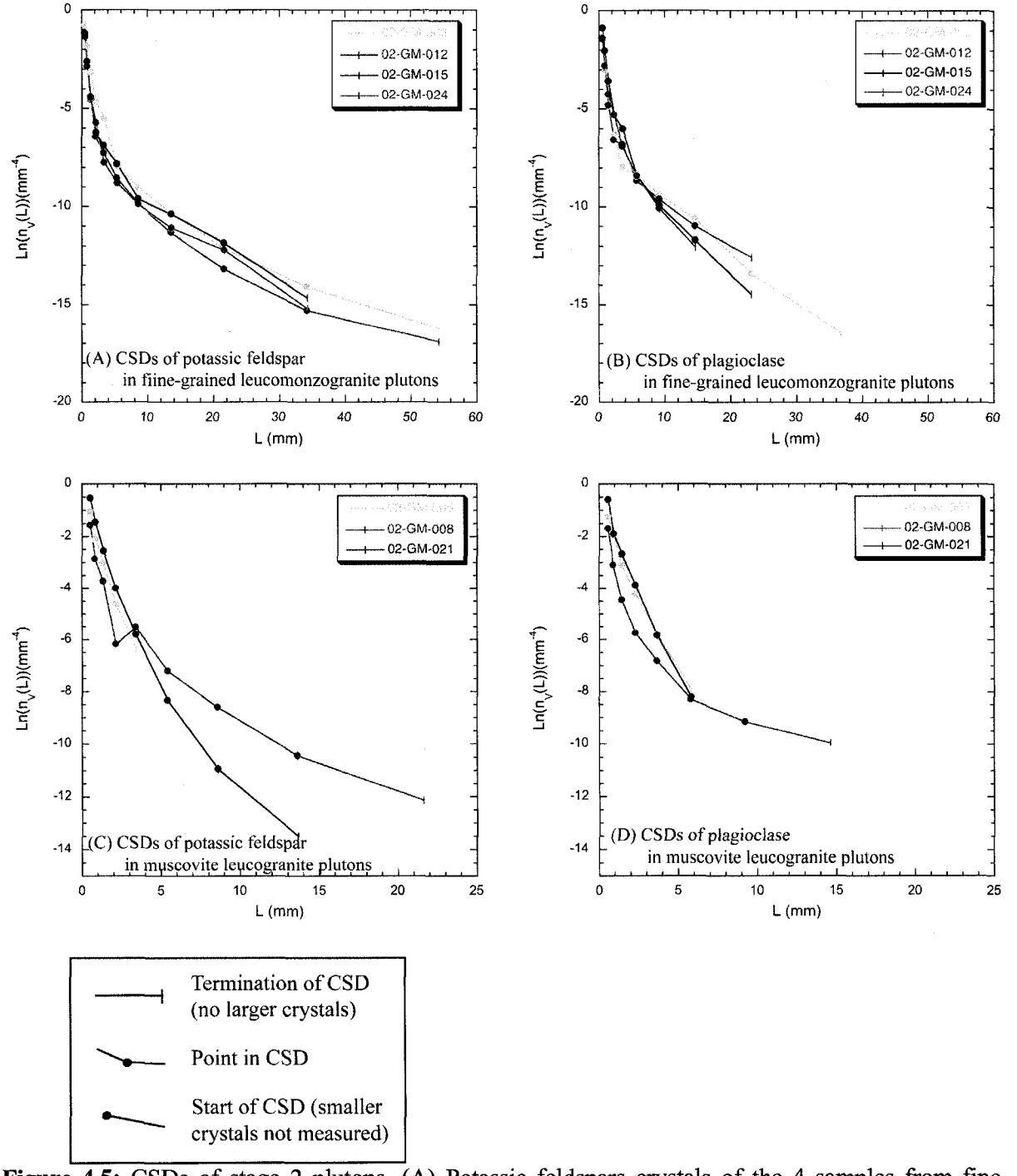

Figure 4.5: CSDs of stage 2 plutons. (A) Potassic feldspars crystals of the 4 samples from fine-grained leucomonzogranite plutons as measured on rock slabs and thin sections. (B) Same specimens as (A) but for plagioclase crystals. (C) Potassic feldspars crystals of the 3 samples from muscovite leucogranite plutons as measured on rock slabs and thin sections. (D) Same specimens as (C) but for plagioclase crystals.

CSDs of early stage 1 plutons show that, all biotite granodiorite plutons CSDs have a maximum population density at sizes between 0.6 and 0.8 mm, while CSDs of biotite monzogranite plutons have a maximum population density at sizes between 0.5 and 0.6 mm for both plagioclase and potassic feldspar crystals (Figure 4.3). The maximum crystal size showed by CSDs varies from 9 to 34 mm for potassic feldspar and from 23 to 37 mm for plagioclase in biotite granodiorite plutons. In the biotite monzogranite plutons it varies from 14 to 55 mm for potassic feldspar and from 23 to 37 mm for plagioclase. For both plutons, the CSD curves for values less than the maximum have negative slopes and are concave upward.

Four rock types compose the late stage 2 plutons and CSDs show that: all muscovite-biotite monzogranite plutons have a maximum population density at sizes 0.6 mm for both plagioclase and potassic feldspar crystals: all coarse-grained leucomonzogranite plutons have a maximum population density at sizes between 0.3 and 1.0 mm for both plagioclase and potassic feldspar crystals: all fine-grained leucomonzogranite plutons have a maximum population density at sizes between 0.4 and 0.5 mm for both plagioclase and potassic feldspar crystals, and: all muscovite leucogranite plutons have a maximum population density at sizes ≈0.6 mm for both plagioclase and potassic feldspar crystals (Figure 4.4 and 4.5). The maximum crystal size, as shown by CSDs, is approximately 34 mm for potassic feldspar and about 23 mm for plagioclase in muscovite-biotite monzogranite plutons. In the coarse-grained leucomonzogranite plutons it varies from 14 to 86 mm for potassic feldspar and from 23 to 58 mm for plagioclase. In the fine-grained leucomonzogranite plutons it varies from 34

to 54 mm for potassic feldspar and from 15 to 37 mm for plagioclase. And finally for the muscovite leucogranite plutons it varies from 3.5 to 22 mm for potassic feldspar and from 3.4 to 15 mm for plagioclase. For all plutons, except two samples of muscovite leucogranite, the part of the CSDs to the right of the maximum have a negative slope and are concave upwards. Two samples of muscovite leucogranite have straight CSDs and a negative slope.

Since most of the CSDs are curved it is not appropriate to estimate slopes and intercepts. By separating CSDs curves in two, at the point of flexure, and by doing a linear regression on both parts, the slope and intercept of both parts were estimated with relative confidence (see chapter 3). The linear regressions are named groundmass and phenocrysts, the former for the smaller sizes of crystals and the latter for the larger. Points in each CSD are separated into these 2 groups. The point of separation (crystal size) was chosen for each sample in a way to attain the highest degree of confidence for each regression line (phenocrysts and groundmass), but in most case the separation is usually done around 5 mm.

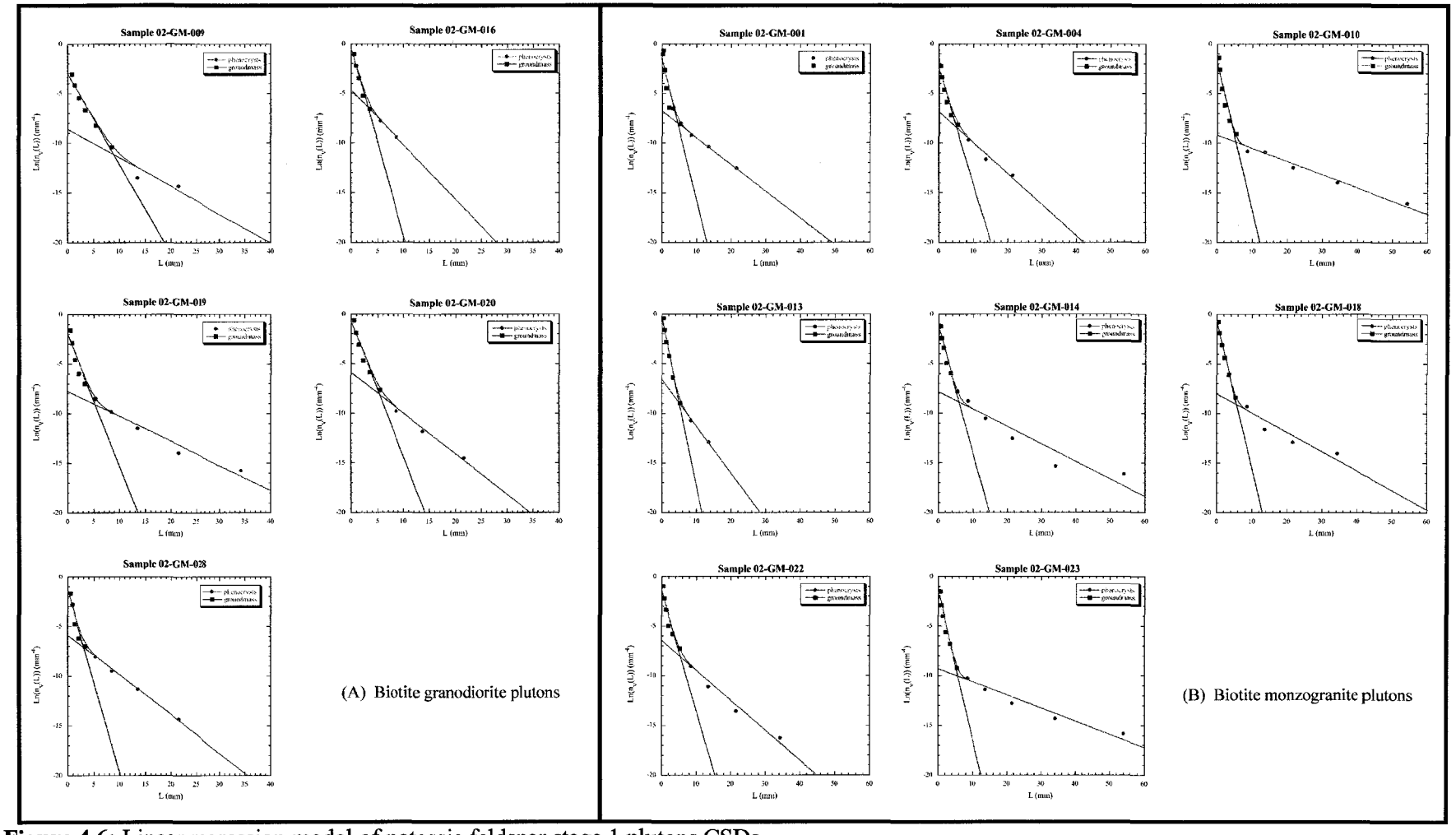

Figure 4.6: Linear regression model of potassic feldspar stage 1 plutons CSDs.

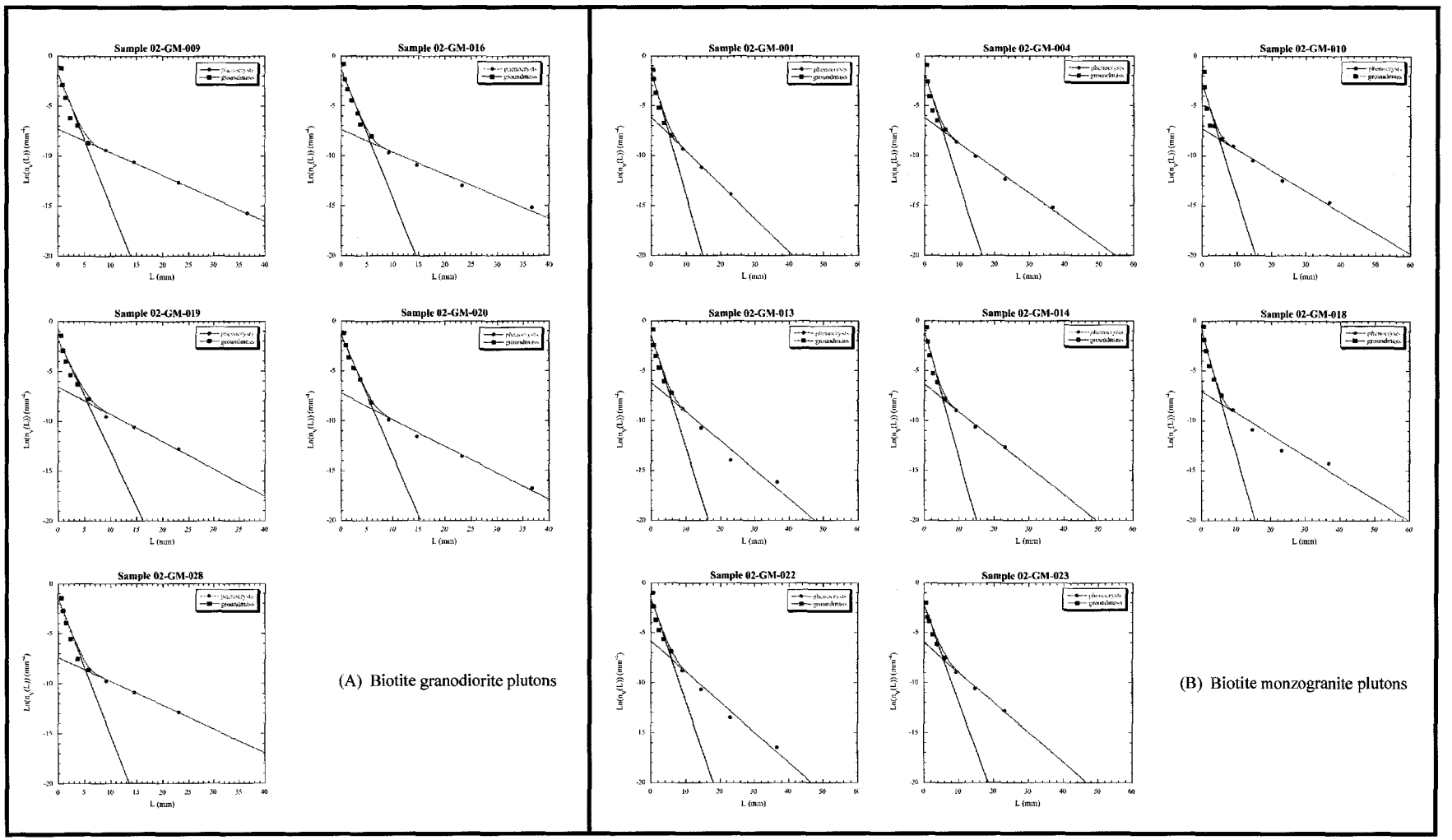

Figure 4.7: Linear regression model of plagioclase stage 1 plutons CSDs.

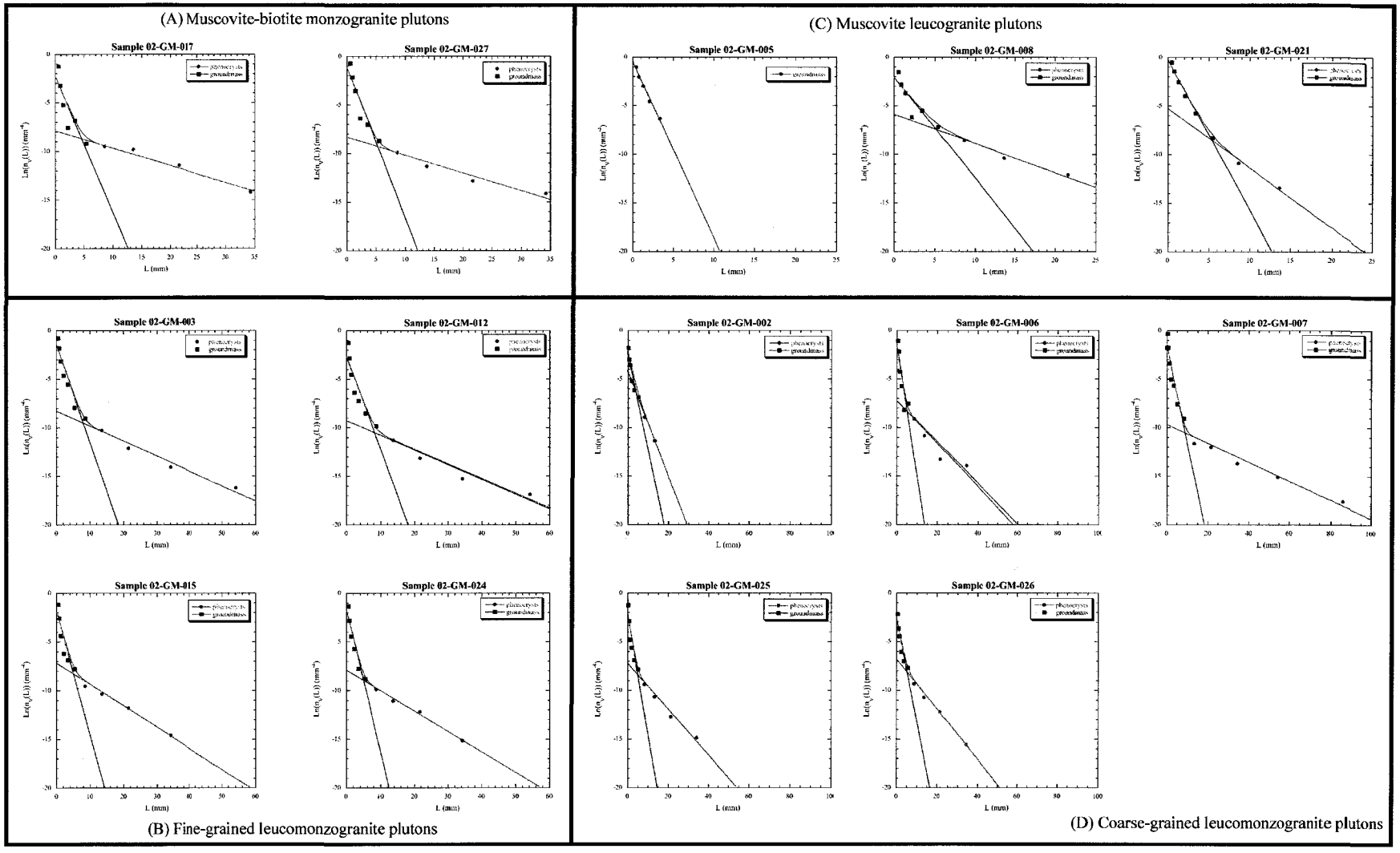

Figure 4.8: Linear regression model of potassic feldspar stage 2 plutons CSDs.

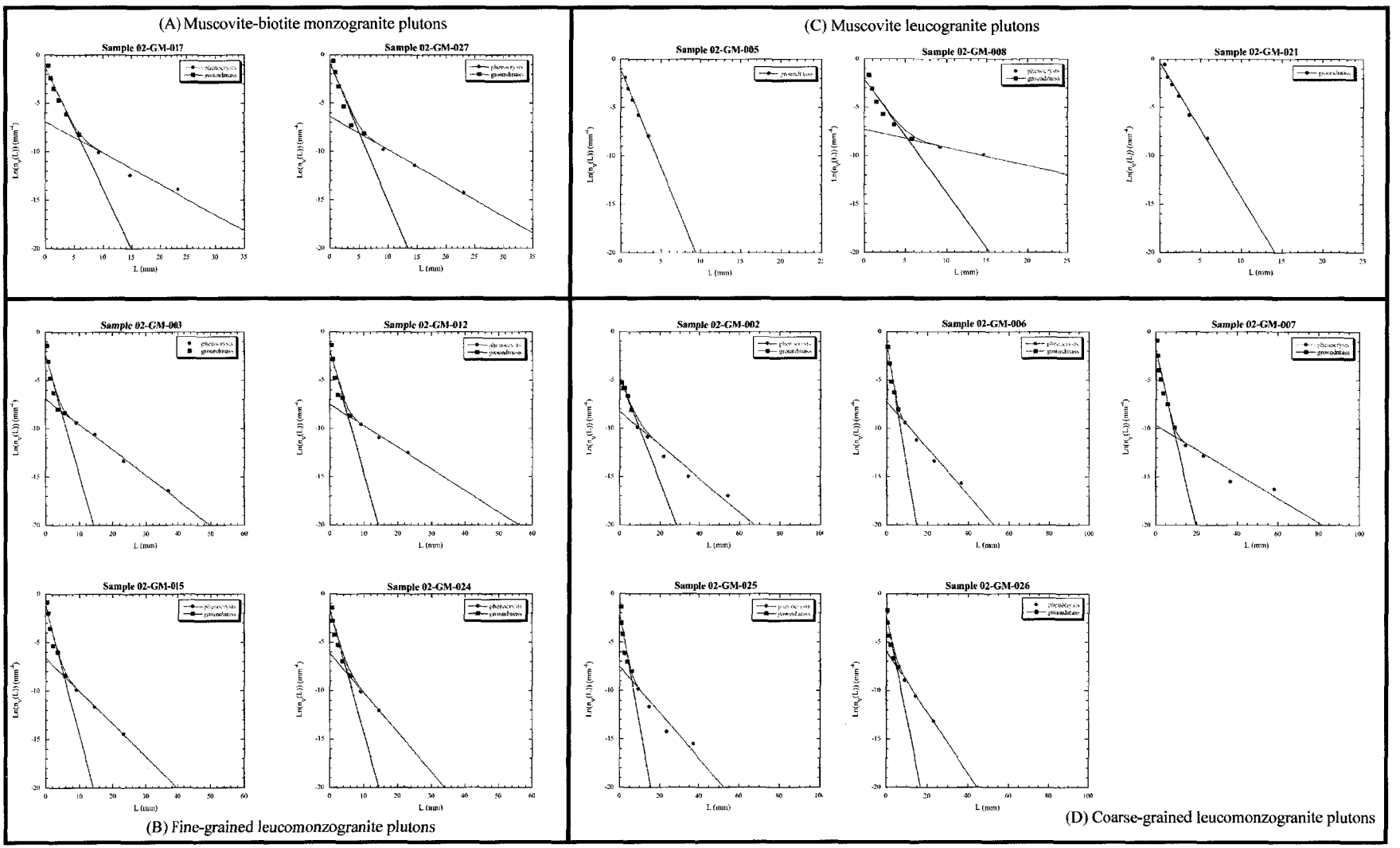

Figure 4.9: Linear regression model of plagioclase stage 2 plutons CSDs

This CSDs separation is presented in Figures 4.6 to 4.9. The blue and green lines are linear regression curves of the phenocrysts and groundmass. In theses figures, there is also a third curve (red) attained by adding the two regression curves of the phenocrysts and groundmass as (see chapter 3). This summation of the regression lines represents the model CSD of each sample and facilitates comparison.

For the Early stage 1 plutons potassic feldspar crystals (Figure 4.10 A), CSDs of biotite granodiorite are less curved than the CSDs of biotite monzogranite, whereas CSDs of plagioclase feldspar crystal (Figure 4.10 C) for both rock types have the same curvature and are similar. In the case of the Late stage 2 plutons, CSDs of potassic feldspar crystals (Figure 4.10 B), all plutons show curved CSDs except for muscovite leucogranite, it seems that the degree of curvature increases as the maximum crystal size increases. For plagioclase feldspar crystals (Figure 4.10 D), the degree of curvature goes from straight with muscovite leucogranite, to almost straight with muscovite-biotite leucogranite to leucomonzogranites that are the more curved. Once again the degree of curvature increases as the maximum crystal size increases.

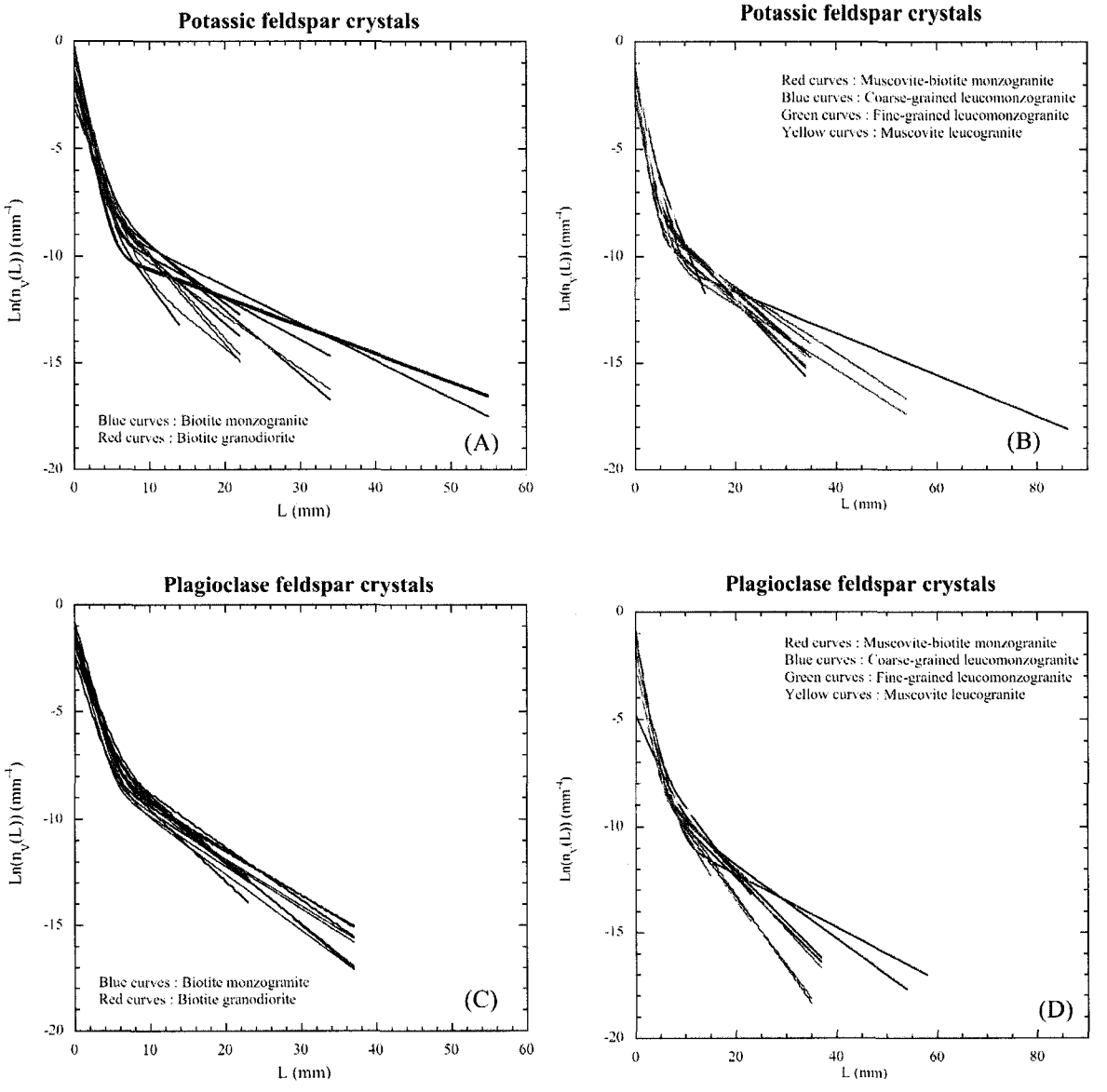

Figure 4.10: Compilation of CSDs calculated from addition of the linear regressions curves. (A) Early stage 1 plutons potassic feldspar; (B) Late stage 2 potassic feldspar; (C) Early stage 1 plutons plagioclase feldspar; (D) Late stage 2 plagioclase feldspar.

Since most CSDs are curved it is not appropriate to estimate slopes and intercepts. By separating CSDs curves in two, at the point of flexure, and by doing a linear regression on both parts (groundmass and phenocrysts), the slope and intercept can be estimated with relative confidence because the two linear regressions have a high confidence level. So for each samples the two were obtained. The characteristic length of the CSD was calculated from the slope (see chapter 1 and 3).

A histogram of characteristic length (CL) has been plotted in Figure 4.11 for both stages of plutons. In the Early stage 1 plutons (Figure 4.11 (A)), CL of the groundmass is between 0 and 2 mm for potassic and plagioclase feldspar, while CL of the phenocrysts of potassic feldspar is between 1 and 8 mm with a gap between 6 and 7 mm. The CL of the phenocrysts of plagioclase feldspar is between 2 and 5 mm. In the Late stage 2 plutons (Figure 4.11 (B)), CL of the groundmass is between 0 and 2 mm for potassic and plagioclase feldspar, while CL of the phenocrysts of potassic feldspar is between 1 and 12 mm with gaps between 2 and 3 mm and 7 mm and 10 mm. The CL of the phenocrysts of plagioclase feldspar is between 2 and 8 mm with gap between 6 and 7 mm. The CL of the groundmass is the same for both stages plutons, while the distribution of phenocrysts is similar, stage 2 plutons have larger CL.

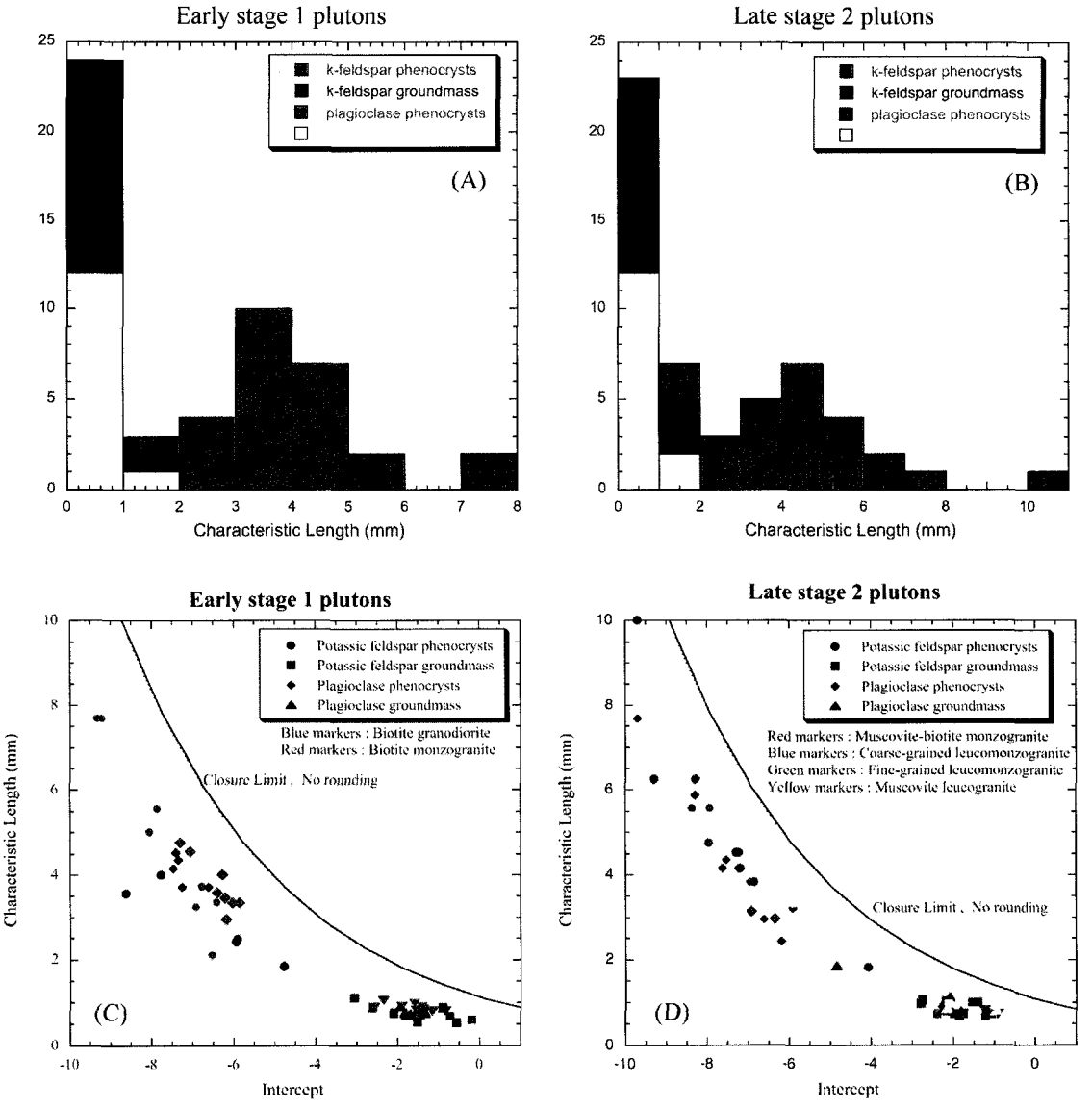

Figure 4.11: (A) Histogram of characteristic lengths as calculated with the linear regression lines for Early stage 1 plutons; (B) Histogram of characteristic lengths as calculated with the linear regression lines for Late stage 2 plutons; (C) Characteristic lengths and intercepts of linear regressions of CSDs for Early stage 1 plutons. The curves represent 100% of crystals of the given shape of plagioclase and potassic feldspar; (D) Characteristic lengths and intercepts of linear regressions of CSDs for Late stage 2 plutons. The curve represents 100% of crystals (for the given shape 1:1.9:2.7) of plagioclase and potassic feldspar.

The characteristic length has been plotted against the intercept in Figure 4.11. The 100% closure limit was calculated and described by Higgins (2002a) for an ellipsoid of the same dimensions (1:1.9:2.7) as used in the data reduction of potassic feldspar. For clarity the closure limit of plagioclase, has been omitted because it is almost the same as potassic feldspar. Both plagioclase and potassic feldspar crystals have been plotted together. For the Early stage 1 plutons (Figure 4.11 C), the groundmass data is grouped into a single cluster of points, while the phenocrysts data are more scattered. All data points are below the closure limit.

The Late stage 2 plutons (Figure 4.11 D) show a different trend. Groundmass data are still clustered in one group while phenocrysts data show a linear correlation, with increasing characteristic length, going from muscovite leucogranite to coarse-grained leucomonzogranite. The phenocrysts points range from a value of 1.5 mm up to 10 mm in a linear manner. The points follow very closely the curve defined by the closure limit. The texture appears to have evolved in the Late stage 2 plutons such that with chemical differentiation described by MacDonald *et al.* (1992), the rock types with the higher values of characteristic length are the least evolved.

Discussion of the results

Crystal size distributions

The SMB is composed of 13 plutons divided into 2 stages: The early stage 1 is mostly comprised of biotite granodiorite, biotite monzogranite and minor fine-grained leucomonzogranite, and; the late stage 2 plutons are composed mostly of two-mica monzogranite, coarse- and fine grained leucomonzogranite, and leucogranite. Petrographic differences noted throughout the SMB define a sequence from least evolved granodiorite to most evolved leucogranite, in the sense of differentiation (MacDonald *et al.*, 1992). Alkali feldspar is perthitic, dominantly so in granodiorite and monzogranite units, whereas in leucogranite units the alkali feldspar is rarely perthitic (MacDonald *et al.*, 1992). Plagioclase is typically either normally or reverse zoned in granodiorite and biotite monzogranite units and unzoned in leucogranite units (MacDonald *et al.*, 1992).

The magma necessary for the SMB was developed by anatexis of a predominantly sedimentary or mixed sedimentary-altered volcanic source (Clarke *et al.*, 1993) during the Acadian Orogeny. Anatexis is responsible for generating the melts and fractional crystallization for the differentiation from the chemically least-evolved granodiorite to the most-evolved leucogranite (MacDonald *et al.*, 1992). The SMB is made up of numerous tabular bodies, laccoliths, which were fed by dykes, and the plutons were progressively built up from countless sheet like intrusions representing periodic magma pulses (Benn *et al.*, 1999) during a very narrow time interval (MacDonald *et al.*, 1992).

Granodiorite and biotite monzogranite units in the early stage 1 are generally medium to coarse grained with or without megacrystic textures, with prominent primary flow textures and are the older units in the SMB. CSDs of stage 1 plutons (Figures 4.3 and 4.10) are, slightly concave up for large crystal sizes (more than 5 mm). This is true for both plagioclase and potassic feldspars, but the CSDs of the potassic feldspars from the biotite granodiorite are less curved than those of the biotite monzogranite.

Late stage 2 plutons are intrusive into Early stage 1 plutons during a very narrow time interval (5 Ma interval) (MacDonald *et al.,* 1992). They were also emplaced as laccolithic plutons fed from dykes, but were emplaced at shallower depth and within cooler crust because the roof was uplifted during the emplacement of stage 1 plutons (Benn *et al.,* 1997). Muscovite-biotite monzogranite and coarse-grained leucomonzogranite units are medium to coarse grained with megacrystic or seriate textures. Fine-grained leucomonzogranite units are fine to medium grained with porphyritic or equigranular textures. Muscovite leucogranite units are fine to medium grained with porphyritic, equigranular or pegmatitic textures and contain topaz. CSDs of stage 2 plutons (Figures 4.4, 4.5 and 4.10) show a curve for large crystal sizes that is slightly concave up. The curvature diminishes with differentiation from leucomonzogranite to almost straight lines for leucogranite for both plagioclase and potassic feldspar.

Solidification of the South Mountain Batholith, stages 1 and 2 plutons, must have started with nucleation and growth of crystals likely producing initial linear CSDs. As mentioned in chapters 1 and 3, initial CSDs for simple steady-state dynamics with linearly increasing undercooling should be straight lines on a conventional CSD plot (Figure 3.12A) for closed and open systems (Figure 1.3 and 1.4), however an initial straight CSD may be modified by geological processes.

Since CSDs of SMB plutons are not straight but concave up (except for muscovite leucogranite), let's take a look at some geological processes that could give rise to the measured CSDs and discuss them in light of the geochemical and other petrologic data accumulated.

Accumulation of crystals in the magma chamber under the influence of gravity will skew the right side of the CSD upwards (Higgins, 2002b; Marsh, 1998) (Figure 1.5 and 3.12B) however MacDonald *et al.* (1994) and others have not reported accumulation of crystals in these plutons. It is true that the megacrysts are aligned in stage 1 plutons and indistinctly aligned in stage 2 plutons, but Benn *et al.* (1999) interprets this to represent magmatic foliation due to horizontal magma flow into the plutons or crystal settling within individual sheets. If the alignment of megacrysts was due to crystal settling this would affect CSDs only by shallowing the slope and increasing the intercept (Higgins, 2002b), that is not the case here, but it is true that CSDs characteristics of crystal settling could have been modified and obscured by a later process. Since there is no clear evidence of crystal settling and granitoids

are very viscous, it will be assumed that aligment of megacrysts in the SMB is due to magmatic foliation rather than accumulation in specific layers, meaning that the megacrysts must have formed at a deeper level or, perhaps during ascent.

Fractional crystallization is another process considered to be a prevalent magma chamber differentiation process and it will skew the right side of the CSD (Figure 3.12B and E) downward because it removes the larger crystals from the crystallization site. This process did not seem to happen at SMB because no CSDs are curved downward and again the process is unlikely due to the high viscosity of silica-rich magmas, unless other later process obscured evidences of it. MacDonald *et al.,* (1992) suggest that fractional crystallization caused the differentiation from the chemically least-evolved granodiorite to the most-evolved leucogranite. CSDs of SMB do not affirm this, so it is proposed that the differentiation observed may come from anatexis of different sources or by partial melting of the same source, rather than crystal fractionation in the laccolith.

An important natural process that can modify CSDs significantly, skew CSDs upwards, is textural coarsening if undercooling remains small for a period of time. As described in chapter 1 (Figure 1.8) and chapter 3, the theory of the Communicating Neighbors (CN) (DeHoff, 1991) can explain the right part of the observed curved CSDs at SMB.

Early stage 1 plutons CSDs seem to follow the textural coarsening CN model, but not completely because the left parts of the CSDs do not fan around a particular size, so

something must have happened after coarsening. In addition, the textural coarsening CN model can explain the upward curvature seen in the stage 1 plutons CSDs. The shapes of CSDs conform to the model and also the correlation between characteristic length and intercept (Figures 4.3, 4.6, 4.7 and 4.11), this shows coarsening between groundmass and phenocrysts and thus supports a textural ripening model. As seen in Figure 4.11 there are 2 populations of crystals, phenocrysts and groundmass, but there is no difference between plagioclase and potassic feldspar. Both rock types composing the first stage plutons have very similar CSDs for both feldspars (Figure 4.3, 4.6 and 4.7). This means that similar processes of coarsening have affected both types of feldspars.

Late stage 2 plutons also follow the textural coarsening model, more specifically curves and shapes follow the CN model. This model can explain the upward bending seen in the stage 2 plutons CSDs. It is shown by the correlation between characteristic lengths and intercept (Figure 4.11) because there are two populations of crystals and there is coarsening between groundmass and phenocrysts. There is no difference between plagioclase and potassic feldspar in terms of shape of CSDs. All rock types, except for muscovite leucogranites, comprising the second stage plutons show very similar CSDs for both feldspars (Figure 4.4, 4.5, and 4.10) and their populations, interpreted to mean that similar processes of coarsening have affected both type of feldspars. Some CSDs from muscovite leucogranite are straight and were produced only by nucleation and growth with no other geological processes modifying them. Muscovite leucogranite are the last rock type to form and be emplaced.

However as said earlier, the CN coarsening model cannot alone explain CSDs measured at SMB because in the model, which is a closed system model, fine crystals are depleted on the final CSD (Figures 1.8 and 3.12 D) because they are used to produce larger crystals. As it was observed (Figures 4.3, 4.4 and 4.5) in the SMB CSDs, smallest crystals are present in the granitoids and are an important part of the crystal population. This can possibly be explained by the fact that SMB components were formed in an open-system environment and that the plutons were progressively built up from countless sheet-like intrusions representing periodic magma pulses (Benn *et al.*, 1999).

Concave up CSDs, as observed at SMB, can also be obtained by changing the crystallization conditions in the plutons. Since plagioclase zoning, reverse and normal, is commonly seen in most of the plutons it may indicate changing magmatic conditions or slightly different chemical conditions caused by a injection of a magma pulse.

Stage 1 plutons: potassic and plagioclase feldspars growth model

As previously demonstrated, it appears that textural coarsening was an important process in the formation of the stage 1 plutons, but before coarsening can begin initial nucleation and initial growth of crystals must occur. It is interpreted that initial growth and nucleation occurred at first in the conduits ascending from where anatexis took place. Growth and nucleation continued, as undercooling increased, in the laccoliths. As the feeder dykes brought warmer new material to the cooling forming plutons, this heat from newer material slowed the undercooling and along with heat of fusion from the plutons buffered the

temperature (Figure 4.12). This heat was enough to induce coarsening in the laccolithic plutons yielding the megacrysts seen in the field and termed phenocrysts in the CSDs. This phase of coarsening would have continued as long as new material buffered temperature near that of the feldspar liquidus. The liquidus temperatures for potassic feldspar and for plagioclase in the SMB are almost the same because the anorthite content is less than 5% in all rocks except for the granodiorite where it can attain 35% (MacDonald *et al.,* 1992). When magma supply waned or because of uplift of the roof during emplacement (Benn *et al.,* 1997), undercooling would have been invigorated, restarting nucleation and growth producing the groundmass, while megacrysts/phenocrysts continued to grow, thus yielding the two crystals populations (Figure 4.12). But since the curvature of CSDs is pronounced and as seen in Figures 4.3 and 4.10 there is a large size difference between phenocrysts and groundmass, the period of coarsening must have happened for as long as new material was fed into the laccolithic plutons.

Early stage 1 plutons are 5 different plutons composed mostly of biotite monzogranite with a biotite granodiorite component (MacDonald *et al.,* 1992). Differentiation between rock types (granodiorite and monzogranite), which are geographically close-spaced, must have occurred during anatexis of the magma source or partly in the laccolithic plutons probably by crystal fractionation, but this process, if it occured, may have been obscured on the CSDs by textural coarsening. Zoning of plagioclase seen mostly in the megacrysts/phenocrysts occurred in plutons at the same time as coarsening was occurring in response to recharge.

Stage 2 plutons: potassic and plagioclase feldspars growth model

As it was stated for stage 1 plutons, initial growth and nucleation of stage 2 plutons occurred at first in the dykes ascending from where anatexis had taken place. Growth and nucleation continued, as undercooling increased, in the laccoliths. Since the stage 2 plutons were emplaced at shallower levels and within cooler crust than stage 1 plutons, they would likely have cooled and crystallized more rapidly (Benn *et al.,* 1997), meaning that grain size should be smaller than the stage 1 plutons. However, CSDs show that sizes of both stages are approximately equal and even that sizes of late stage 2 plutons are a little larger (Figure 4.11).

As the feeder dykes brought warmer new material to the cooling forming plutons, this heat slowed the undercooling in the plutons. Another factor helped buffer temperature near the liquidus, is the size of the plutons. Although the margins of late stage 2 plutons are chilled, their km-scale preclude rapid heat loss from the interior (MacDonald *et al.,* 1992). As stated in chapter 3, conduction (diffusion) is likely the main process for heat loss because the thickness of SMB plutons is approximately 7 km and they were emplaced at depth (Benn *et al.*, 1999), thus causing small undercooling and buffering temperature. This heat was enough to induce coarsening in the laccolithic plutons giving the megacrysts, termed phenocrysts in the CSDs. Coarsening would have continued as long as new material was injected so as to buffer temperature. In common with the stage 1 plutons, nucleation and growth resumed and groundmass was formed when new material stopped being injected allowing for

undercooling. As the groundmass formed, megacrysts/phenocrysts continued to grow, resulting in the size difference between the two crystals populations (Figure 4.12).

Late stage 2 plutons comprise 8 different plutons composed mostly of leucomonzogranite (coarse and fine grained) with a muscovite-biotite monzogranite and a small leucogranite component (MacDonald *et al.,* 1992). Differentiation between rock types, that are spatially close, must have occurred during anatexis or in the laccolithic plutons by crystal fractionation or by mixing these two processes. If fractional crystallization happened in the plutons, evidence was obscured on the CSDs by textural coarsening. CSDs of the leucogranite are different from other CSDs since they are straight. Leucogranites were produced by in-situ fractional crystallization (Dostal & Chatterjee, 1995), but the CSDs do not show any processes modified them. This could be explained by the fact that they formed from a fluorine rich magma (Dostal & Chatterjee, 1995) as seen by the fact that topaz and muscovite is magmatic rather than metasomatic (Kontak, 1990). Zoning of plagioclase is not as prominent as in stage 1 plutons, possibly because there was less plagioclase.

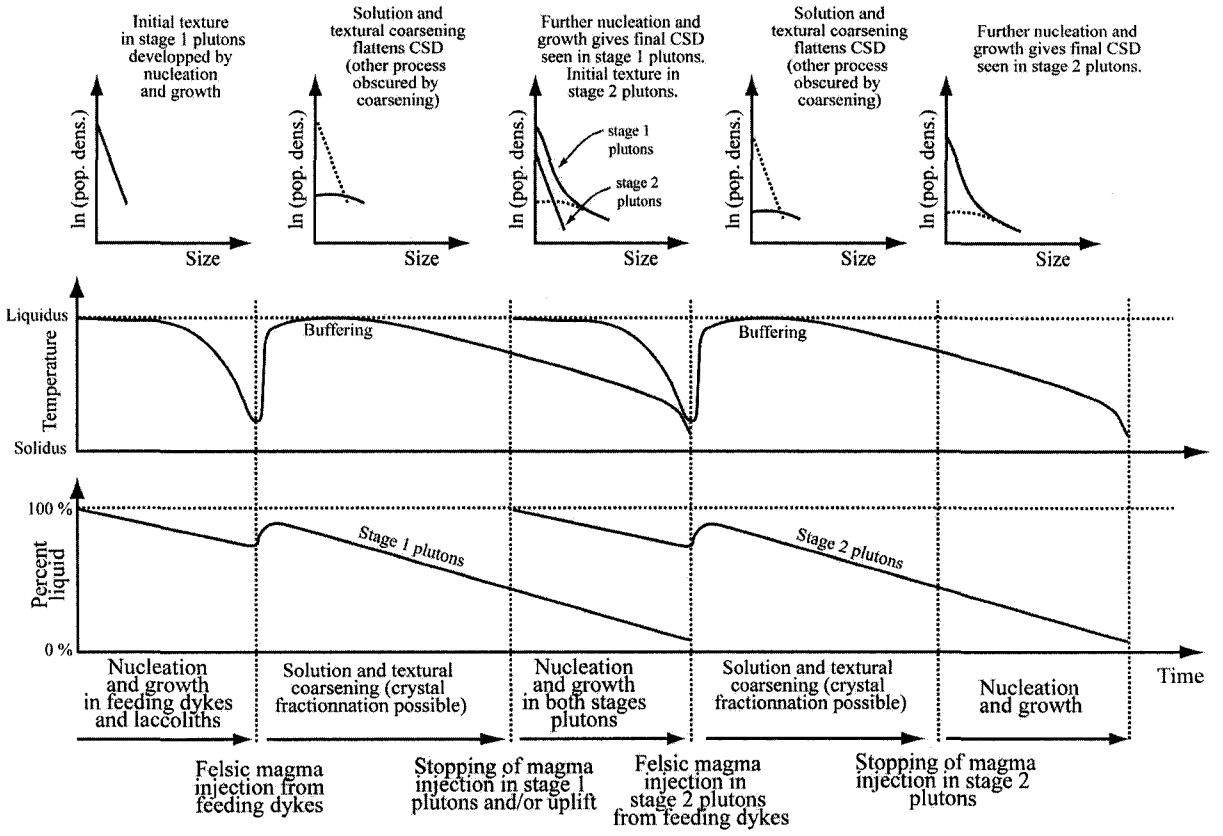

Figure 4.12: Dynamic model for the development of textures in plutons from the South Mountain Batholith.

Conclusion

Quantitative textural analysis of a series of samples from the South Mountain Batholith indicate that feldspars crystals have been texturally coarsened. Coarsening followed in part the communicating neighbors model of De Hoff (1991).

In the stage 1 plutons, an episode of textural coarsening is interpreted to have occurred so as to produce the megacrysts/phenocrysts crystals. This episode of coarsening was possible due to ascent of constant new magma to the plutons, which slowed undercooling, and buffered temperature near the liquidus of potassic and plagioclase feldspars. Textural coarsening may have obscured other process, such as fractional crystallization, which may have occurred.

In the stage 2 plutons, textural coarsening plays also a role in producing the textures seen. Coarsening was possible due to the constant feeding of new material and because the temperature gradient was small (low diffusion), helping to keep the latent heat of stage 2 plutons inside, slowing undercooling and buffering the temperature near the liquidus of potassic and plagioclase feldspar. Once again, textural coarsening seen on the CSDs may have obscured other processes.

Chapter 5

Conclusions

Crystal size distributions (CSD) is a technique that allows the quantification of some aspects of rock textures, for the formulation and testing of hypotheses about the crystallization conditions and processes that occur in a magma chambers and lead to rock formation.

To date, with a few exceptions most CSD studies of igneous rocks have been restricted to mafic volcanic and plutonic rocks and to a lesser extent on felsic volcanic. Because the few studies of felsic plutonic rocks have focused mostly on accessory minerals rather than essential minerals, it was decided to do a in-depth study of feldspars in felsic plutonic rocks of two well-known localities

The two chosen localities were the Eurajoki stock in Finland and the South Mountain Batholith (SMB) in Nova Scotia, Canada. CSDs done on rocks of these two localities are used with other work to quantify crystal sizes and to test hypotheses of crystal growth mechanisms in order to decipher the processes that likely occurred during magma chamber consolidation.

In order to do CSDs on a large number of samples from the two localities, a method was developed using sodium cobaltinitrite staining on rock-slabs and thin sections and colour

thresholding using computer software. Software was used to extract digital files of the different minerals, plagioclase and potassic feldspar, from images made from stained rocks and thin sections. Crystal sizes were measured and CSDs were then calculated using the software *CSD corrections.*

CSDs of a series of samples from the Eurajoki stock, composed of various granite phases of the Tarkki and Väkkärä intrusives, indicate that the potassic feldspar crystals in theses granites have been texturally coarsened and coarsening was an important process in granite formation. In the Tarkki granite, two distinct episodes, of textural coarsening have occurred to produce the megacrysts and phenocrysts. These episodes of coarsening, the last one relatively short, were possibly due to the influence of the still-hot Laittila Batholith which retarded undercooling in the granite and buffered temperature near that of the liquidus of potassic feldspar. In the Väkkärä granite textural coarsening also played a role in producing some of the textures. In contrast the biotite granite, has little evidence of textural coarsening because it intruded into the Tarkki granite that was already cold when the Väkkärä granite was emplaced. The associated topaz bearing granite shows evidence of textural coarsening likely because the biotite granite played a role of insulator slowing undercooling.

CSDs of a series of samples from the South Mountain Batholith indicate that feldspars crystals, both plagioclase and potassic feldspars, have also been texturally coarsened. In the stage 1 plutons, an episode of textural coarsening occurred to produce the megacrysts/phenocrysts crystals. This episode of coarsening was facilitated by the constant

ascent of new hot material into the many plutons. It is plausible that other processes such as crystal settling and fractional crystallization may have occured but if so evidence was obscured on the CSDs by textural coarsening. In the stage 2 plutons, textural coarsening also plays a role in producing the textures seen. Again, coarsening was possible due to the constant feeding of new material and because the surrounding rocks were cooled.

CSDs are easily and rapidly calculated on a large scale using modern computer techniques and they reveal information not available from other techniques on the processes that occurred during rock formation. Textural coarsening, as revealed by CSDs, is an important process in the formation of the granites from Eurajoki and the SMB, and more generally, may be an important process in the formation of other plutonic felsic rocks. Thus this research should alert others that the process might be widespread. Certainly it is highly unlikely that granitic magmas are superheated and given their deep-seated nature, those that cool by conduction, without the aid of hydrothermal circulation may very well be expected to produce the conditions necessary for textural coarsening. Unfortunately, it is not possible to quantify the period of textural coarsening.

It has been demonstrated here that CSDs of major rock-forming minerals are useful in the interpretation of textures from plutonic felsic rocks. CSDs are a useful complement to petrographic observation, structural observations and geochemistry of granitic rocks and provide useful information to help decipher their mechanisms of formation.

Contributions to new knowledge

- CSDs applied to large scale felsic plutonic rocks and petrologic studies involving a significant number of specimens. Very few studies have been done on major rock forming minerals of felsic plutonic rocks;
- CSDs on potassic feldspar of the Eurajoki stock, including rock slabs and thin sections from 13 samples covering all components of the stock;
- CSDs on plagioclase and potassic feldspar of the South Mountain Batholith, including rock slabs and thin sections from 28 samples covering all major components of the batholith;
- Integrating CSDs measured on outcrop, rock slabs and thin sections into one compilation CSD. This method allows the overlapping of CSDs calculated at different scale, for example small crystals measured on a rock slabs represent larger crystals measured on a thin section;
- Using two different linear regression to interpret curved CSDs rather than using polynomial fit, it yields physically meaningful results;
- Using staining and computer software to acquire data rapidly, about 8 times faster, instead of tracing the contours of every crystal;
- Discovery of the importance of textural coarsening in the studied granites and how this process could also be important in other rocks.

References

Armienti, P., Pareschi, M. T., Innocenti, F. & Pompilio, M. (1994). Effects of magma storage and ascent on the kinetics of crystal growth. *Contributions to Mineralogy and Petrology* 115, 402-414.

Bell, K. & Blenkinshop, J. (1960). Mississippian Horton Group of type Windsor-Horton district, Nova Scotia. *Geological Survey of Canada,* Memoir 314, 112.

Benn, K., Horne, R. J., Kontak, D. J., Pignotta, G. S. & Evans, N. G. (1997). Syn-Acadian emplacement model for the South Mountain Batholith, Meguma Terrane, Nova Scotia: magnetic fabric and structural analyses. *Geological Society of America Bulletin* 109, 1279-1293.

Benn, K., Roest, W. R., Rochette, P., Evans, N. G. & Pignotta, G. S. (1999). Geophysical and structural signatures of syntectonic batholith construction: the South Mountain Batholith, Meguma Terrane, Nova Scotia. *Geophysical Journal* 136, 144-158.

Bindeman, I. (2003). Crystal sizes in evolving silicic magma chambers. *Geology* 31, 367-370.

Bindeman, I. & Valley, J. W. (2001). Low del18 O rhyolites from Yellowstone: Magmatic evolution bases on analyses of zircons and individual phenocrysts. *Journal of Petrology* 42, 1491-1517.

Boone, G. M. & Wheeler, E. P. (1968). Staining for cordierite and feldspars in thin section. *American Mineralogist* 53, 327-331.

Boudreau, A. E. (1995). Crystal aging and the formation of fine-scale igneous layering. *Mineralogy and Petrology* 54, 55-69.

Cashman, K. V. (1988). Crystallization of Mount St Helens dacite; a quantitative textural approach. *Bulletin of Volcanology* 50, 194-209.

Cashman, K. V. (1992). Groundmass crystallization of Mount St Helens dacite 1980-1986: a tool for interpreting shallow magmatic processes. *Contributions to Mineralogy and Petrology* 109, 431-449.

Cashman, K. V. & Marsh, B. D. (1988). Crystal size distribution (CSD) in rocks and the kinetics and dynamics of crystallization II: Makaopuhi lava lake. *Contibutions to Mineralogy and Petrology* 99, 292-305.

Castro, J. M., Cashman, K. V. & Manga, M. (2003). A technique for measuring 3D crystal-size distributions of prismatic microlites in obsidian. *American Mineralogist* 88, 1230-1240.

Charest, M. H. (1976). Petrology, geochemistry and mineralization of the New Ross area, Lunenburg County, Nova Scotia. Halifax: Dalhousie University, 154 pages.

Clarke, B. D., Macdonald, M. A., Reynolds, P. H. & Longstaffe, F. J. (1993). Leucogranites from the Eastern Part of the South Mountain Batholith, Nova Scotia. *Journal of Petrology* 34, 653-679.

Clarke, D. B. & Halliday, A. N. (1980). Strontium isotope geology of the South Mountain Batholith, Nova Scotia. *Geochimica et Cosmochimica Acta* 44, 1045-1058.

Clemens, J. D. (1998). Observations on the origins and ascent mechanisms of granitic magmas. *Journal of the Geological Society of London* 155, 843-851.

DeHoff, R. T. (1991). A geometrically general theory of diffusion controlled coarsening. *Acta Metallurgica et Materiala* 39, 2349-2360.

Dostal, J. & Chatterjee, A. K. (1995). Origin of topaz-bearing and related peraluminous granites of the Late Devonian Davis Lake pluton, Nova Scotia, Canada: crystal versus fluid fractionation. *Chemical Geology* 123, 67-88.

Fairbairn, H. W., Hurley, P. M. & Pinsen, W. H. (1964). Preliminary age study and initial Sr87/Sr86 of Nova Scotia granitic rocks by the Rb-Sr whole rock method. *Geological Society of America Bulletin* 75, 253-258.

Fairbault, E. R. (1908). City of Halifax sheet, Map No. 68. *Geological Survey of Canada, Publication No. 1019.*

Fairbault, E. R. (1924). Chester Basin. Geological Survey of Canada, Map 87.

Fowler, A. D. & Roach, D. E. (1996). A model and simulation of branching mineral growth from cooling contacts and glasses. *Mineralogical Magazine* 60, 595-601.

Gualda, G., Cook, D. & Chopra, R. (2004). Fragmentation, nucleation and migration of crystals and bubbles in the Bishop Tuff rhyolitic magma. *Transactions of the Royal Society of Edinburgh: Earth Sciences* 95, 375-390.

Haapala, I. (1977). Petrography and geochemistry of the Eurajoki stock; a rapakivi-granite complex with greisen-type mineralization in southwestern Finland. *Geological Survey of Finland, Bulletin* 186, 1-128.

Haapala, I. (1997). Magmatic and postmagmatic processes in Tin-mineralized granites: Topaz-bearing leucogranites in the Eurajoki rapakivi granite stock, Finland. *Journal of Petrology*, 1645-1659.

Haapala, I. & Rämö, O. T. (1992). Tectonic setting and origin of the Proterozoic rapakivi granites of southeastern Fennoscandia. *Transactions of the Royal Society of Edinburgh: Earth Sciences* 83, 165-171.

Haapala, I. & Thomas, R. (2000). Melt inclusions in quartz and topaz of the topaz granite from Eurajoki, Finland. *Journal of the Czech Geological Society* 45, 149-154.

Hammer, J. E., Cashman, K. V., Hoblitt, R. P. & Newman, S. (1999). Degassing and microlite crystallization during pre-climatic events of the 1991 eruption of Mt. Pinatubo, Philipines. *Bulletin of Volcanology* 60, 355-380.

Higgins, M. D. (1991). The origin of laminated and massive anorthosite, Sept Iles intrusion, Quebec, Canada. *Contributions to Mineralogy and Petrology* 106, 340-354.

Higgins, M. D. (1994). Numerical modeling of crystal shapes in thin sections: Estimation of crystal habit and true size. *American Mineralogist* 79, 113-119.

Higgins, M. D. (1996). Magma dynamics beneath Kameni volcano, Thera, Greece, as revealed by crystal size and shape measurements. *Journal of Volcanology and Geothermal Research* 70, 37-48.

Higgins, M. D. (1998). Origin of anorthosite by textural coarsening: Quantitative measurements of a natural sequence of textural development. *Journal of Petrology* 39, 1307-1323.

Higgins, M. D. (1999). Origin of megacrysts in granitoids by textural coarsening: A crystal size distribution (CSD) study of microcline in the Cathedral Peak Granodiorite, Sierra Nevada, California. In: Castro, A. a. F., C. (ed.) *Understanding granites: integrating modern and classical techniques*: Geological Society of London Special Publications 158, 207-219.

Higgins, M. D. (2000). Measurement of crystal size distributions. *American Mineralogist* 85, 1105-1116.

Higgins, M. D. (2002a). Closure in crystal size distributions (CSD), verification of CSD calculations, and the significance of CSD fans. *American Mineralogist* 87, 160-164.

Higgins, M. D. (2002b). A crystal size-distribution study of the Kiglapait layered mafic intrusion, Labrador, Canada: evidence for textural coarsening. *Contributions to Mineralogy and Petrology* 144, 314-330.

Higgins, M. D. (2006). *Quantitative textural measurements in petrology*: Cambridge University press, 265 pages.

Higgins, M. D. & Roberge, J. (2003). Crystal size distribution of plagioclase and amphibole from Soufrière Hills Volcano, Montserrat: Evidence for dynamic crystallization-textural coarsening cycles. *Journal of Petrology* 44, 1401-1411.

Hodson, M. E. (1998). The origin of igneous layering in the Nunarssuit syenite, south Greenland. *Mineralogical Magazine* 62, 9-27.

Horne, R. J., Macdonald, M. A., Corey, M. C. & Ham, L. J. (1992). Structure and emplacement of the South Mountain batholith, southwestern Nova Scotia. *Atlantic Geology* 28, 29-50.

Howard, V. & Reed, M. G. (1998). *Unbiased stereology : three-dimensional measurement in microscopy*. Oxford, U.K.: Bios Scientific Publisher/Springer, 246 pages.

Howie, R. D. & Barss, M. S. (1975). Upper Paleozoic rocks of the Atlantic Provinces, Gulf of St. Lawrence, and adjacent continental shelf. *Offshore Geology of Eastern Canada*: Geological Survey of Canada, Paper 74-30, 285.

Hunter, R. H. (1992). Textural development in cumulate rocks. In: Cawthorn, R. G. (ed.) *Layered intrusions. Developments in petrology.* Amsterdam: Elsevier, 77-101.

Hutchison, C. S. (1974). *Laboratory handbook of petrographic techniques*: John Wiley & Sons.

Jerram, D. A., Cheadle, M. J. & Philpotts, A. R. (2003). Quantifying the building blocks of igneous rocks: Are clustered crystal framework the foundation? *Journal of Petrology* 44, 2033-2051.

Keppie, J. D. c. (1979). Geological map of the province of Nova Scotia. Nova Scotia Department of Mines and Energy.

Kontak, D. J. (1990). The east Kemptville Topaz-muscovite Leucogranite, Nova Scotia I. Geological setting and whole-rock geochemistry. *Canadian Mineralogist* 28, 787-825.

Korja, A., Korja, T., Luosto, U. & Heikkinen, P. (1993). Seismic and geoelectric evidence for collisional and extensional events in the Fennoscandian Shield - implications for Precambrian crustal evolution. *Tectonophysics* 219, 129-152.

Kretz, R. (1966). Grain-size distribution for certain metamorphic minerals in relation to nucleation and growth. *Journal of Geology* 74, 147-173.

Launeau, P. & Cruden, A. R. (1998). Magmatic fabric acquisition mechanisms in a syenite: results of a combined AMS and image analysis study. *Journal of Geophysical Research* 103, 5067-5089.

Lifshitz, I. M. & Slyozov, V. V. (1961). The kinetics of precipitation from supersaturated solid solutions. *Journal of Physics and Chemistry of Solids* 19, 35-50.

MacDonald, M. A., Horne, R. J., Corey, M. C. & Ham, L. J. (1992). An overview of recent bedrock mapping and follow-up petrological studies of the South Mountain Batholith, southwestern Nova Scotia, Canada. *Atlantic Geology* 28, 7-28.

MacDonald, M. A., Horne, R. J., Corey, M. C. & Ham, L. J. (1994). Geological map of the South Mountain Batholith, Western Nova Scotia. Map 94-01. Halifax: Nova Scotia Department of Natural Resources, Mines and Energy Branches.

Marsh, B. D. (1988). Crystal size distribution (CSD) in rocks and the kinetics and dynamics of crystallization. I: Theory. *Contributions to Mineralogy and Petrology* 99, 277-291.

Marsh, B. D. (1998). On the interpretation of crystal size distributions in magmatic systems. *Journal of Petrology* 39, 553-599.

McConnell, J. (1975). Microstructures of minerals as petrogenetic indicators. *Annual Review of Earth and Planetary Sciences* 3, 129-155.

McKenzie, C. B. & Clarke, B. D. (1975). Petrology of the South Mountain Batholith, Nova Scotia. *Canadian Journal of Earth Sciences* 12, 1209-1218.

Meurer, W.P. & Boudreau, A.E. (1998). Compaction of igneous cumulates; Part II, Compaction and the development of igneous foliations. *Journal of Geology* 106, 293-304.

Mock, A. & Jerram, D. A. (2005). Crystal Size Distributions (CSD) in Three Dimensions: Insights from the 3D Reconstruction of a Highly Porphyritic Rhyolite. *Journal of Petrology* 46, 1525-1541.

Mock, A., Jerram, D. A. & Breitkreuz, C. (2003). Using quantitative textural analysis to understand the emplacement of shallow-level rhyolitic laccoliths - A case study from the Halle Volcanic Complex, Germany. *Journal of Petrology* 44, 833-849.

Oze, C. & Winter, J. D. (2005). The occurrence, vesiculation, and solidification of dense blue glassy pahoehoe. *Journal of Volcanology and Geothermal Research* 142, 285-301.

Peterson, T. D. (1996). A refined technique for measuring crystal size distributions in thin section. *Contributions to Mineralogy and Petrology* 124, 395-405.

Randolf, A. D. & Larson, M. A. (1971). *Theory of particulate processes*: Academic Press, New York.

Reynolds, P. H., Elias, P., Muecke, G. K. & Grist, A. M. (1987). Thermal history of the southwestern Meguma Zone, Nova Scotia, from an 40Ar/39Ar and fission track dating study of intrusive rocks. *Canadian Journal of Earth Sciences* 24, 1952-1965.

Reynolds, P. H., Zentilli, M. & Muecke, G. K. (1981). K-Ar and 40Ar/39Ar geochronology of granitoid rocks from southern Nova Scotia: its bearing on the geological evolution of the Meguma Zone of the Appalachians. *Canadian Journal of Earth Sciences* 18, 386-394.

Royet, J.-P. (1991). Stereology: A method for analysing images. *Progress in Neurobiology* 37, 433-474.

Sahagian, D. L. & Proussevitch, A. A. (1998). 3D particle size distributions from 2D observations: stereology for natural applications. *Journal of Volcanology and Geothermal Research* 84, 173-196.

Saltykov, S. A. (1967). The determination of the size distribution of particles in an opaque matrix from a measurement of the size distributions of their sections. In: H., E. (ed.) *Stereology*. Berlin Heidelberg New-York: Spinger, 163-173.

Smith, T. E. (1974). The geochemistry of the granitic rocks of Halifax County, Nova Scotia. *Canadian Journal of Earth Sciences* 11, 650-656.

Smitheringale, W. G. (1973). *Geology of parts of Digby, Bridgetown, and Gaspereau Lake map areas, Nova Scotia.*

Streckeisen, A. (1975). To each plutonic rocks its proper name. *Earth Sciences Reviews* 12, 1-33.

Taylor, F. C. (1969). *Geology of the Annapolis-St. Mary's Bay map-area, Nova Scotia.*

Underwood, E. E. (1970). *Quantitative stereology*. Reading, Massachusetts: Addison-Wesley.

Vaasjoki, M. (1977). Rapakivi granites and other postorogenic rocks in Finland, their age and the lead isotopic composition of certain associated galena mineralizations. *Geological Survey of Finland, Bulletin* 294, 1-64.

Voorhees, P. W. (1992). Ostwald ripening of two-phases mixtures. *Annual Review of Material Science* 22, 197-215.

Zieg, M. J. & Marsh, B. D. (2002). Crystal size distributions and scaling laws in the quantification of igneous textures. *Journal of Petrology* 43, 85-101.

Appendix A

Description of samples from the Eurajoki stock

All samples locations are illustrated on Figure 3.1 (see chapter 3).

Tarkki granite

00-GM-011

This sample was taken in a rock quarry. It is reddish pink, mostly equigranular, with potassic feldspar megacrysts (3-5 cm) roughly distributed at one per m^2. The granite is in contact with a diabase which melted the granite and caused the formation of pegmatite near the contact. A quartz-feldspar porphyry dike, 1 meter large, cross cuts the whole assemblage.

00-GM-013

This is a medium grained, reddish, equigranular and homogeneous granite. It is made of turbid potassic feldpar, plagioclase and quartz. It seems to contain two generations of quartz, the first generation is turbid and subhedral to euhedral, almost by-pyramidal. The second generation is of crystals that are clear and anhedral. The mafic minerals present are biotite, hornblende and less than 1% fayalite, and trace rutile.

00-GM-014

This is a medium to fine grained, homogeneous, pinkish equigranular granite similar to 00-GM-013. It is made of the same minerals as previously. The difference is the presence of micrographic textures.

00-GM-015

It is a homogeneous, reddish, equigranular medium grained rock, with some 1.5 cm alkali feldspar megacrysts. It also contains biotite and abundant micrographic texture.

00-GM-016

It is a reddish-pink, homogeneous, medium to coarse-grained granite resembling 00-GM-011. It contains less than 0.5% alkali feldspar megacrysts. The mineral phases present are: potassic feldspar, quartz, biotite, amphibole, plagioclase, topaz, iddingsite and olivine. Micrographic texture is present. The feldspars grains are sericitised.

Väkkärä granite

Biotite granite

00-GM-010

This sample is a equigranular, medium grained, reddish biotite granite containing mostly turbid and sericitised potassic feldspar (65%), 30% quartz, almost no albite (less than 2%) and some muscovite and biotite. Micrographic texture, intergrowth between vermicular quartz and potassic feldspar, is common.

00-GM-020

It is light pink, equigranular homogeneous medium grained biotite granite. It is composed of potassic feldspar, quartz, plagioclase, biotite and topaz. Perthitic and micrographic textures are present. Topazatisation of the plagioclase crystals was observed. No euhedral quartz like that of the topaz granite was found.

Porphyritic and coarse-grained topaz bearing granite

00-GM-009

It is fine-grained, homogeneous reddish granite with small phenocrysts (0.5 cm) of quartz and alkali feldspar. Some of the quartz phenocrysts are euhedral with a by-pyramidal shape. The groundmass is composed of quartz, potassic feldspar, plagioclase (An_{40}), green brown biotite and 1% topaz. Plagioclase grains are sericitised.

00-GM-012

A light pink granite medium to coarse grained in size, with some euhedral quartz and alkali feldspar crystals, with rare euhedral feldspar megacrysts (2 cm) (0,01%). These megacrysts are turbid, altered and contain euhedral plagioclase crystals. Besides the major minerals, it contains biotite, topaz and sericite. A pegmatite phase is also present.

00-GM-017

It is a homogeneous, coarse grained, salmon red granite with some alkali feldspar megacrysts (2 cm). It is composed of potassic feldspar, quartz (some euhedral grains), plagioclase, biotite altered to chlorite and topaz in inclusions within quartz.

00-GM-018

This sample is a little different from the other topaz-granite samples. It is more purple-red color, homogeneous and coarse grained. Feldspar crystals are euhedral and as long as 3 cm. It contains biotite altered to chlorite, topaz (seen with eye) and fluorite. Two generations of feldpars, one is sericitised and the other one not.

00-GM-019

This sample is salmon pink in color, fine to medium grained in size and homogeneous similar to 00-GM-017 but finer grain size. Euhedral feldpars (1 cm) and quartz crystals are present. It is composed of potassic feldspar, quartz, plagioclase, biotite and topaz. The first generation of K-feldspar crystals are turbid and bigger than the clear plagioclase crystals and bigger than the second generation of K-feldspar.

00-GM-021

It is a fine-grained, homogeneous, reddish, massive granite. A greisen zone cuts the outcrop and even the granite is hematised. Some euhedral quartz crystals are present. It is composed of potassic feldspar, quartz, and plagioclase, biotite altered to chlorite, topaz and fluorite.

Plagioclase crystals are albitised and topazitised. This sample contains the most topaz crystals of all samples studied.

Appendix B

Eurajoki Electron Microprobe data

Tarkki granite electron microprobe analysis

SAMPLE	011A-1	011A-2	011A-3	011A-5	011A-6	011A-7	011A-8	011A-9	14-1	14-2	14-3	14-4	14-5	14-6	14-7	14-8	14-9	14-10	14-11	14-12
MINERAL	K-feldspar	albite	K-feldspar	K-feldspar	K-feldspar	biotite	chlorite	bytownite	K-feldspar	K-feldspar	K-feldspar	K-feldspar	K-feldspar	albite	oligoclase	oligoclase	andesine	K-feldspar	albite	K-feldspar
SIO2	66.1	68.84	65.61	65.09	65.13	29.46	29.98	36.74	65.58	64.77	65.4	64.45	65.34	69.69	64.5	62.55	57.75	65.09	64.64	65.71
AL2O3	18.51	19.7	18.41	18.49	18.46	12.7	14.82	15.32	19.1	18.88	18.89	18.23	18.79	19.75	22.96	24.53	27.19	18.61	23.59	19.25
TIO2	0	0	0	0	0	2.98	0.07	0.07	0	0	0	0	0	0	0	0	0	0	0	0
CR2O3	0	0	0	0	0	0.02	0	0	0	0	0	0	0	0	0	0	0	0	0	0
FEO	0	0.06	0	0.05	0.08	33.32	16.08	9.91	0.06	0.08	0.11	0.17	0.1	0.02	0.1	0.09	0.11	0.1	0.26	0.08
MGO	0	0	0	0	0	3.01	20.1	21.52	0	0	0	0	0	0	0	0	0	0	0	0
MNO	0	0	0	0	0	0.28	0.16	0.1	0	0	0	0	0	0	0	0	0	0	0	0
NIO	0	0	0	0	0	0	0	0	0	0	0	0	0	0	0	0	0	0	0	0
K2O	13.87	1.69	15.68	16.56	15.26	6.94	0.02	0.04	13.55	16.18	16.54	17.01	15.92	0.07	0.91	0.5	0.32	16.66	1.38	13.33
CAO	0.16	0.6	0.03	0.05	0.07	0.11	0.3	0.67	0.13	0.13	0.01	0.01	0.05	0.15	2.38	5.33	8.5	0.05	1.91	0.15
NA2O	2.3	11.03	1.28	0.74	1.76	0.21	0.12	0.1	2.42	0.69	0.32	0.18	0.88	11.48	9.39	8.63	6.63	0.31	9.51	2.68
BAO	0.38	0.08	0.66	0.48	0.41	0.11	0.04	0.04	0.43	0.44	0.27	0.18	0.37	0	0	0	0	0.29	0.05	0.38
CL	0	0	0	0	0	0.3	0.2	0.4	0	0	0	0	0	0	0	0	0	0	0	0
F	0	0	0	0	0	0.87	0.24	0.83	0	0	0	0	0	0	0	0	0	0	0	0
TOTAL	101.32	102	101.67	101.46	101.17	90.31	82.13	85.74	101.27	101.17	101.54	100.23	101.45	101.16	100.24	101.63	100.5	101.11	101.34	101.58
TOT-O	101.32	102	101.67	101.46	101.17	89.88	81.98	85.3	101.27	101.17	101.54	100.23	101.45	101.16	100.24	101.63	100.5	101.11	101.34	101.58
SI	8.998	8.931	8.982	8.956	8.951	5.662	5.5	6.14	8.928	8.919	8.955	8.973	8.951	9.01	8.509	8.206	7.726	8.964	8.461	8.914
AL	2.969	3.012	2.971	2.998	2.99	2.877	3.205	3.017	3.066	3.064	3.048	2.991	3.034	3.009	3.57	3.793	4.287	3.021	3.639	3.077
TI	0	0	0	0	0	0.431	0.009	0.009	0	0	0	0	0	0	0	0	0	0	0	0
CR	0	0	0	0	0	0.003	0	0	0	0	0	0	0	0	0	0	0	0	0	0
FE	0	0.006	0	0.006	0.009	5.356	2.467	1.386	0.007	0.009	0.013	0.02	0.012	0.002	0.011	0.01	0.012	0.012	0.029	0.009
MG	0	0	0	0	0	0.861	5.497	5.361	0	0	0	0	0	0	0	0	0	0	0	0
MN	0	0	0	0	0	0.046	0.025	0.014	0	0	0	0	0	0	0	0	0	0	0	0
NI	0	0	0	0	0	0	0	0	0	0	0	0	0	0	0	0	0	0	0	0
K	2.409	0.28	2.738	2.907	2.676	1.701	0.006	0.009	2.353	2.842	2.888	3.022	2.783	0.011	0.154	0.083	0.054	2.927	0.231	2.307
CA	0.024	0.064	0.005	0.008	0.011	0.022	0.058	0.119	0.019	0.019	0.002	0.001	0.008	0.021	0.337	0.749	1.219	0.008	0.268	0.022
NA	0.606	2.774	0.339	0.197	0.468	0.076	0.041	0.031	0.639	0.185	0.085	0.049	0.234	2.877	2.403	2.195	1.721	0.083	2.412	0.704
BA	0.02	0.004	0.035	0.026	0.022	0.009	0.003	0.003	0.023	0.024	0.015	0.01	0.02	0	0	0	0	0.016	0.002	0.02
CL	0	0	0	0	0	0.097	0.062	0.114	0	0	0	0	0	0	0	0	0	0	0	0
F	0	0	0	0	0	0.529	0.139	0.437	0	0	0	0	0	0	0	0	0	0	0	0
SUBT	15.026	15.091	15.07	15.098	15.127	17.67	17.012	16.64	15.035	15.062	15.006	15.066	15.042	14.93	14.984	15.036	15.019	15.031	15.042	15.053

SAMPLE	14-13	14-14	14-15	15-1-1	15-1-2	15-2-3	15-1-4	16-1-1	16-1-2	16-1-3	16-1-4	16-1-5	16-1-6	16-1-7	16-2-1	16-2-2	16-2-3	16-2-4	16-2-5
MINERAL	K-feldspar	albite	K-feldspar	K-feldspar	albite	oligoclase	albite	K-feldspar	albite	K-feldspar	K-feldspar	albite	K-feldspar	K-feldspar	biotite	amphibole	biotite	fayalite	biotite
SIO2	64.93	67.82	64.69	66.2	68.98	62.34	67.16	64.6	67.79	66.11	65.62	69.58	66.56	65.08	34.42	41.64	47.47	29.55	41.22
AL2O3	18.87	20.88	18.57	19.07	20.95	25.09	21.92	18.88	20.85	19.08	18.77	20.47	19.05	19.01	11.49	8.74	0.09	0.01	0
TIO2	0	0	0	0	0	0	0	0	0	0	0	0	0	0	3.22	0.4	0	0.01	0.03
CR2O3	0	0	0	0	0	0	0	0	0	0	0	0	0	0	0	0	0	0.02	0
FEO	0.03	0.24	0.21	0.06	0.06	0.08	0.23	0.02	0	0.05	0.03	0.07	0.02	0.05	32.45	29.94	47.23	68.43	41.61
MGO	0	0	0	0	0	0	0	0	0	0	0	0	0	0	4.36	3.07	1.44	1.13	1.2
MNO	0	0	0	0	0	0	0	0	0	0	0	0	0	0	0.07	0.27	1.07	1.43	0.64
NIO	0	0	0	0	0	0	0	0	0	0	0	0	0	0	0	0	0	0	0
K2O	16.82	0.25	16.75	14.35	0.59	0.22	0.49	15.43	0.63	12.12	15.03	0.21	11.87	15.23	8.49	1.39	0	0.01	0.16
CAO	0.07	1.34	0.01	0.05	1.03	6.26	1.43	0.05	0.9	0.16	0.07	0.53	0.17	0.06	0.03	10.59	0.63	0.08	0.3
NA2O	0.41	10.79	0.39	1.78	11.2	8.43	10.49	0.76	10.33	3.19	1.04	11.52	3.45	0.96	0.12	1.81	0.05	0.09	0
BAO	0.33	0	0.53	0.18	0.1	0.01	0.03	0.79	0.07	0.46	0.36	0	0.54	0.58	0	0	0	0	0
CL	0	0	0	0	0	0	0	0	0	0	0	0	0	0	0.32	0.3	0.02	0.01	0
F	0	0	0	0	0	0	0	0	0	0	0	0	0	0	1.1	0.79	0	0	0
TOTAL	101.46	101.32	101.15	101.69	102.91	102.43	101.75	100.53	100.57	101.17	100.92	102.38	101.66	100.97	96.07	98.94	98	100.77	85.16
TOT-O	101.46	101.32	101.15	101.69	102.91	102.43	101.75	100.53	100.57	101.17	100.92	102.38	101.66	100.97	95.53	98.54	98	100.77	85.16
SI	8.926	8.807	8.94	8.968	8.833	8.126	8.699	8.934	8.849	8.956	8.986	8.917	8.968	8.939	6.108	6.908	8.233	5.956	8.241
AL	3.057	3.196	3.025	3.045	3.162	3.854	3.346	3.078	3.208	3.047	3.03	3.091	3.025	3.076	2.403	1.708	0.018	0.002	0
TI	0	0	0	0	0	0	0	0	0	0	0	0	0	0	0.429	0.05	0	0.002	0.005
CR	0	0	0	0	0	0	0	0	0	0	0	0	0	0	0	0	0	0.003	0
FE	0.004	0.026	0.025	0.007	0.006	0.009	0.025	0.003	0	0.005	0.004	0.008	0.003	0.006	4.815	4.153	6.85	11.498	6.956
MG	0	0	0	0	0	0	0	0	0	0	0	0	0	0	1.152	0.759	0.371	0.338	0.359
MN	0	0	0	0	0	0	0	0	0	0	0	0	0	0	0.011	0.039	0.157	0.243	0.108
NI	0	0	0	0	0	0	0	0	0	0	0	0	0	0	0	0	0	0	0
K	2.95	0.041	2.954	2.479	0.097	0.037	0.082	2.722	0.105	2.094	2.626	0.034	2.04	2.668	1.923	0.294	0	0.003	0.04
CA	0.01	0.187	0.002	0.007	0.141	0.874	0.199	0.007	0.126	0.022	0.01	0.073	0.024	0.009	0.006	1.882	0.116	0.016	0.064
NA	0.109	2.717	0.104	0.468	2.78	2.131	2.634	0.205	2.614	0.838	0.275	2.864	0.902	0.255	0.042	0.582	0.018	0.036	0
BA	0.018	0	0.029	0.01	0.005	0	0.001	0.043	0.003	0.024	0.019	0	0.029	0.031	0	0	0	0	0
CL	0	0	0	0	0	0	0	0	0	0	0	0	0	0	0.097	0.084	0.006	0.002	0.002
F	0	0	0	0	0	0	0	0	0	0	0	0	0	0	0.615	0.416	0.002	0	0
SUBT	15.074	14.974	15.079	14.984	15.024	15.031	14.986	14.992	14.905	14.986	14.95	14.987	14.991	14.984	17.601	16.875	15.771	18.079	15.775

Väkkärä granite electron microprobe analysis

SAMPLE	9/1/01	9/1/02	9/2/01	9/2/02	9/2/03	9/2/04	010A-1	010A-2	010A-3	010A-4	010A-5	010A-6	010A-7	010A-8	12/1/01	12/1/02	12/2/01	12/3/01	12/3/02	12/3/03	12/3/04	12/3/05	17-1
MINERAL	K-feldspar	albite	albite	albite	k-feldspar	albite	k-feldspar	k-feldspar	k-feldspar	k-feldspar	oligoclase	k-feldspar	albite	k-feldspar	albite	k-feldspar	albite	k-feldspar	albite	albite	k-feldspar	albite	albite
SIO2	66.18	69.14	70.31	70.42	65.71	69.98	66.22	66.44	66.71	65.92	64.4	65.86	69.04	66.27	65.39	69.42	69.6	65.28	69.66	69.55	66.56	70.76	69.52
AL2O3	18.74	20.25	20.01	20.21	18.82	19.99	18.42	18.32	18.64	18.32	22.5	18.45	19.3	18.57	18.83	19.86	19.81	18.62	19.89	20.28	18.72	20.05	19.75
TIO2	0	0	0	0	0	0	0	0	0	0	0	0	0	0	0	0	0	0	0	0	0	0	0
CR2O3	0	0	0	0	0	0	0	0	0	0	0	0	0	0	0	0	0	0	0	0	0	0	0
FEO	0	0.03	0	0.02	0.02	0	0.04	0	0	0	0.06	0.03	0.07	0.02	0.08	0	0	0.03	0.04	0.04	0.06	0.02	0.04
MGO	0	0	0	0	0	0	0	0	0	0	0	0	0	0	0	0	0	0	0	0	0	0	0
MNO	0	0	0	0	0	0	0	0	0	0	0	0	0	0	0	0	0	0	0	0	0	0	0
NIO	0	0	0	0	0	0	0	0	0	0	0	0	0	0	0	0	0	0	0	0	0	0	0
K2O	16.48	0.17	0.21	0.22	16.49	0.29	14.76	15.7	12.42	15.15	0.78	16.83	1.38	14.18	16.42	0.25	0.07	16.26	0.2	0.25	16.41	0.21	0.11
CAO	0	0.14	0.11	0.22	0	0.1	0.04	0.03	0.06	0.03	3.88	0	0.53	0.02	0	0.01	0.03	0.01	0.08	0.1	0	0.02	0.02
NA2O	0.32	11.51	11.71	11.9	0.29	11.7	2.02	1.3	3.61	1.48	9.07	0.57	10.4	2.29	0.4	11.77	12.02	0.38	11.92	11.94	0.46	11.83	11.41
BAO	0	0.04	0.1	0.03	0	0	0.1	0.05	0.03	0	0	0.01	0.01	0.01	0	0	0	0.14	0.12	0	0.02	0	0.01
CL	0	0	0	0	0	0	0	0	0	0	0	0	0	0	0	0	0	0	0	0	0	0	0
F	0	0	0	0	0	0	0	0	0	0	0	0	0	0	0	0	0	0	0	0	0	0	0
TOTAL	101.72	101.28	102.45	103.02	101.33	102.06	101.6	101.84	101.47	100.9	100.69	101.75	100.73	101.36	101.12	101.31	101.53	100.72	101.91	102.16	102.23	102.89	100.86
TOT-O	101.72	101.28	102.45	103.02	101.33	102.06	101.6	101.84	101.47	100.9	100.69	101.75	100.73	101.36	101.12	101.31	101.53	100.72	101.91	102.16	102.23	102.89	100.86
SI	9.009	8.944	8.993	8.966	8.986	8.985	9.005	9.029	9.001	9.022	8.489	8.998	9.016	9.002	8.968	8.98	8.983	8.988	8.972	8.934	9.015	9.005	9.012
AL	3.006	3.087	3.017	3.032	3.033	3.024	2.952	2.935	2.964	2.956	3.496	2.971	2.97	2.974	3.044	3.028	3.014	3.021	3.02	3.071	2.989	3.006	3.017
TI	0	0	0	0	0	0	0	0	0	0	0	0	0	0	0	0	0	0	0	0	0	0	0
CR	0	0	0	0	0	0	0	0	0	0	0	0	0	0	0	0	0	0	0	0	0	0	0
FE	0	0.004	0	0.002	0.003	0	0.005	0	0	0	0.007	0.004	0.007	0.002	0.009	0	0	0.004	0.004	0.004	0.007	0.002	0.004
MG	0	0	0	0	0	0	0	0	0	0	0	0	0	0	0	0	0	0	0	0	0	0	0
MN	0	0	0	0	0	0	0	0	0	0	0	0	0	0	0	0	0	0	0	0	0	0	0
NI	0	0	0	0	0	0	0	0	0	0	0	0	0	0	0	0	0	0	0	0	0	0	0
K	2.861	0.028	0.034	0.035	2.876	0.047	2.561	2.722	2.139	2.645	0.131	2.932	0.229	2.457	2.873	0.041	0.011	2.856	0.033	0.041	2.835	0.034	0.019
CA	0	0.019	0.015	0.03	0	0.014	0.006	0.005	0.008	0.004	0.548	0.001	0.074	0.003	0	0.001	0.004	0.001	0.012	0.013	0	0.003	0.003
NA	0.086	2.887	2.904	2.937	0.077	2.913	0.532	0.342	0.945	0.393	2.317	0.152	2.632	0.604	0.106	2.951	3.008	0.102	2.976	2.974	0.122	2.919	2.868
BA	0	0.002	0.005	0.002	0	0	0.005	0.003	0.001	0	0	0	0.001	0	0	0	0	0.007	0.006	0	0.001	0	0.001
CL	0	0	0	0	0	0	0	0	0	0	0	0	0	0	0	0	0	0	0	0	0	0	0
F	0	0	0	0	0	0	0	0	0	0	0	0	0	0	0	0	0	0	0	0	0	0	0
SUBT	14.962	14.971	14.968	15.004	14.975	14.983	15.066	15.036	15.058	15.02	14.988	15.058	14.929	15.042	15	15.001	15.02	14.979	15.023	15.037	14.969	14.969	14.924

SAMPLE	17-2	17-3	17-4	17-5	17-6	17-7	18A-1	18A-1	18A-2	18A-3	20-1-1	20-1-2	20-2-1	20-2-2	20-2-3	20-2-4	21-1	21-2	21-3	21-4	21-5	21-6
MINERAL	k-feldspar	albite	albite	albite	k-feldspar	albite	albite	albite	k-feldspar	k-feldspar	albite	k-feldspar	albite	oligoclase	albite	k-feldspar	k-feldspar	albite	albite	k-feldspar	albite	k-feldspar
SIO2	66.04	68.92	68.36	69.24	65.03	69.12	65.24	70.02	65.28	65.5	68.02	65.56	67.81	22.46	69.3	65.42	66.23	69.03	68.53	65.42	70.36	66.18
AL2O3	18.79	20.41	19.89	19.99	18.88	20.04	18.05	19.45	17.69	18.02	20.34	18.65	20.45	20.61	20.11	18.51	17.72	19.28	17.35	18.51	18.78	17.53
TIO2	0	0	0	0	0	0	0	0	0	0	0	0	0	0.01	0	0	0	0	0	0	0	0
CR2O3	0	0	0	0	0	0	0	0	0	0	0	0	0	0.02	0	0	0	0	0	0	0	0
FEO	0.07	0.29	0.16	0.06	0	0.67	0.11	0.03	0.07	0.45	0.03	0.13	0	43.77	0.06	0.31	0.09	0.05	0.01	0.06	0.07	0
MGO	0	0	0	0	0	0	0	0	0	0	0	0	0	0.49	0	0	0	0	0	0	0	0
MNO	0	0	0	0	0	0	0	0	0	0	0	0	0	0.22	0	0	0	0	0	0	0	0
NIO	0	0	0	0	0	0	0	0	0	0	0	0	0	0	0	0	0	0	0	0	0	0
K2O	17.21	0.41	0.23	0.19	16.87	0.17	17.08	0.16	16.77	16.96	0.19	16.27	0.15	0	0.18	16.51	17.17	0.23	0.15	17.29	0.07	17.41
CAO	0.04	0.11	0.22	0.07	0	0	0	0.12	0	0.01	0.79	0.01	0.76	0.01	0.38	0	0	0.36	0.19	0	0.09	0
NA2O	0.41	11.59	11.37	11.52	0.42	11.75	0.44	11.73	0.47	0.58	11.08	0.34	11.52	0.01	11.64	0.33	0.35	11.59	11.37	0.32	11.7	0.32
BAO	0	0.01	0.01	0.01	0	0	0	0	0	0.02	0	0	0.05	0.03	0.01	0.04	0	0.01	0.02	0	0.02	0
CL	0	0	0	0	0	0	0	0	0	0	0	0	0	0.01	0	0	0	0	0	0	0	0
F	0	0	0	0	0	0	0	0	0	0	0	0	0	0.3	0	0	0	0	0	0	0	0
TOTAL	102.56	101.74	100.24	101.08	101.2	101.75	100.92	101.51	100.28	101.54	100.45	100.96	100.74	87.94	101.68	101.12	101.56	100.55	97.62	101.6	101.09	101.44
TOT-O	102.56	101.74	100.24	101.08	101.2	101.75	100.92	101.51	100.28	101.54	100.45	100.96	100.74	87.81	101.68	101.12	101.56	100.55	97.62	101.6	101.09	101.44
SI	8.966	8.904	8.944	8.971	8.939	8.931	9.009	9.032	9.054	9.002	8.885	8.996	8.851	4.513	8.941	8.988	9.076	9.006	9.185	8.974	9.105	9.088
AL	3.007	3.108	3.067	3.052	3.058	3.052	2.938	2.957	2.892	2.918	3.132	3.016	3.146	4.881	3.058	2.997	2.861	2.964	2.74	2.992	2.864	2.837
TI	0	0	0	0	0	0	0	0	0	0	0	0	0	0.002	0	0	0	0	0	0	0	0
CR	0	0	0	0	0	0	0	0	0	0	0	0	0	0.003	0	0	0	0	0	0	0	0
FE	0.008	0.031	0.018	0.007	0	0.072	0.012	0.003	0.008	0.052	0.003	0.015	0	7.356	0.007	0.035	0.01	0.005	0.001	0.007	0.008	0
MG	0	0	0	0	0	0	0	0	0	0	0	0	0	0.148	0	0	0	0	0	0	0	0
MN	0	0	0	0	0	0	0	0	0	0	0	0	0	0.038	0	0	0	0	0	0	0	0
NI	0	0	0	0	0	0	0	0	0	0	0	0	0	0	0	0	0	0	0	0	0	0
K	2.981	0.067	0.039	0.031	2.958	0.028	3.008	0.026	2.967	2.973	0.031	2.848	0.025	0.001	0.03	2.895	3.001	0.038	0.026	3.025	0.012	3.05
CA	0.006	0.015	0.031	0.01	0	0	0	0.017	0	0.002	0.111	0.001	0.106	0.002	0.053	0	0	0.051	0.027	0	0.012	0
NA	0.108	2.903	2.885	2.893	0.113	2.944	0.117	2.935	0.126	0.156	2.805	0.092	2.916	0.006	2.911	0.088	0.092	2.931	2.955	0.086	2.936	0.086
BA	0	0	0	0.001	0	0	0	0	0	0.001	0	0	0.003	0.002	0.001	0.002	0	0.001	0.001	0	0.001	0
CL	0	0	0	0	0	0	0	0	0	0	0	0	0	0.003	0	0	0	0	0	0	0	0
F	0	0	0	0	0	0	0	0	0	0	0	0	0	0.189	0	0	0	0	0	0	0	0
SUBT	15.076	15.028	14.984	14.965	15.068	15.027	15.084	14.97	15.047	15.104	14.967	14.968	15.047	17.144	15.001	15.005	15.04	14.996	14.935	15.084	14.938	15.061

Appendix B: Väkkärä granite, sample 00-GM-009

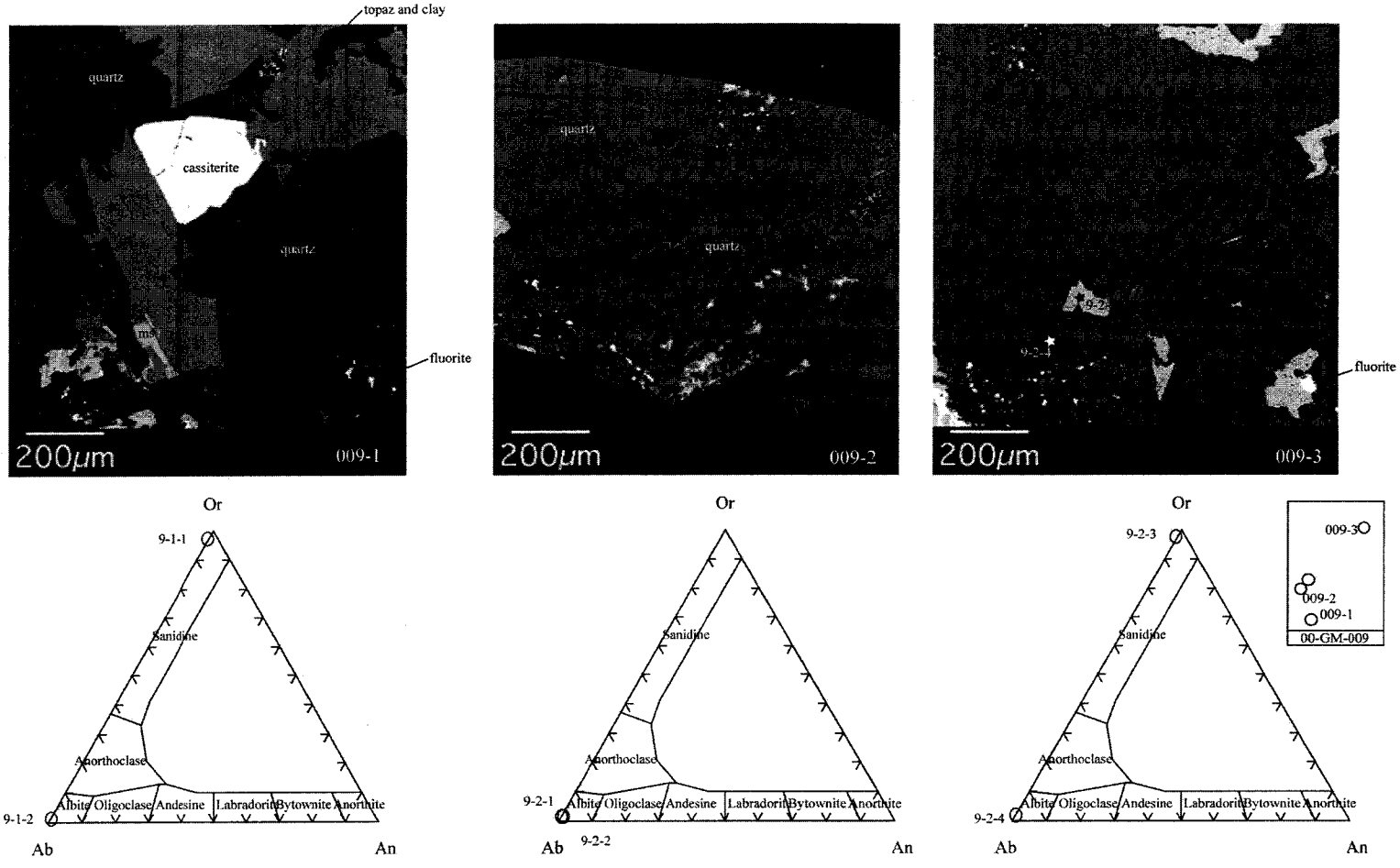

Location of electron microprobe analysis made on sample 00-GM-009 and relationship between important rock-forming minerals. Notice that feldspars are pure albite or sanidine and that topaz and quartz are found together.

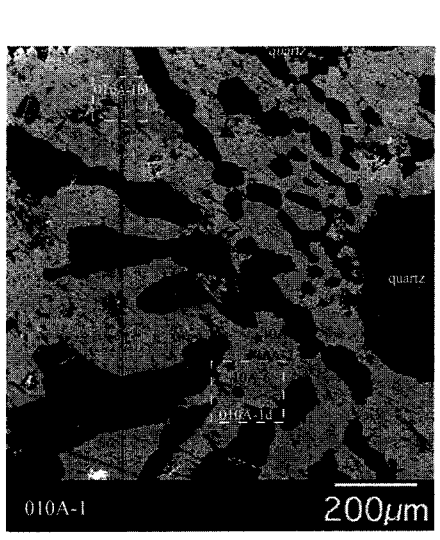

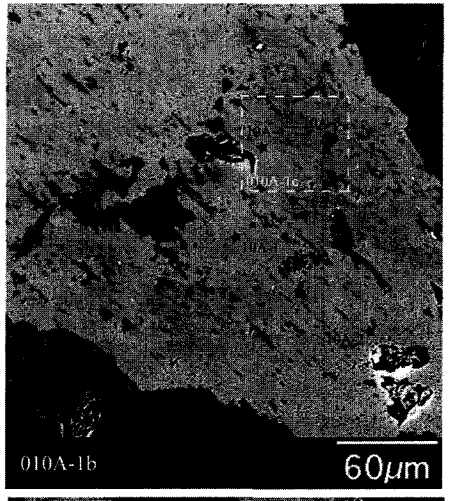

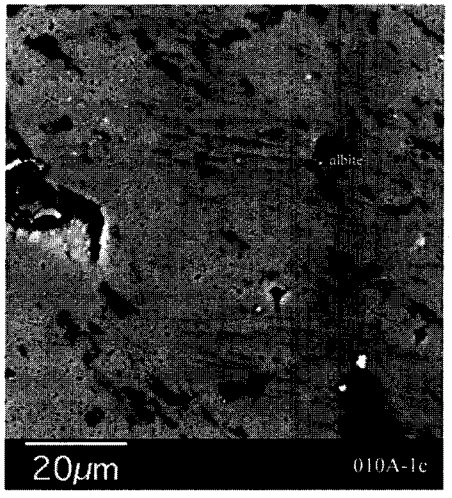

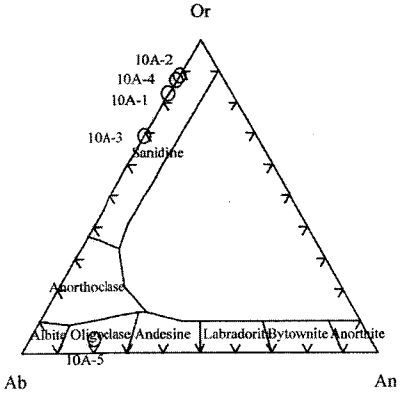

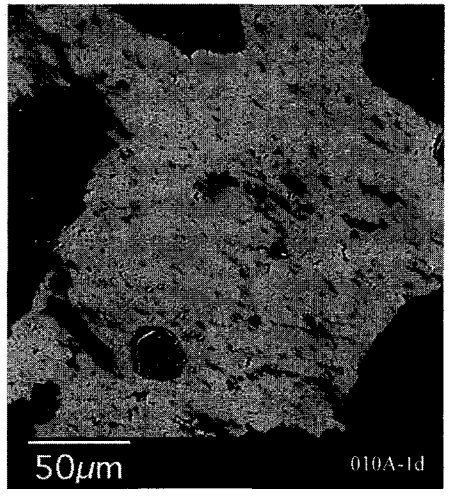

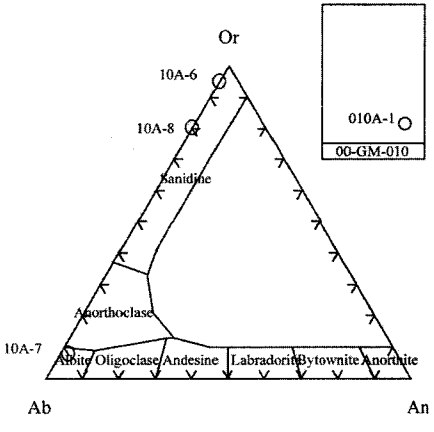

Location of electron microprobe analysis made on sample 00-GM-010. Feldspars compositions are varied. Feldspar and quartz form micrographic texture (010A-1)

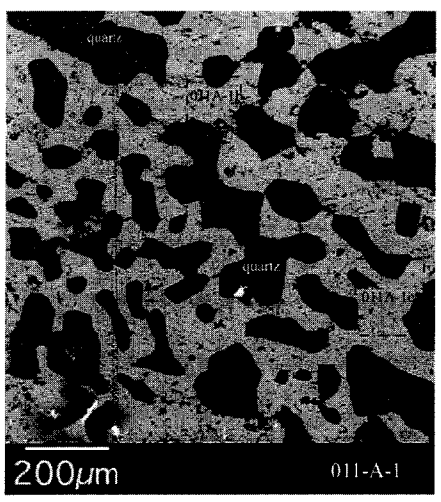

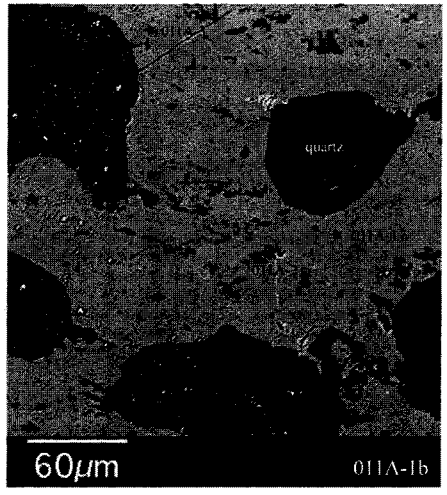

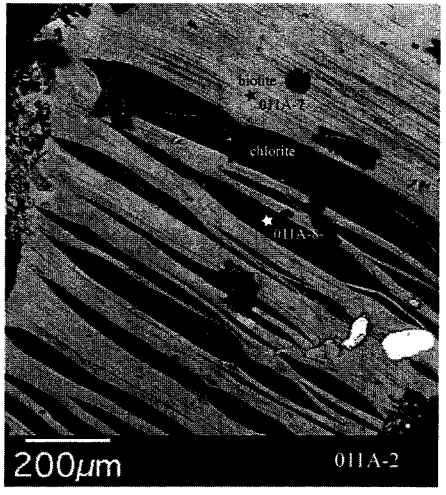

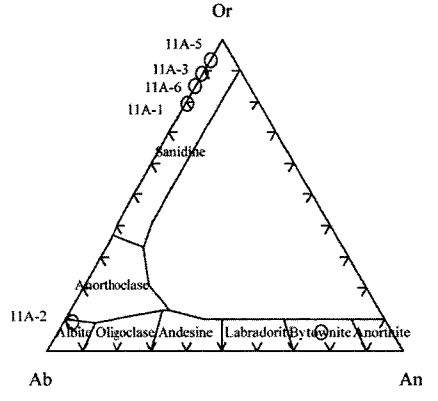

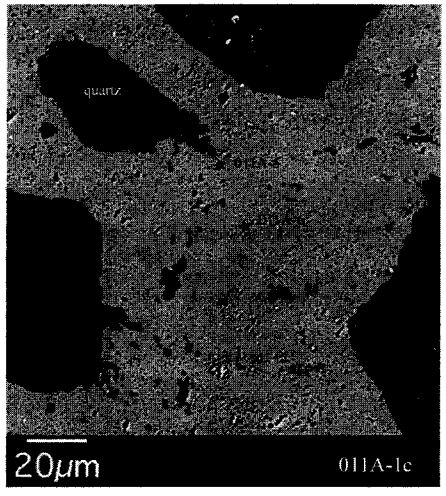

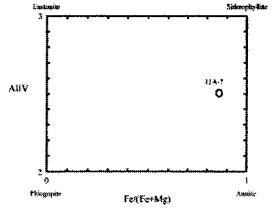

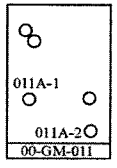

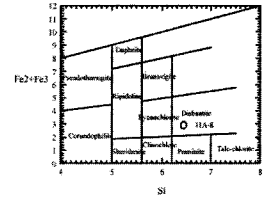

Location of electron microprobe analysis made on sample 00-GM-011. Notice relationship quartz and feldspar, while biotite is altered to chlorite (011A-2). Feldspar composition varies from bytownite to sanidine.

Appendix B: Väkkärä granite, sample 00-GM-012

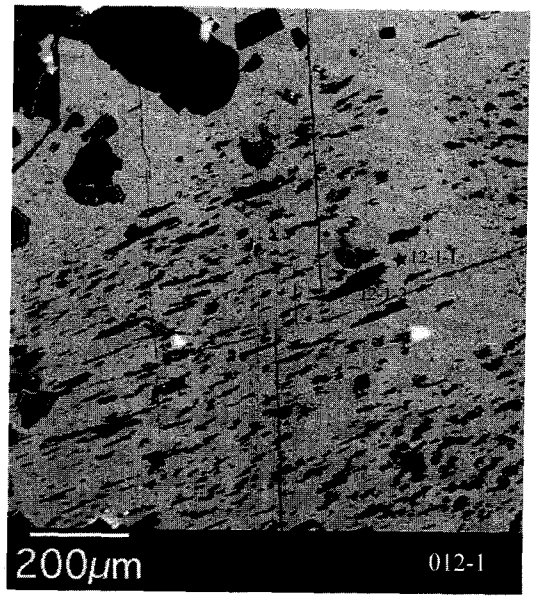

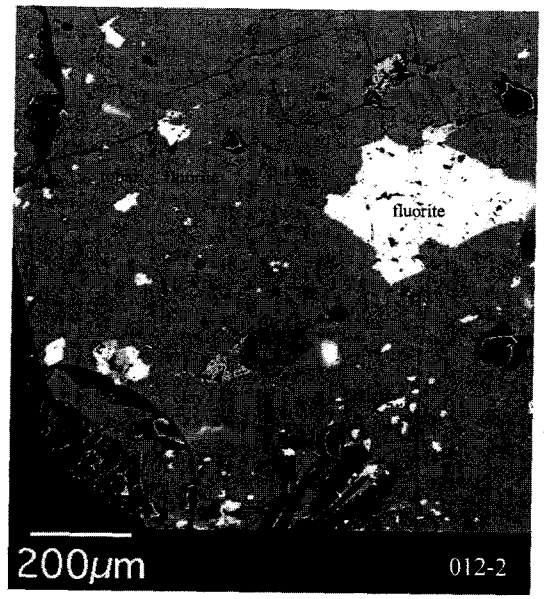

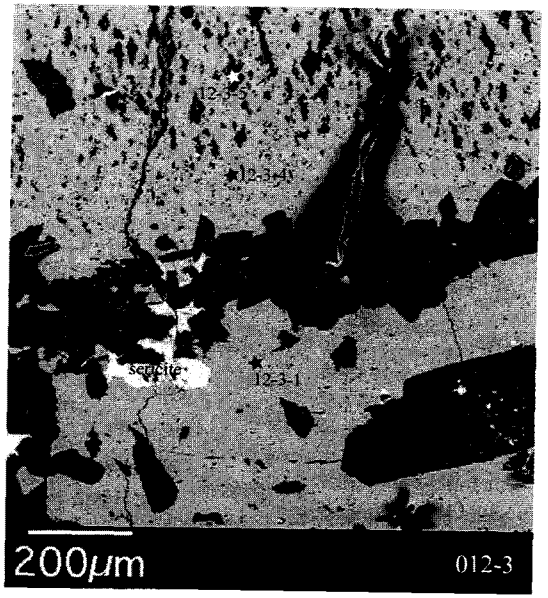

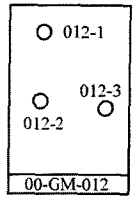

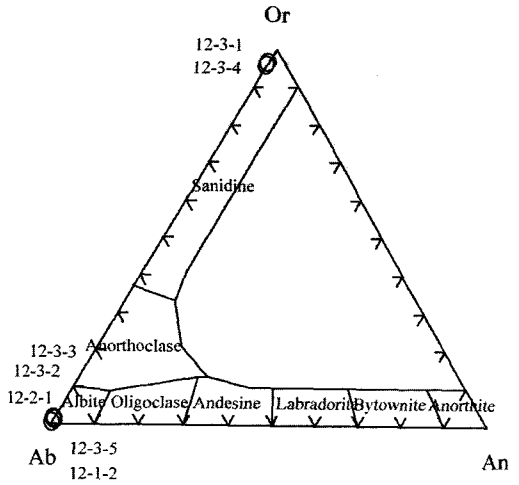

Location of electron microprobe analysis made on sample 00-GM-012. Notice the relationship between all the minerals and perthitic texture (012-1). Feldspar composition is pure albite or sanidine.

Appendix B: Tarkki granite, sample 00-GM-014

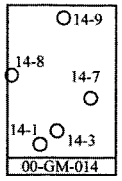

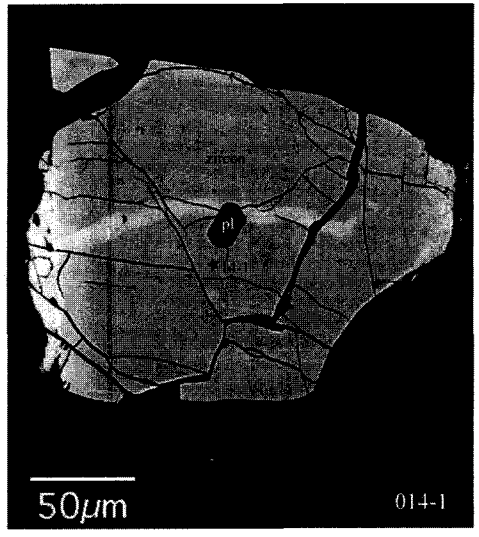

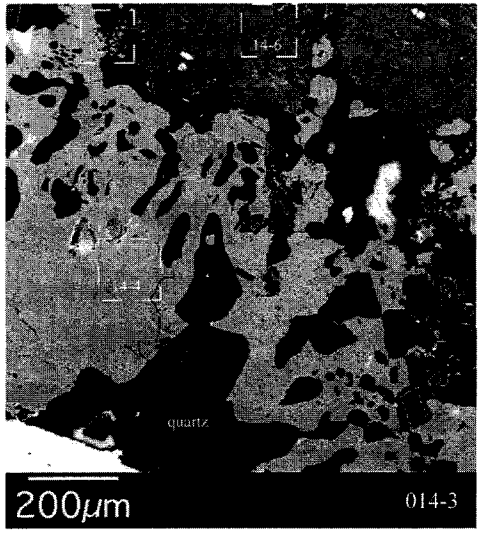

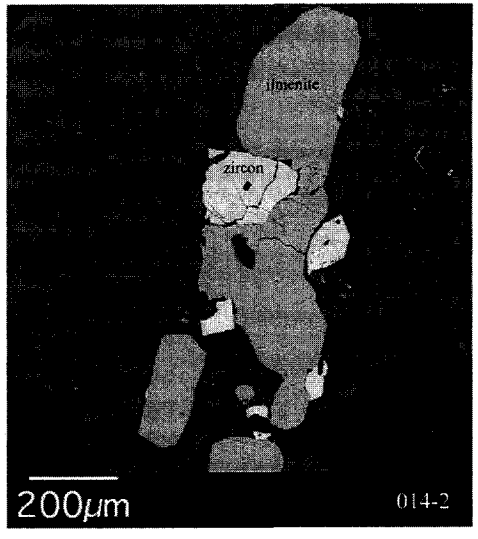

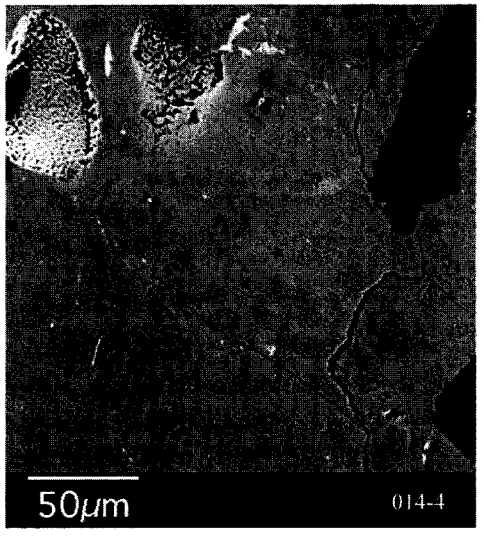

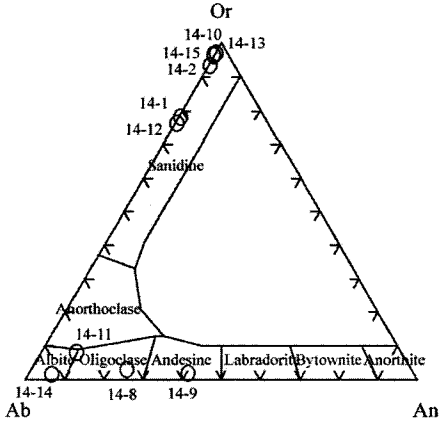

Location of electron microprobe analysis made on sample 00-GM-014. Notice the relationship between all the minerals, the zoning in zircon (014-1) and micrographic texture (014-3). Feldspar composition varies from andesine to sanidine.

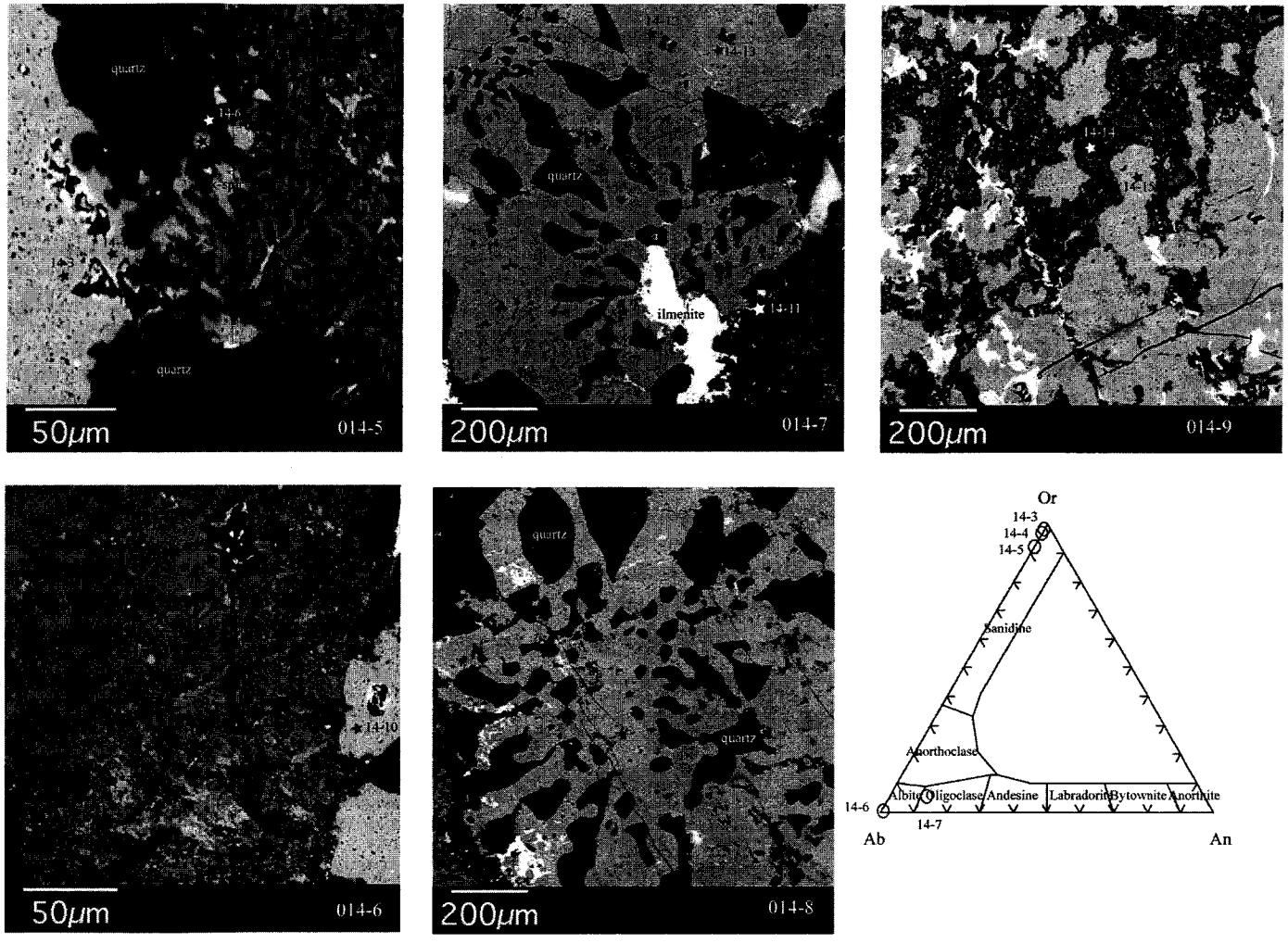

Location of electron microprobe analysis made on sample 00-GM-014 (continued). Notice the relationship between all the minerals and micrographic texture (014-7 and 014-8). Feldspar varies from oligoclase to sanidine.

Appendix B: Tarkki granite, sample 00-GM-015

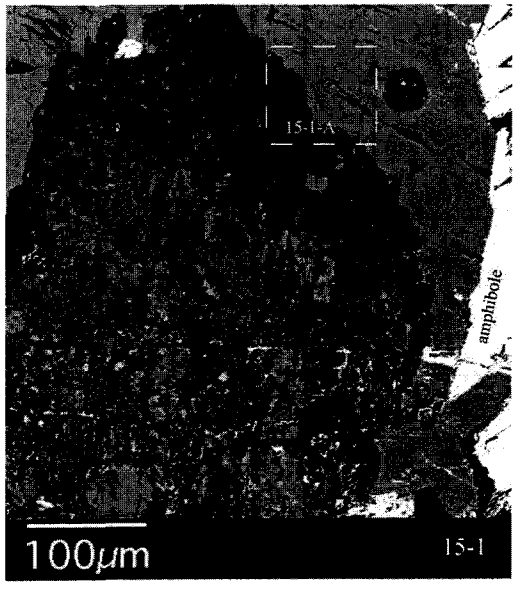

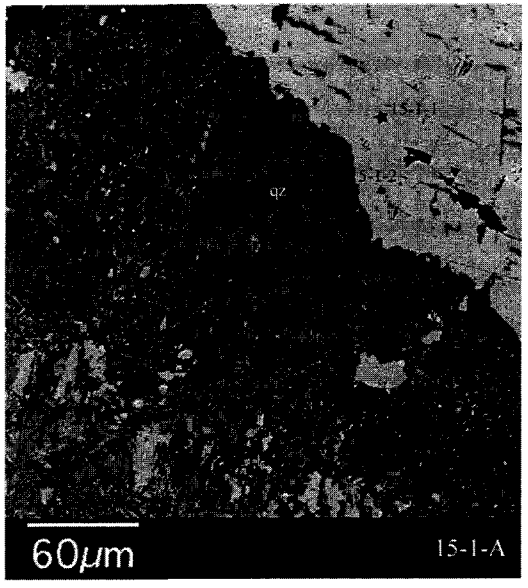

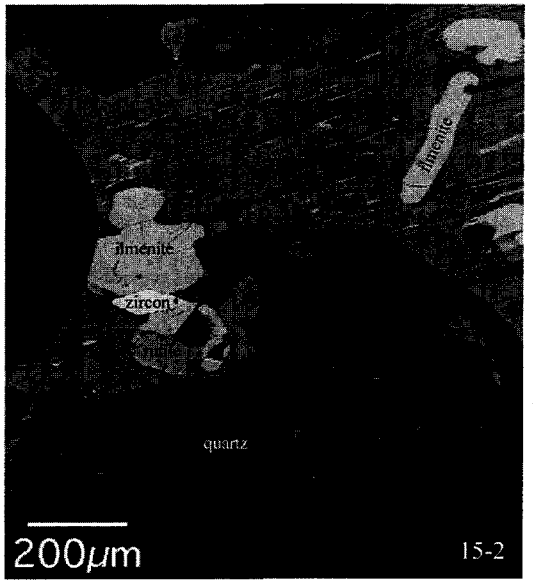

Location of electron microprobe analysis made on sample 00-GM-015. Notice the relationship between all the minerals. Feldspar composition varies from oligoclase to sanidine.

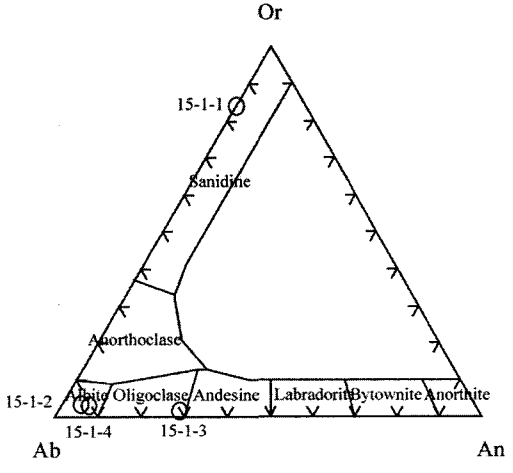

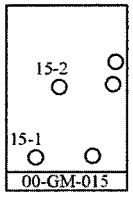

Appendix B: Tarkki granite, sample 00-GM-016

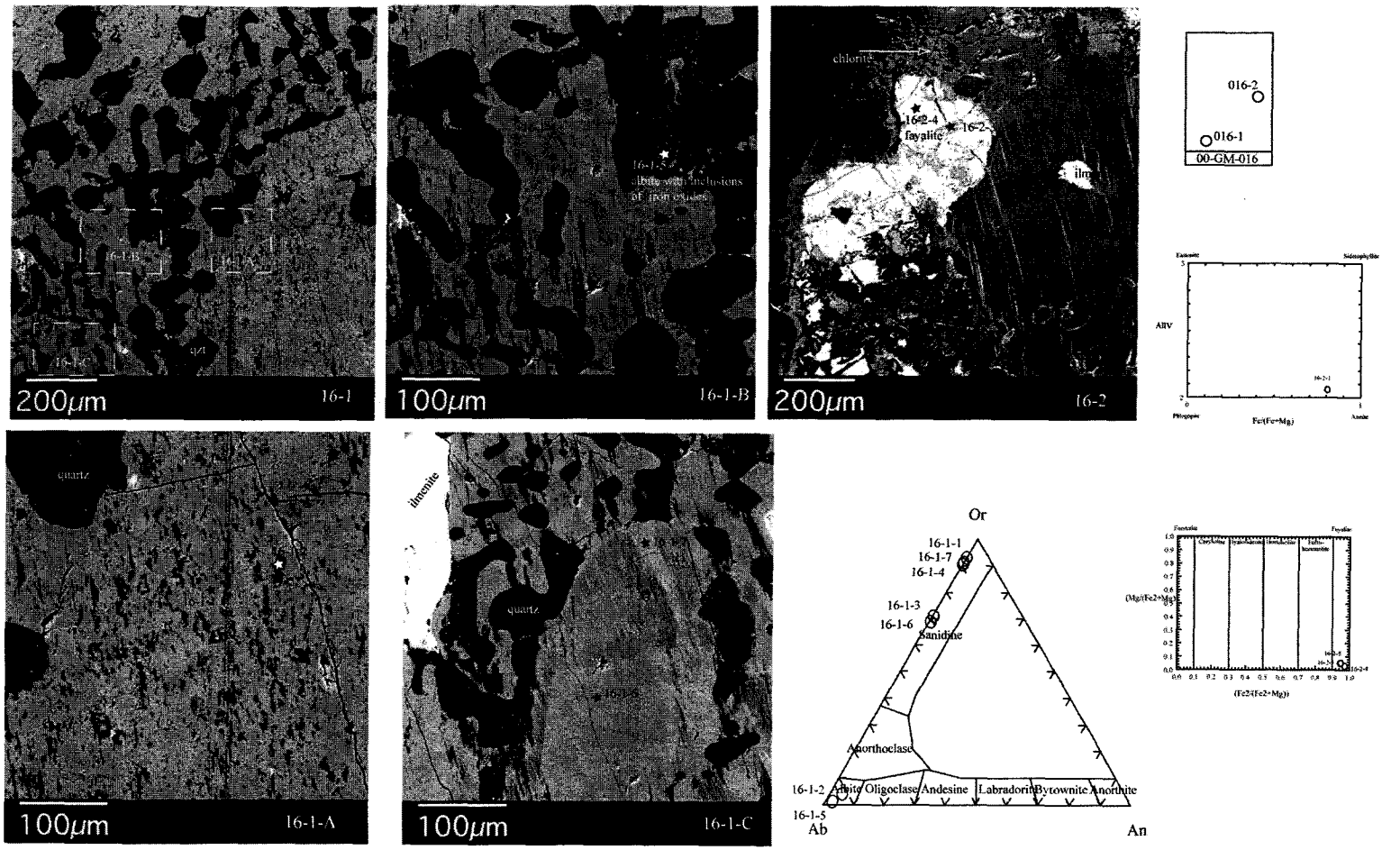

Location of electron microprobe analysis made on sample 00-GM-016. Notice the relationship between all the minerals and micrographic texture (16-1, 16-1-B, 16-1-C). Feldspar composition is pure albite or sanidine, while olivine is fayalite and biotite is annite.

Appendix B: Väkkärä granite, sample 00-GM-017

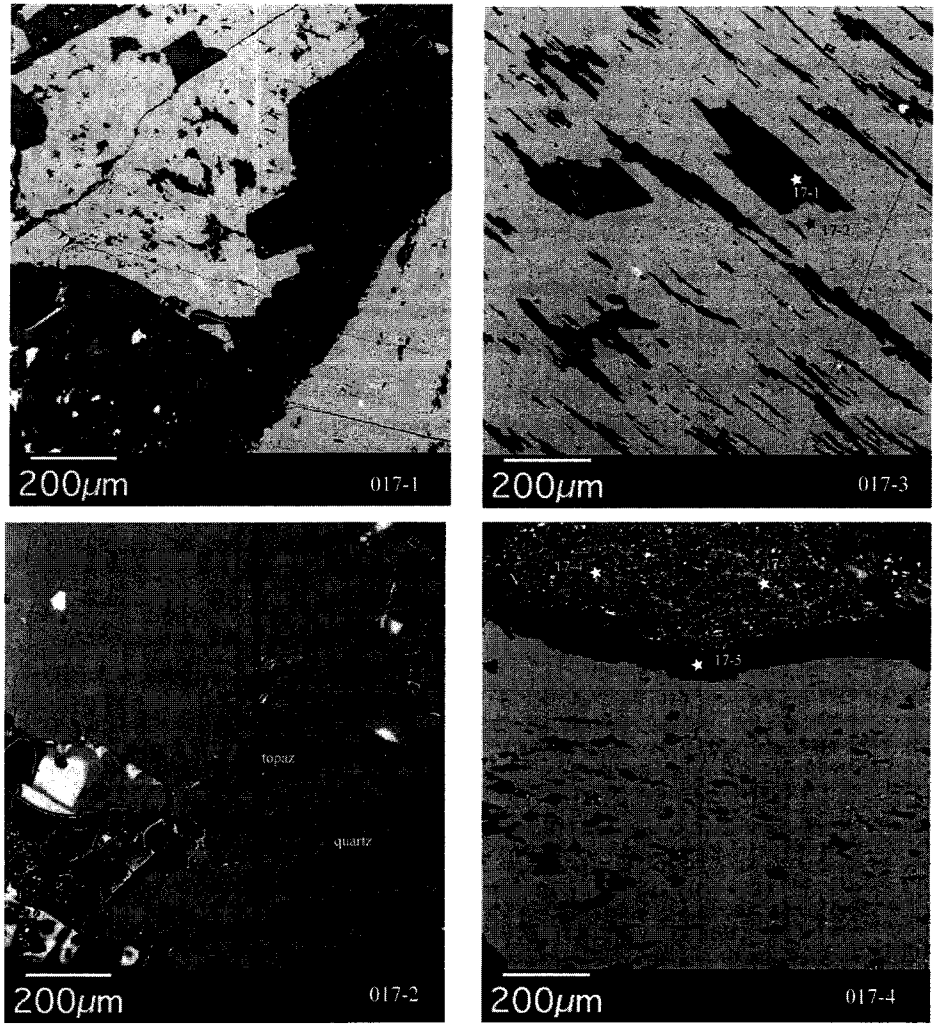

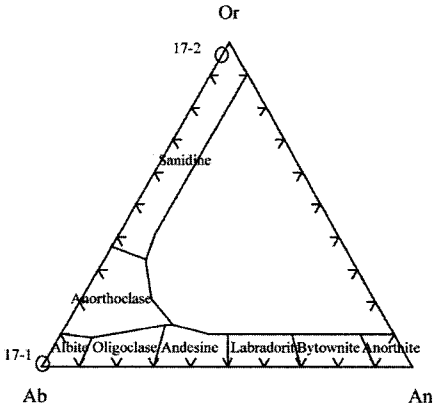

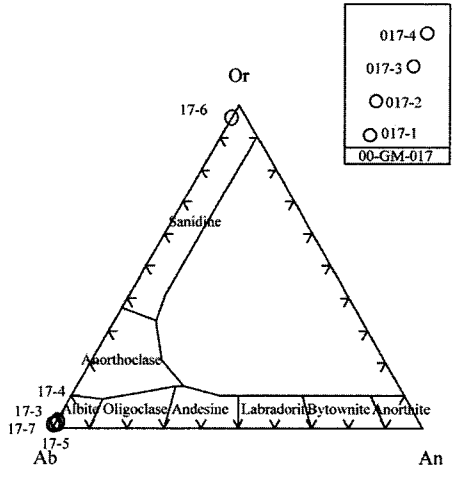

Location of electron microprobe analysis made on sample 00-GM-017. Notice the relationship between all the minerals and perthitic texture (017-3). Feldspar composition is pure albite or sanidine.

Appendix B: Väkkärä granite, sample 00-GM-018

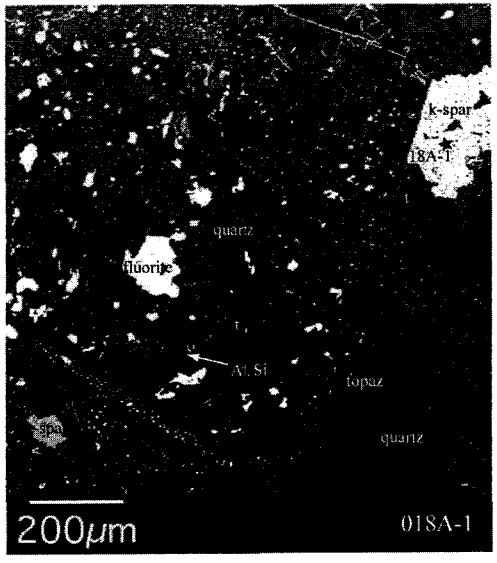

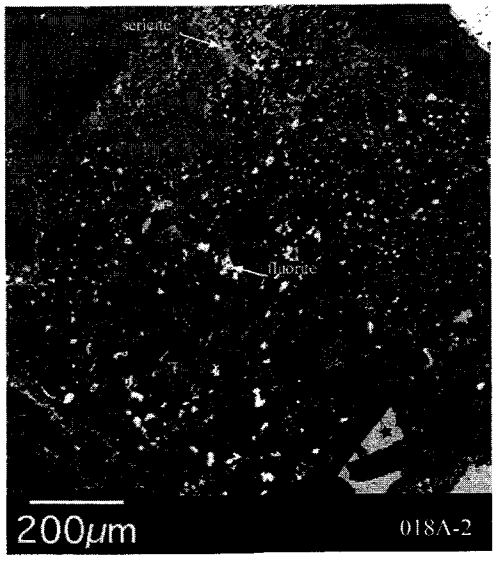

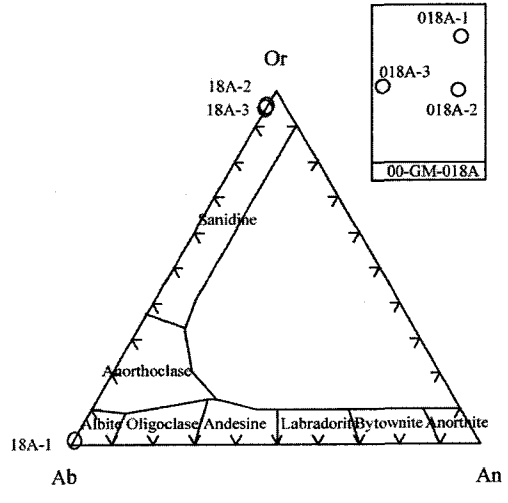

Location of electron microprobe analysis made on sample 00-GM-018. Notice the relationship between all the minerals. Feldspar composition is pure albite or sanidine.

Appendix B: Väkkärä granite, sample 00-GM-020

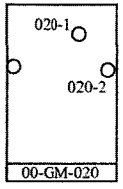

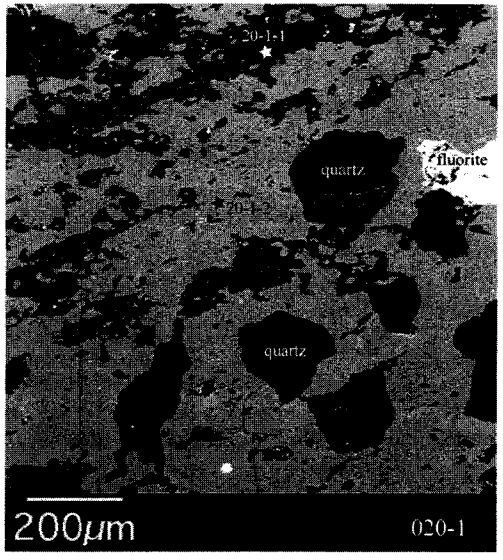

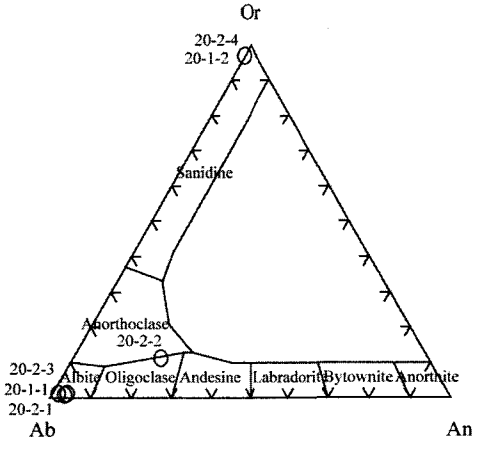

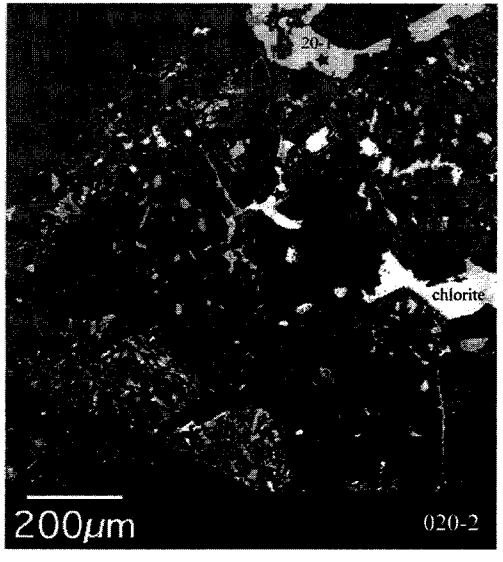

Location of electron microprobe analysis made on sample 00-GM-020. Notice the relationship between all the minerals. Feldspar composition is albite, sanidine or oligoclase.

Appendix B: Väkkärä granite, sample 00-GM-021

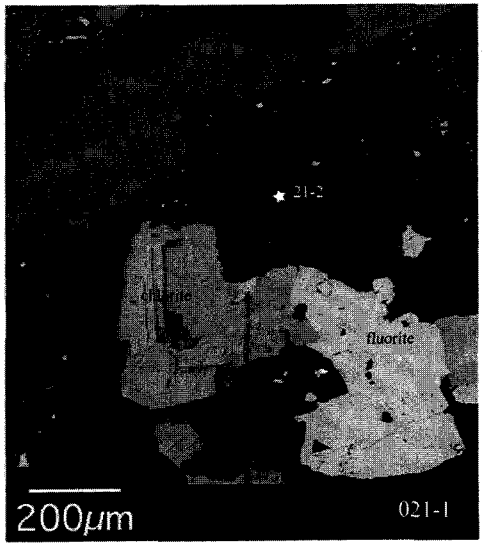

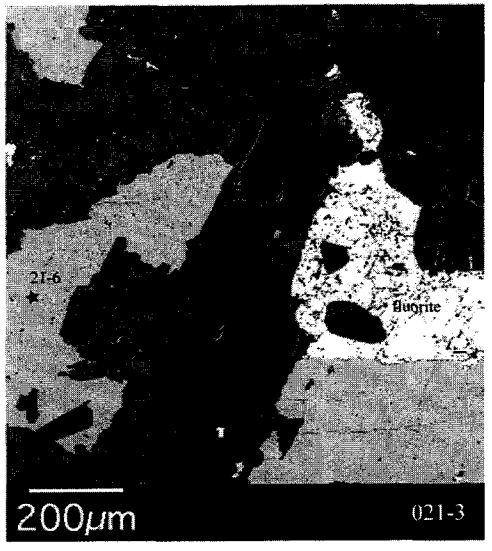

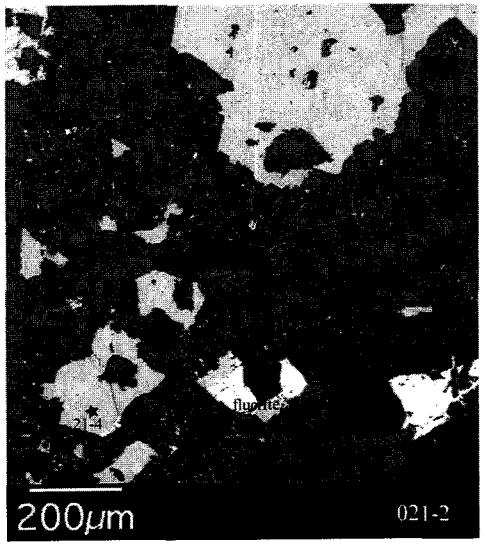

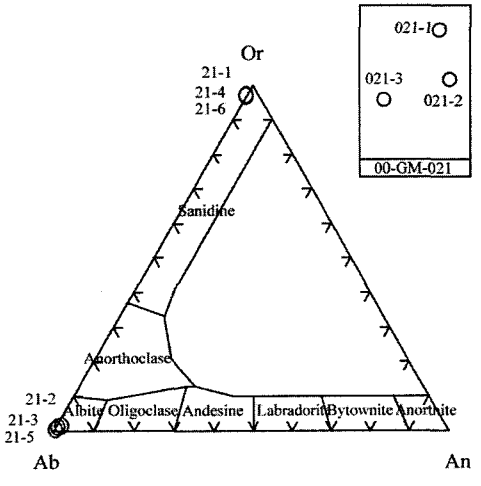

Location of electron microprobe analysis made on sample 00-GM-021. Notice the relationship between all the minerals. Feldspar composition is pure albite or sanidine.

Appendix C

Description of samples from the South Mountain Batholith

All samples locations are illustrated on Figure 4.1 (see chapter 4).

Early Stage 1 Plutons

02-GM-009 (Biotite granodiorite from Scrag Lake Pluton)

It is a white rock with pinkish alteration, coarse grained, with plagioclase feldspar euhedral megacrysts 5 cm long (less than 1% of the rock). Approximately 45% of plagioclase, 25 % quartz, 15% potassic feldspar and 15 % biotite compose this rock. Except for the megacryst, grain size is around 1-2 cm.

02-GM-016 (Biotite granodiorite from Scrag Lake Pluton)

It is a white rock with pinkish alteration and coarse grained. Approximately 45% of plagioclase, 25 % quartz, 10% potassic feldspar and 20 % biotite compose this rock. The grain size is around 0.5 – 1.5 cm, a few plagioclase megacrysts (3-4 cm long) are seen on outcrop.

02-GM-019 (Biotite granodiorite from Gaspereau Lake Pluton)

It is a coarse grained (1-2 cm) homogeneous white granodiorite. Approximately 50% of plagioclase, 25 % quartz, 10% potassic feldspar and 15 % biotite compose this rock. Plagioclase crystal are twinned and zoned.

02-GM-020 (Biotite granodiorite from Gaspereau Lake Pluton)

It is a coarse grained (1-2 cm) homogeneous pink-red granodiorite. Approximately 40% of plagioclase, 30 % quartz, 25% potassic feldspar and 5 % biotite compose this rock. Plagioclase crystals are twinned. Potassic feldspars grains are anhedral and fill spaces between quartz and plagioclase crystals.

02-GM-028 (Biotite granodiorite from an unnamed Pluton)

It is a white, with traces of pink color, homogeneous, coarse-grained granodiotite. It contains less than 0.5% alkali feldspar megacrysts. Approximately 40% plagioclase, 25 % quartz, 30% potassic feldspar and 5 % biotite compose this rock. Plagioclase crystals are twinned, zoned and euhedral while potassic feldspars grains are subhedral and 0.5 to 1.5 cm long.

02-GM-001 (Biotite monzogranite from Peggy's Cove Pluton)

It is a white rock, with traces of pink color, homogeneous, coarse-grained (1 to 4 cm) monzogranite composed of approximately 40% plagioclase, 15 % quartz, 40% potassic feldspar and 5 % biotite. Plagioclase crystals are twinned and subhedral to euhedral. Potassic feldspars grains are subhedral and are the larger crystals in the rock (1 to 2.5 cm long). A few

potassic feldspar megacrysts (1 per 100 m^2) are seen. Mafic xenoliths with very different shapes (rounded to rectangular) are also seen.

02-GM-004 (Biotite monzogranite from Sandy Lake Pluton)

It is a white, with traces of pink color, homogeneous, medium to coarse-grained monzogranite composed of approximately 40% plagioclase, 15 % quartz, 35% potassic feldspar and 10 % biotite. Plagioclase crystals are twinned and subhedral to euhedral while potassic feldspars grains are subhedral. At this outcrop, monzonite is in contact with sedimentary rocks from the Cambrian to Devonian period.

02-GM-010 (Biotite monzogranite from Scrag Lake Pluton)

It is a white, with traces of pink color, homogeneous, coarse-grained monzogranite with potassic feldspar euhedral megacrysts up to 8 cm long containing approximately 35% plagioclase, 10 % quartz, 40% potassic feldspar and 15 % biotite. Plagioclase and potassic feldspars crystals are subhedral to euhedral.

02-GM-013 (Biotite monzogranite from Little Round Lake Pluton)

It is a white, homogeneous, coarse-grained porphyritic monzogranite with plagioclase plagioclase euhedral megacrysts up to 5 cm long containing approximately 45% plagioclase, 15 % quartz, 30% potassic feldspar and 10 % biotite. Plagioclase crystals are euhedral and twinned. Potassic feldspars grains are subhedral to anhedral and fill space between plagioclase crystals.

02-GM-014 (Biotite monzogranite from Little Round Lake Pluton)

It is a white, homogeneous, coarse-grained monzogranite containing approximately 45% plagioclase, 15 % quartz, 30% potassic feldspar and 10 % biotite. Plagioclase crystals are euhedral, zoned and twinned. Potassic feldspars grains are subhedral. Macroscopically, this sample is very similar to 02-GM-013 except for the megacrysts.

02-GM-018 (Biotite monzogranite from Cloud Lake Pluton)

It is a light pink, homogeneous, coarse-grained monzogranite with plagioclase euhedral megacrysts up to 5 cm long containing approximately 45% plagioclase, 15 % quartz, 25% potassic feldspar and 15 % biotite. Plagioclase crystals are subhedral to euhedral, twinned and some are mantled by potassic feldspar crystal. Potassic feldspars grains are subhedral to anhedral and fill space between plagioclase crystals.

02-GM-022 (Biotite monzogranite from Salmontail Pluton)

It is a pink, homogeneous, medium to coarse-grained monzogranite with plagioclase euhedral phenocrysts up to 3 cm long conataining approximately 45% plagioclase, 15 % quartz, 35% potassic feldspar and 5 % biotite. Plagioclase crystals are euhedral, zoned and twinned. Potassic feldspars grains are subhedral to anhedral and fill space between plagioclase crystals.

02-GM-023 (Biotite monzogranite from Salmontail Pluton)

It is a white, homogeneous, coarse-grained monzogranite with plagioclase euhedral phenocrysts up to 3 cm long containing approximately 45% plagioclase, 15 % quartz, 30% potassic feldspar and 10 % biotite. Plagioclase crystals are euhedral, zoned and twinned. Potassic feldspars grains are subhedral to anhedral and fill space between plagioclase crystals. Besides the color, it is very similar to 02-GM-022.

Late Stage 2 plutons

02-GM-017 (Muscovite-biotite monzogranite from West Dalhousie Pluton)

It is a pink, homogeneous, coarse-grained monzogranite with potassic feldspar euhedral aligned megacrysts up to 5 cm long containing approximately 35% plagioclase, 15 % quartz, 40% potassic feldspar, 5% muscovite and 5% biotite. Plagioclase crystals are euhedral, zoned and twinned. Potassic feldspars grains are euhedral and twinned.

02-GM-027 (Muscovite-biotite monzogranite from Sherwood Pluton)

It is a white, homogeneous, coarse-grained monzogranite with potassic feldspar euhedral aligned megacrysts up to 5 cm long containing approximately 35% plagioclase, 15 % quartz, 40% potassic feldspar, 1% muscovite and 9% biotite. Plagioclase crystals are euhedral, zoned and twinned. Potassic feldspars grains are euhedral and twinned.

02-GM-002 (Coarse-grained leucomonzogranite from Halifax Peninsula Pluton)

It is a white, homogeneous, coarse-grained monzogranite with potassic feldspar euhedral megacrysts up to 8 cm long containing approximately 35% plagioclase, 18 % quartz, 35% potassic feldspar, 2% cordierite, 5% muscovite and 5% biotite. Plagioclase crystals are euhedral and twinned. Potassic feldspars grains are euhedral.

02-GM-006 (Coarse-grained leucomonzogranite from Davis Lake Pluton)

It is a white to grayish blue, homogeneous, coarse-grained monzogranite containing approximately 35% plagioclase, 15 % quartz, 40% potassic feldspar, 5% muscovite and 5% biotite. All feldspars crystals are altered, sericitized and broken.

02-GM-007 (Coarse-grained leucomonzogranite from Davis Lake Pluton)

It is a white to pink, homogeneous, coarse-grained monzogranite with potassic feldspar euhedral aligned megacrysts up to 7 cm long containing approximately 35% plagioclase, 15 of quartz, 40% potassic feldspar, 5% muscovite and 5% biotite. Plagioclase and potassic feldspars crystals are euhedral, sericitized and twinned. This outcrop is very similar to 02-GM-006 except for the megacrysts.

02-GM-025 (Coarse-grained leucomonzogranite from New Ross Pluton)

It is a light pink, homogeneous, coarse-grained monzogranite with potassic feldspar euhedral phenocrysts up to 2 cm long containing approximately 40% plagioclase, 15 % quartz, 35%

potassic feldspar, 5% muscovite and 5% biotite. Plagioclase crystals are euhedral, sericitized and twinned while potassic feldspars grains are euhedral, perthitic and twinned.

02-GM-026 (Coarse-grained leucomonzogranite from Spectacle Road Pluton)

It is a light pink, homogeneous, coarse-grained monzogranite with potassic feldspar euhedral aligned megacrysts up to 4 cm long containing approximately 40% plagioclase, 15 % quartz, 35% potassic feldspar, 5% muscovite and 5% biotite. Plagioclase crystals are euhedral, zoned and twinned while potassic feldspars grains are euhedral.

02-GM-003 (Fine-grained leucomonzogranite from Tantallon Pluton)

It is a white, homogeneous, coarse-grained monzogranite with potassic feldspar euhedral aligned megacrysts up to 10 cm long containing approximately 30% plagioclase, 15 % quartz, 45% potassic feldspar, 5% muscovite and 5% biotite. Plagioclase crystals are euhedral. Potassic feldspars grains are euhedral and twinned.

02-GM-012 (Fine-grained leucomonzogranite from an unnamed Pluton)

It is a white, homogeneous, coarse-grained monzogranite containing approximately 40% plagioclase, 15 % quartz, 35% potassic feldspar, 2% muscovite and 8% biotite. Plagioclase crystals are euhedral and twinned. Potassic feldspars grains are euhedral and perthitic.

02-GM-015 (Fine-grained leucomonzogranite from East Dalhousie Pluton)

It is a pink, homogeneous, coarse-grained monzogranite with potassic feldspar euhedral aligned phenocrysts up to 3 cm long containing approximately 40% plagioclase, 15 % quartz, 35% potassic feldspar, 5% muscovite and 5% biotite. Plagioclase crystals are euhedral, zoned, sericitized and twinned. Potassic feldspars grains are euhedral and twinned.

02-GM-024 (Fine-grained leucomonzogranite from Panuke Lake Pluton)

It is a pink, homogeneous, coarse-grained monzogranite with potassic feldspar euhedral aligned megacrysts up to 5 cm long containing approximately 40% plagioclase, 15 % quartz, 35% potassic feldspar, 5% muscovite and 5% biotite. Plagioclase crystals are euhedral, zoned and twinned. Potassic feldspars grains are euhedral, perthitic and twinned.

02-GM-005 (Muscovite leucogranite from East Kemptville Pluton)

It is a pink, homogeneous, fine-grained granite containing approximately 25% plagioclase, 30 % quartz, 35% potassic feldspar and 10% muscovite. The whole rock is silicified, grains are all anhedral and altered. The sample was taken near the mineralized zone of the East Kemptville tin mine.

02-GM-008 (Muscovite leucogranite from East Kemptville Pluton)

It is a pink, homogeneous, fine to medium-grained granite composed of approximately 30% plagioclase, 30 % quartz, 30% potassic feldspar and 10% muscovite. Plagioclase crystals are euhedral and twinned. Potassic feldspars grains are euhedral.

02-GM-021 (Muscovite leucogranite from Murphy Lake Pluton)

It is a red, homogeneous, fine-grained granite containing approximately 25% plagioclase, 30 % quartz, 30% potassic feldspar and 15% muscovite. The outcrop is cross-cut by numerous pegmatite dykes.